

UNIVERSITÄTSKLINIKUM HAMBURG-EPPENDORF

Aus der Klinik und Poliklinik für Kinder- und Jugendmedizin, Sektion
Biochemie, des Zentrums für Geburtshilfe, Kinder- und Jugendmedizin

Direktor: Prof. Dr. med. Kurt Ullrich

Generation and analysis of a cell-based model of CLN7 disease

Dissertation

zur Erlangung des Grades eines Doktors der Medizin an
der Medizinischen Fakultät der Universität Hamburg.

vorgelegt von:

Jana Farhana Galal, geb. Helal

aus Köln

Hamburg 2014

Für meine Eltern
Christel und Rakib-Al Helal

Angenommen von der Medizinischen Fakultät

der Universität Hamburg am: 26.03.2015

Veröffentlicht mit Genehmigung der Medizinischen

Fakultät der Universität Hamburg

Prüfungsausschuss, der /die Vorsitzende: PD Dr. rer. nat. Stephan Storch

Prüfungsausschuss: 2. Gutachter/in: Prof. Dr. rer. nat. Thomas Braulke

Prüfungsausschuss: 3. Gutachter/in: Prof. Dr. Christian Hagel

Table of contents

1.	Introduction	1
1.1	Lysosomes.....	1
1.2	Biosynthesis and transport of soluble lysosomal hydrolases.....	2
1.3	Biosynthesis and transport of lysosomal membrane proteins.....	3
1.4	Functions of lysosomal membrane proteins	3
1.5	Degradative pathways to lysosomes	5
1.5.1	Endocytosis.....	5
1.5.2	Autophagy	5
1.6	Lysosomal storage disorders.....	6
1.7	The neuronal ceroid lipofuscinoses (NCLs)	7
1.8	Classification of NCLs.....	8
1.9	Molecular basis of CLN7 disease	11
1.10	Organization of the <i>MFSD8/CLN7</i> gene and <i>MFSD8/CLN7</i> expression	12
1.11	Membrane topology and localisation of the CLN7 protein	13
1.11.1	Lysosomal targeting of CLN7	14
1.11.2	Function of CLN7.....	14
2.	Aim of the study	15
3.	Materials and Methods	16
3.1	Materials	16
3.1.1	Equipment and consumables	16
3.1.2	Chemicals and Kits.....	18
3.1.3	Buffers and Solutions	20
3.1.4	Enzymes	21
3.1.5	Protein and DNA standards	22
3.1.6	Mammalian cell lines	22
3.1.7	Media and solutions for cell culture	22
3.1.7.1	Bacterial strains and bacteria medium	23
3.1.8	Antibodies.....	23
3.1.9	siRNA	24

Table of contents	II
3.1.10 Vectors and primers.....	25
3.1.11 Sequencing of DNA samples.....	27
3.2 Methods.....	27
3.2.1 Cell Biology Methods.....	27
3.2.1.1 General note	27
3.2.1.2 Cell culture cultivation and trypsinization	27
3.2.1.3 Cryoconservation and revitalisation of cells	28
3.2.1.4 Transfection of siRNA	28
3.2.1.5 Transfection of expression- and shRNA vectors	28
3.2.1.6 Double immunofluorescence microscopy.....	30
3.2.2 Analysis of clathrin-mediated endocytosis.....	31
3.2.3 Molecular biological methods	31
3.2.3.1 Retransformation/ Transformation of <i>E. coli</i> cells	31
3.2.3.2 Extraction of plasmid DNA from <i>E. coli</i>	31
3.2.3.3 Preparation of glycerol stocks.....	32
3.2.3.4 Photometric measurement of DNA and RNA concentrations	32
3.2.3.5 Cloning of shRNA	32
3.2.4 Enzymatic phosphorylation of DNA	34
3.2.5 Linearization of pSuper.GFP/neo.....	34
3.2.6 Ligation of DNA.....	35
3.2.7 Identification of recombinant clones	35
3.2.8 Cloning of pSuper.RFP.shRNA and pSuper.GFP-LC3.shRNA.....	36
3.2.9 Site-directed mutagenesis	37
3.2.10 Sequencing of DNA constructs	38
3.2.11 Agarose gel electrophoresis.....	38
3.2.12 RNA extraction from cultured cells.....	39
3.2.13 Synthesis of cDNA	39
3.2.14 Quantitative real-time PCR	39
3.2.15 Biochemical methods	41
3.2.15.1 Protein extraction	41
3.2.15.2 Protein quantification.....	41
3.2.15.3 SDS-PAGE	41
3.2.15.4 Western blot analysis	43
4. Results	45

Table of contents	III
4.1	<i>MFSD8/CLN7</i> mRNA expression in cultured human cell lines 45
4.2	siRNA-mediated down-regulation of <i>MFSD8/CLN7</i> mRNA..... 46
4.3	shRNA-mediated down-regulation of <i>MFSD8/CLN7</i> mRNA..... 46
4.3.1	Generation of vector pSuper.GFP.CLN7-shRNA 46
4.3.2	shRNA-mediated down-regulation of <i>MFSD8/CLN7</i> mRNA in HeLa cells 48
4.3.3	Reduced amounts of <i>CLN6</i> and <i>CLN8</i> mRNAs in <i>MFSD8/CLN7</i> -depleted HeLa cells..... 49
4.3.4	<i>MFSD8/CLN7</i> -depletion does not alter mRNA expression levels of lysosomal proteins 50
4.3.5	Clathrin-mediated endocytosis of the transferrin receptor is not altered in <i>MFSD8/CLN7</i> -depleted HeLa cells..... 51
4.3.6	Number, size and distribution of LAMP-1 and LAMP-2 positive compartments were not affected in <i>MFSD8/CLN7</i> -depleted cells..... 54
4.3.7	Expression of LAMP-1 and LAMP-2 in <i>MFSD8/CLN7</i> -depleted cells 56
4.3.8	Proteolytic processing of cathepsin D and Z is not altered in <i>MFSD8/CLN7</i> -depleted HeLa cells 58
4.3.9	Number, size and distribution of early endosomes are not changed in <i>MFSD8/CLN7</i> -depleted HeLa cells 59
4.4	Effects of <i>MFSD8/CLN7</i> depletion on macroautophagy 60
4.4.1	Detection of autophagosomes by imaging the autophagosomal marker GFP-LC3-II in <i>MFSD8/CLN7</i> -down-regulated cells 63
4.4.2	Increased number of autophagosomes in <i>MFSD8/CLN7</i> -depleted HeLa cells 64
4.4.3	Increased number of autophagosomes in CLN7 overexpressing HeLa cells 67
5.	Discussion 69
5.1	Expression analyses of <i>MFSD8/CLN7</i> in cultured human cell lines 69
5.2	Generation of a cell-based model for CLN7 disease 70
5.3	Analyses of <i>MFSD8/CLN7</i> -depleted cells 71
5.3.1	Expression of NCL-related and lysosomal genes in <i>MFSD8/CLN7</i> -depleted cells 71
5.3.2	Unaltered transferrin-receptor mediated endocytosis in <i>MFSD8/CLN7</i> -depleted cells 72
5.3.3	Decreased LAMP-1 protein amounts in <i>MFSD8/CLN7</i> -depleted cells..... 74
5.3.4	Analysis of expression, biosynthetic sorting and proteolytic processing of soluble lysosomal enzymes in <i>MFSD8/CLN7</i> -depleted cells 76
5.3.5	Increased number of autophagosomes in <i>MFSD8/CLN7</i> -depleted cells 77

5.4	Comparison of <i>MFSD8/CLN7</i> -downregulated cells with <i>Cln7</i> -deficient fibroblasts from <i>Mfsd8/Cln7</i> -knockout mice	80
5.5	Outlook	81
6.	Summary	83
7.	References	85
8.	Curriculum Vitae	95
9.	Affidavit (Eidesstattliche Erklärung)	96
10.	Acknowledgements	97

Abbreviations

ANCL	Adult neuronal ceroid lipofuscinosis
APS	Ammonium peroxydisulfate
Atg	Autophagy-related genes
BMP	Bi(monoacyl-glycerol) phosphate
Bp	Base pairs
BSA	Bovine serum albumin
CLEAR	Coordinated Lysosomal Expression and Regulation
C-terminal	Carboxyl-terminal
cDNA	Complementary DNA
CSP	Cysteine string protein
Ctsb	Cathepsin B
Ctsd	Cathepsin D
DAPI	4',6-Diamidino-2-phenylindole
DMSO	Dimethylsulfoxide
DMEM	Dulbecco's minimal essential medium
DNA	Deoxyribonucleic acid
dNTP	Deoxynucleoside triphosphate
ECL	Enhanced chemiluminescence
EEA-1	Early endosome antigen 1
ER	Endoplasmic reticulum
FCS	Fetal calf serum
GFP	Green fluorescent protein
GlcNAc	N-Acetyl glucosamine
HEK293	Human embryonic kidney cell line 293
HeLa	Human cell line from cervical cancer (<u>Henrietta Lacks</u>)
HRP	Horse radish peroxidase
IB	Immunoblot
IF	Immunofluorescence
INCL	Infantile neuronal ceroid lipofuscinosis
IRES	Internal ribosome entry site
Kb	Kilobase
kDa	Kilodalton
LAMP	Lysosome-associated membrane protein
LC3	Microtubule-associated protein 1A/1B-light chain 3
LF 2000	Lipofectamine 2000
LIMP	Lysosomal integral membrane protein
LINCL	Late-infantile neuronal ceroid lipofuscinosis
LMPs	Lysosomal membrane proteins
LRO	Lysosome-related organelles
LSDs	Lysosomal storage disorders
MFS	Major facilitator superfamily
MFSD8	Major facilitator superfamily domain-containing 8
Min	Minutes
MPR46	Mannose 6-phosphate receptor of 46 kDa
MPR300	Mannose 6-phosphate receptor of 300 kDa

mRNA	Messenger ribonucleic acid
M6P	Mannose 6-phosphate
NPC1	Nieman-Pick Type C1
N-terminal	Amino-terminal
NCL	Neuronal ceroid lipofuscinosis
ON	Overnight
PBS	Phosphate buffered saline
PCR	Polymerase chain reaction
PPT1	Palmitoyl protein thioesterase 1
RT	Room temperature
SDS	Sodium dodecyl sulfate
SDS-PAGE	SDS Polyacrylamide gel electrophoresis
siRNA	Silencing RNA
shRNA	Short hairpin RNA
Sec	Seconds
TAE	Tris-acetate-EDTA buffer
TEMED	NNN`N`-Tetramethylethylenediamine
TFEB	Transcription factor EB
TGN	Trans-Golgi network
TM	Transmembrane domain
TPP1	Tripeptidyl-peptidase 1
Tris	Tris(hydroxymethyl)aminomethane
WB	Western blotting
Wt	Wild-type

1. Introduction

1.1 Lysosomes

Lysosomes are primary degradative compartments, which are confined by a single phospholipid bilayer from the cytosol and are characterized by their heterogeneous size, their high intraluminal concentration of protons and the lack of mannose 6-phosphate receptors (Kornfeld and Mellman, 1989). The low pH of 4.5-5.0 is generated and maintained by V-type H⁺-ATPase pumps and is required for the activation of soluble lysosomal hydrolases and the denaturation of macromolecules (Mindell, 2012). The main function of lysosomes consists in the degradation of endogenous and exogenous macromolecules, like proteins, carbohydrates, nucleic acids and lipids, which are delivered by phagocytosis, autophagy and endocytosis. In addition to lysosomes, lysosome-related organelles (LRO), like cytotoxic T-cell granules, platelet-dense bodies, major histocompatibility complex class II compartments and melanosomes, exist which contain both subset of lysosomal proteins and cell-type specific proteins (Saftig and Klumperman, 2009). Furthermore, lysosomes play an important role in iron metabolism, supplying the cytosol with Fe²⁺ either from substrates delivered by autophagy or by release from endocytosed transferrin (Kurz et al., 2008).

Lysosomes and LROs are important for many physiological processes such as cholesterol homeostasis, cell death, pathogen defence, cell energy metabolism and plasma membrane repair (Saftig and Klumperman, 2009; Settembre et al., 2013).

Lysosomes contain 60 different soluble lysosomal enzymes, which are essential for bulk degradation, processing of pro-proteins and antigens, degradation of the extracellular matrix and initiation of apoptosis (Lübke et al., 2009). Approximately 250 different lysosomal membrane proteins exist which are required for acidification of the lysosomal lumen, protein import from the cytosol, membrane fusion and transport of degradation products into the cytosol (Schröder et al., 2010). Defects in soluble lysosomal enzymes or lysosomal membrane proteins lead to dysfunctional lysosomes and the storage of non-degraded macromolecules or monomeric catabolic products inside organelles of the endosomal-autophagic-lysosomal system finally resulting in lysosomal storage diseases (Futerman and van Meer, 2004).

1.2 Biosynthesis and transport of soluble lysosomal hydrolases

The biogenesis and function of lysosomes require the continuous supply of newly synthesized soluble lysosomal enzymes and membrane proteins, the maintenance of an acidic pH and high Ca^{2+} concentrations. Soluble lysosomal enzymes can be categorized into glycosidases, lipases, nucleases, peptidases, phospholipases, phosphatases and sulfatases depending on the nature of their substrates (Lübke et al., 2009). Lysosomal enzymes were also identified in LROs (Dell'Angelica et al., 2000).

The sorting of newly synthesized soluble enzymes to lysosomes depends on the presence of the mannose 6-phosphate (M6P) recognition marker, which is synthesized in a two-step reaction (Kollmann et al., 2010). After translocation into the endoplasmic reticulum (ER), newly synthesized soluble lysosomal precursor proteins are folded and *N*-linked core oligosaccharide are transferred to selected asparagine residues, which conform to the consensus sequence N X(S/T), where X can be any amino acid except proline, in the ER (Pohl et al., 2009). After vesicular transport from the ER to the Golgi apparatus the hexameric *N*-Acetylglucosamine (GlcNAc)-1-phosphotransferase complex transfers GlcNAc-1-phosphate residues from UDP-GlcNAc to selected terminal mannose residues of high-mannose-type oligosaccharides (Tiede et al., 2005). In the *trans*-Golgi network (TGN) the GlcNAc residues are removed by the uncovering enzyme which exposes the M6P recognition marker (Kornfeld et al., 1998). The M6P recognition marker is recognized and bound by two types of M6P-receptors in the TGN, the 46 kDa cation-dependent M6P-receptor (MPR46) and the 300 kDa cation-independent MPR300 (Braulke and Bonifacino, 2009). The receptor-ligand complexes are packed into clathrin-coated vesicles which are transported from the TGN to endosomal/prelysosomal compartments. After dissociation of the receptor-ligand complexes in prelysosomal compartments, the lysosomal enzymes are delivered to lysosomes where they are processed to the catalytically active forms. The MPRs recycle back to the TGN to mediate further rounds of transport between the TGN and endosomal compartments (Ghosh et al., 2003).

1.3 Biosynthesis and transport of lysosomal membrane proteins

Proteomic analyses combined with identification of proteins by mass spectrometry revealed the presence of approximately 250 different lysosomal membrane proteins (Bagshaw et al., 2005; Schröder et al., 2007). These lysosomal membrane proteins are required for different functions including stabilization of the lysosomal membrane, the separation of the lysosomal hydrolases from the cytosol, fusion with endosomes, autophagosomes and the plasma membrane, the import and export of substrates out and into lysosomes, acidification of the lysosomal lumen, and transport of lysosomes along the cytoskeleton (Eskelinen et al., 2003; Saftig and Klumperman, 2009). It is estimated that the lysosome-associated membrane proteins (LAMPs) and the lysosomal integral membrane proteins (LIMPs) account for about 50% of all lysosomal membrane proteins (Saftig, 2005).

Two pathways are involved in the biosynthetic sorting of membrane proteins to lysosomes: i) an indirect pathway from the TGN via the plasma membrane to endosomes and ii) a direct pathway from the TGN to early and late endosomes (Braulke and Bonifacino, 2009; Hunziker and Geuze, 1996). The sorting between late endosomes and lysosomes occurs identically for both transport routes. The transport of membrane proteins to the lysosomes is independent of the M6P recognition marker. The sorting of type I membrane proteins to endosomal/ lysosomal compartments is mediated by sorting signals, which are located in the short cytosolic tails of the proteins (Bonifacino and Traub, 2003). Sorting signals are composed of short linear amino acid sequences which are typically 4-7 residues in length. They can be divided into tyrosine-based signals, which conform to the consensus sequence YXX Φ , where X is any amino acid and Φ are amino acids with bulky side chains, and dileucine-based signals, which fit to the consensus sequence [DE]XXXL[LI] (Bonifacino and Traub, 2003).

1.4 Functions of lysosomal membrane proteins

The lysosomal membrane consists of a single phospholipid bilayer and contains mainly phospholipids, cholesterol, dolichol derivatives, bismonoacylglycerol and highly glycosylated membrane proteins (Schulze et al., 2009). Lysosomal membranes have multiple functions. They are important for the separation of lysosomal hydrolases from the cytosol and other cellular organelles and the import of molecules into the lysosomes

and the export of degraded substances out of lysosomes. Lysosomal membranes contain transmembrane transporters required for carrying solutes and degradation products across the membrane. Lysosomal membrane proteins, like vacuolar-type H⁺ ATPases and chloride channels, maintain the acidic lysosomal pH and heavily glycosylated integral membrane proteins coordinate the fusion and fission of lysosomes with other organelles (Winchester, 2001).

Over 20 lysosomal transport systems exist for the transport of amino acids, peptides, inorganic ions, nutrients and sugar derivatives (neutral and acidic monosaccharides, amino sugars, myo-inositol, Sagne and Gasnier, 2008). Lysosomal transporters for amino acids (lysosomal amino acid transporter 1 (LYAAT-1), cystinosis, proton-coupled oligopeptide transporter protein 2 (PHT2), PQ loop protein 2 (PQLC2), carbohydrates (sialin, H⁺ myo-inositol transporter HMIT), inorganic ions (v-ATPase, SLC26A11, mucolipin-1, dimetal transporter 1 (DMT1), K-Cl co-transporter (KCC1), zinc transporter 2 (ZnT2), nucleosides (equilibrative nucleoside transporter 3, ENT3), fatty acids (Niemann-Pick disease type C protein 1 (NPC1), p40, spinster like protein), vitamins (cobalamine) and peptides (ABCB9) have been functionally characterized (Jezegou et al., 2012; Rutsch et al., 2009; Sagne and Gasnier, 2008), but the functions of the majority of lysosomal membrane proteins and transporters responsible for the export of lysosomal catabolites are unknown. Few lysosomal membrane proteins belong to the major facilitator superfamily (MFS) of transporters including Disrupted in Renal Carcinoma 2 protein (DIRC2, Savalas et al., 2011), sialin (Laridon et al., 2008), spinster (Rong et al., 2011) and CLN7 (Siintola et al., 2007).

To date more than ten lysosomal storage diseases, including action myoclonus renal failure syndrome, cobalamin F-type disease, cystinosis, Danon disease, Niemann-Pick type C, mucopolidosis type IV, mucopolysaccharidosis type IIIC, malignant osteopetrosis, CLN3 disease, CLN7 disease, and Salla disease are known, which are caused by the deficiency of single membrane proteins (Schwake et al., 2013; Verheijen FW, 2005).

1.5 Degradative pathways to lysosomes

1.5.1 Endocytosis

Lysosomes receive their substrates by endocytosis, phagocytosis or macroautophagy (Saftig and Klumperman, 2009). Extracellular ligands and proteins are targeted to the lysosome through receptor-mediated endocytosis and pinocytosis, and exogenous particles are targeted by phagocytosis (Ciechanover, 2005).

Plasma membrane proteins are involved in various important processes such as the transport of metabolites into the cell or output signaling. Concentrations of proteins at the plasma membrane can be regulated by sorting of damaged and downregulated proteins to lysosomes. Firstly, the proteins are internalized from the cell surface and sorted into multi-vesicular bodies (MVB) that deliver the content to lysosomes for degradation (Piper and Lehner, 2011). The posttranslational modification of cell surface proteins with the 76 amino acid ubiquitin tag is required for their internalization and sorting into MVB (Piper and Lehner, 2011).

Receptors, like the transferrin receptor, the low-density lipoprotein (LDL) receptor, the epidermal growth factor (EGF) receptor, bind their ligands at the cell surface and are transported via clathrin-coated vesicles to endosomal compartments (Mellman, 1996). In the endosomal compartments the ligands dissociate from their receptors and are either transported into the cytosol (Fe^{2+}), or are sorted and degraded in lysosomes (EGF and LDL). The receptors recycle back to the plasma membrane to mediate further rounds of uptake.

1.5.2 Autophagy

Autophagy is an evolutionary conserved lysosomal degradation pathway which is activated during stress conditions such as amino acid starvation, unfolded protein response or viral infection (Eskelinen and Saftig, 2009). Three different autophagy pathways have been described including i) macroautophagy, ii) microautophagy and iii) chaperone-mediated autophagy. In macroautophagy, cytosol or organelles are enclosed into a double-membrane bound autophagosome, which fuses with endosomes and lysosomes (Klionsky and Emr, 2000). Then organelles, cytoplasm and the inner limiting

membrane are degraded by lysosomal hydrolases and the degradation products are transported back to the cytosol for re-utilization (Klionsky and Codogno, 2013).

About 30 autophagy-related genes (*Atg*) have been identified in yeast, and several mammalian homologues exist (Levine and Kroemer, 2008). The mammalian *Atg6* homologue beclin 1 is required for the initiation of autophagosome formation (Kang et al., 2011). Beclin 1 forms a complex with the class III phosphatidyl-inositol 3-kinase vacuolar protein sorting 34 proteins (Vps34). In addition, the *Atg12-Atg5* and the *Atg8*-phosphatidylethanol systems are needed for autophagosome formation (Ohsumi, 2001). The mammalian *Atg8* homologue microtubule-associated protein 1A/1B-light chain 3 (LC3) exists in a soluble LC3-I form and a membrane-associated lipidated, autophagosome-specific LC3-II form (Kabeya et al., 2000).

Impaired autophagy has been detected in a large number of lysosomal storage diseases, including CLN2, CLN3, CLN6 and CLN10 disease (Cao et al., 2006; Koike et al., 2005; Lieberman et al., 2012; Micsenyi et al., 2013; Thelen et al., 2012). In most cases, the autophagic flux is reduced leading to secondary accumulation of autophagy substrates such as polyubiquitinated proteins, p62 protein/sequestosome 1 (SQSTM1), and dysfunctional mitochondria (Bjorkoy et al., 2005).

1.6 Lysosomal storage disorders

Lysosomal storage diseases (LSDs) are a group of recessively inherited metabolic disorders with an overall incidence of 1:8000 births. They result from mutations in genes encoding for proteins crucial for lysosomal biogenesis and function (Schultz et al., 2011). To date more than 50 different LSDs are known, which are caused by deficiencies of single (e. g. CLN1 disease) or multiple lysosomal hydrolases (e. g. multiple sulfates deficiency (MSD), mucopolidoses type II and III) and by mutations in lysosomal membrane proteins (e. g. CLN3 disease and Salla disease, Futerman and van Meer, 2004). The deficiency of lysosomal hydrolases results in the accumulation of undegraded material in lysosomes. Defects in lysosomal membrane proteins result in accumulation of monomeric compounds not being exported from the lysosomes or impaired acidification (Ruivo et al., 2009). The accumulation of undegraded macromolecules and monomers in lysosomes can inhibit lysosomal enzymes and transporters that are not genetically deficient resulting in secondary substrate

accumulation (Walkley and Vanier, 2009). Massive lysosomal storage prevents lysosomal functions such as nutrition delivery through the endolysosomal system, leading to a state of cellular starvation (Schulze and Sandhoff, 2011). In addition, lysosomal dysfunction leads to secondary consequences like altered calcium homeostasis, changed signal transduction, oxidative stress, inflammation, altered lipid biosynthesis and trafficking, induction of autophagy, endoplasmic reticulum stress and autoimmune responses (Ballabio and Gieselmann, 2009).

LSDs are characterized by their clinical variability with respect to the onset of the disease (congenital, infantile, late-infantile, juvenile, and adult forms), the severity of clinical features, the affected cell types/tissues and the life span. Variability amongst different LSDs depends on the protein function affected by specific mutations, the biochemistry of the stored material and cell types where storage occurs (Platt et al., 2012). Most of the LSDs involve dysfunction of the central nervous system (CNS) with neurodegeneration, progressive mental decline and motor disabilities (Schultz et al., 2011). One group of childhood-onset lysosomal storage disorders, which are characterized by the storage of autofluorescent lipopigments, the selective loss and damage of photoreceptors and neurons in multiple brain regions, and neuroinflammation was categorized into the group of neuronal ceroid lipofuscinoses (Kollmann et al., 2013). For a number of LSDs enzyme replacement therapies exist (Beck, 2010). Other therapies like hematopoietic stem cell therapy, substrate deprivation therapy, gene therapy and chaperone therapy are currently being tested in clinical trials (Platt and Lachmann, 2009).

1.7 The neuronal ceroid lipofuscinoses (NCLs)

The NCLs are a group of autosomal recessively inherited neurodegenerative LSDs and represent the most common cause for neurodegeneration in childhood (Haltia, 2003; Jalanko and Braulke, 2009). The overall incidence is approximately 1:100.000 live births (Jalanko and Braulke, 2009), with a higher frequency of 1:30.000 live births in Germany (Kohlschütter, 2005) and 1:12.500 live births in the United States (Muzaffar and Pearce, 2008). The NCLs are caused by single gene defects and share typical clinical features with variable onset including progressive degeneration of the central nervous system leading to retinopathy and blindness, ataxia, speech failure, epilepsy,

seizures, mental retardation, paralysis, and premature death (Mole et al., 2005; Santavuori et al., 2001).

Biochemically a characteristic lysosomal autofluorescent storage material, called ceroid lipofuscin, accumulates in cells of the brain and other tissues of NCL patients (Anderson et al., 2013). Two thirds of the storage material are composed of proteins, mainly subunit c of mitochondrial ATP synthase, with the remainder consisting of carbohydrates, phospholipids, glycosphingolipids, the anionic lipid bi(mono-acylglycero)phosphate (BMP), dolichol and metals, mainly iron (Jabs et al., 2008; Palmer et al., 1988). In CLN1 disease, saposins A and D accumulate in the protein fraction of the storage material (Tyynelä et al., 1993). Altered levels of M6P-modified lysosomal enzymes were detected in brain samples of CLN2 and CLN3 patients (Sleat et al., 1998).

1.8 Classification of NCLs

A new nomenclature has been proposed to categorize the thirteen genetically different NCL variants on the basis of the underlying gene defect into CLN1, 2, 3, 4, 5, 6, 7, 8, 10, 11, 12, 13, and 14 disease (Kollmann et al., 2013; Kousi et al., 2012). In addition, the impact of the gene defect on the course of the disease and the clinical presentation is added following the *CLN* gene defect and classified into congenital, infantile, late infantile, juvenile and adult forms (Mole SE, 2011). Different mutations in the same gene can lead to a variety of phenotypes. An example is CLN10 disease where both congenital and juvenile variants exist. Most likely it is caused by different residual enzyme activities of mutant cathepsin D (Siintola et al., 2006b; Steinfeld et al., 2006).

To date, nearly 400 mutations in thirteen genes have been identified in NCL patients (Table 1.1; NCL mutation data base: <http://www.ucl.ac.uk/ncl/mutation.shtml>). The genes encode for soluble lysosomal enzymes (*CLN1*/ Palmitoyl protein thioesterase 1, *CLN2*/ Tripeptidylpeptidase 1, *CLN5*/ CLN5, *CLN10*/ Cathepsin D, and *CLN13*/ Cathepsin F), lysosomal membrane proteins (*CLN3*/ CLN3 und *MFSD8*/ CLN7), and ER membrane proteins (*CLN6*/ CLN6 und *CLN8*/ CLN8). In addition, defects in new genes encoding the secretory protein progranulin (*CLN11*) and the cytosolic proteins cysteine-string protein α (*CSP α* / *CLN4*) and potassium channel tetramerization domain-containing protein (*KTCD7*/ *CLN14*) were identified recently (Table 1.1, Noskova et

al., 2011; Smith et al., 2012; Staropoli et al., 2012). Additionally, mutations in the *CLCN7* gene encoding for the lysosomal chloride channel *CIC7* also lead to a disease characterized by osteopetrosis and storage of subunit C of the mitochondrial ATP synthase (Jentsch, 2008).

To date, no curative treatment for any of the NCLs exists (Hobert and Dawson, 2006). Hence, long-term palliative treatment is of great importance in order to enable these patients the best possible life quality (Kohlschütter and Schulz, 2009). Therapies for NCLs, such as enzyme replacement and immune therapy, are currently at preclinical stages and under phase 1 trials. A better understanding of the pathogenesis of NCL in mouse and human models will be needed to develop successful therapeutic strategies (Kohan et al., 2011).

Table 1.1: Neuronal ceroid lipofuscinoses and underlying gene defects

<i>Disease</i>	<i>Phenotypes</i>	<i>Protein</i>	<i>Protein structure and localisation</i>	<i>Reference</i>
CLN1	infantile, late infantile, juvenile, adult	PPT1, Palmitoyl-protein thioesterase 1	soluble lysosomal matrix protein	(Vesa et al., 1995)
CLN2	Infantile, juvenile, classic late infantile	TPP1 Tripeptidyl peptidase 1	soluble lysosomal matrix protein	(Sleat et al., 1997)
CLN3	juvenile, protracted infantile	CLN3	lysosomal membrane protein	(Lerner et al., 1995)
CLN4	adult (autosomal-dominant)	CSP- α Cysteine-string protein alpha	cytosolic protein associated to vesicular membranes	(Noskova et al., 2011)
CLN5	late infantile variant, juvenile, adult, infantile	CLN5 soluble protein	soluble lysosomal matrix protein	(Savukoski et al., 1998)
CLN6	late infantile variant, adult	CLN6 transmembrane protein	ER-localized membrane protein	(Gao et al., 2002); (Wheeler et al., 2002)
CLN7	late infantile variant, juvenile	CLN7 transmembrane protein	lysosomal membrane protein	(Siintola et al., 2007)
CLN8	late infantile variant, EPMR	CLN8 transmembrane protein	ER/ERGIC-transmembrane protein	(Ranta et al., 1999)
CLN9	juvenile variant	not known	not known	(Schulz et al., 2004)
CLN10	congenital, juvenile	Cathepsin D	soluble lysosomal matrix protein	(Siintola et al., 2006b; Steinfeld et al., 2006)
CLN11	adult (autosomal recessive)	Progranulin	secreted protein	(Smith et al., 2012)
CLN12	juvenile	ATP13A2	lysosomal membrane protein	(Bras et al., 2012)
CLN13	adult (autosomal recessive)	Cathepsin F	soluble lysosomal matrix protein	(Smith et al., 2013)
CLN14	infantile-onset NCL subtype	KCTD7, potassium channel tetramerization domain-containing protein	cytosolic protein	(Staropoli et al., 2012)

1.9 Molecular basis of CLN7 disease

Since the CLN7 protein is in the focus of the present thesis, CLN7 disease, the respective gene and its gene product are described in more detail. CLN7 disease belongs to the group of variant late infantile NCLs (vLINCL), which can also be caused by defects in the *CLN5*, *CLN6* and *CLN8* genes (Kousi et al., 2009; Perez-Poyato et al., 2012). Like other NCL diseases, CLN7 disease is a fatal neurological disease with manifestations mainly restricted to the central nervous system. CLN7 patients have an age of onset ranging from 1.5 to 5 years (Kousi et al., 2009). Initial symptoms are epileptic seizures, visual impairment, worsening mental and motor disabilities (Siintola et al., 2007). In the course of the disease cognitive disabilities develop, and myoclonus and personality changes occur. The life span is severely reduced with a median life expectancy of 11.5 years (Kousi et al., 2009). Clinical manifestations in CLN7 patients with late infantile variant phenotype are generally uniform (Kousi et al., 2012). An exception is a patient with CLN7 disease, juvenile phenotype, having a protracted disease course. This patient was diagnosed with visual failure at the age of 11 and is still alive at the age of 43 (Kousi et al., 2009). Genetic analyses revealed a c.468_469delinsCC mutation in this patient which results in a missense mutation in the CLN7 protein (p.Ala157Pro).

Brain atrophy, a progressive reduction of neurons in the cerebral and cerebellar cortex, degeneration of the retina, activation of microglial cells and astrocytes in the cerebellum, hippocampus and cortex, generalized accumulation of autofluorescent ceroid lipopigments in the brain and peripheral tissues are major hallmarks of CLN7 disease (Anderson et al., 2013; Elleder, 2011; Sharifi et al., 2010). The ultrastructure of the cerebral neuronal storage material is a mixture of rectilinear complex and fingerprint profiles (Elleder, 2011). On magnetic resonance imaging (MRI), patients showed atrophy of the cerebellum and more mildly of cerebrum, and in most cases, also brainstem involvement (Topcu et al., 2004).

To date, 33 different mutations have been identified in patients with CLN7 disease (Aiello et al., 2009; Aldahmesh et al., 2009; Kousi et al., 2012; Kousi et al., 2009; Siintola et al., 2007; Stogmann et al., 2009). Due to the similar clinical course of CLN7 disease in patients with different defects in the *MFSD8/CLN7* gene all mutations with one exception (p.Ala157Pro) are thought to result in a complete loss of CLN7 function.

The most common mutation in CLN7 patients is c.881C>A, which results in the missense mutation p.Thr294Lys in CLN7 (Kousi et al., 2012). Pathogenic mutations in genes encoding lysosomal membrane proteins can cause decreased stability and/or activity of the mutant protein, misfolding, ER retention and associated degradation, or intracellular missorting (Futerman and van Meer, 2004). None of the expressed pathogenic mutations impaired lysosomal localization and trafficking of mutant CLN7 (Kousi et al., 2009; Sharifi et al., 2010; Siintola et al., 2007; Steenhuis et al., 2012). Steenhuis and co-workers could demonstrate that selected mutations in luminal loops of CLN7 lead to an altered stability resulting in increased proteolytic cleavage in lysosomes (Steenhuis et al., 2012).

1.10 Organization of the *MFSD8/CLN7* gene and *MFSD8/CLN7* expression

The human *MFSD8/CLN7* gene is located on chromosome 4q28.1-q28.32 and contains 13 exons. The promotor of the *MFSD8/CLN7* gene contains a Coordinated Lysosomal Expression and Regulation (CLEAR) element, which has been shown to exist in the promoters of other genes important for lysosomal biogenesis, function and autophagy (Sardiello et al., 2009; Settembre et al., 2011). CLEAR elements represent binding sites for the transcription factor EB (TFEB), which regulates the transcription of genes involved in the biogenesis of lysosomes. The human *MFSD8/CLN7* mRNA is around 5 kb long and ubiquitously expressed at very low levels with higher amounts in heart, liver, skeletal muscle and pancreas (Siintola et al., 2007). Differential expression in brain region was observed with highest *MFSD8/CLN7* mRNA concentrations found in the cerebellum and the cerebral cortex in humans and in the granular layer of the cerebellum, in pyramidal cells of the hippocampus and the cerebral cortex in rats (Kousi et al., 2009; Sharifi et al., 2010; Siintola et al., 2007). Analysis of *Mfsd8-lacZ* gene reporter mice showed high expression of *Cln7* in neurons of the cerebral cortex and hippocampus with minor expression in the cerebellar cortex in adult animals (Damme et al., 2014). The amount of *Mfsd8/Cln7* mRNA was reported to be 12- and 6.4-fold more abundant in cultured rat neurons than in astrocytes and microglial cells, respectively (Sharifi et al., 2010).

1.11 Membrane topology and localisation of the CLN7 protein

CLN7 is an ubiquitously expressed integral lysosomal membrane glycoprotein composed of 518 amino acids with a predicted molecular mass of the non-*N*-glycosylated polypeptide of 58 kDa (Siintola et al., 2007). Based on computer algorithm predictions, CLN7 contains 12 transmembrane domains and a large luminal loop L9 between transmembrane domains 9 and 10 (Figure 1.1, Siintola et al., 2007). Consistent with this topology model the large luminal loop L9 contains two used *N*-glycosylation sites in positions N371 and N376 (Steenhuis et al., 2010). Furthermore CLN7 contains sites in loop L9 which are cleaved by lysosomal cysteine proteases (Steenhuis et al., 2012). Fluorescence protease protection assays revealed that CLN7 contains an even number of transmembrane domains with the N- and C-terminal domains projected towards the cytosol (Steenhuis et al., 2010). Prior to the identification of patients with defects in the *MFSD8/CLN7* gene, CLN7 was detected by proteomic analyses combined with identification by mass spectrometry in lysosomal membranes (Bagshaw et al., 2005; Schröder et al., 2007). In agreement, CLN7 has been shown to co-localize with lysosomal marker proteins in non-transfected neuronal cells and in transfected non-neuronal cells (Sharifi et al., 2010; Siintola et al., 2007; Steenhuis et al., 2010).

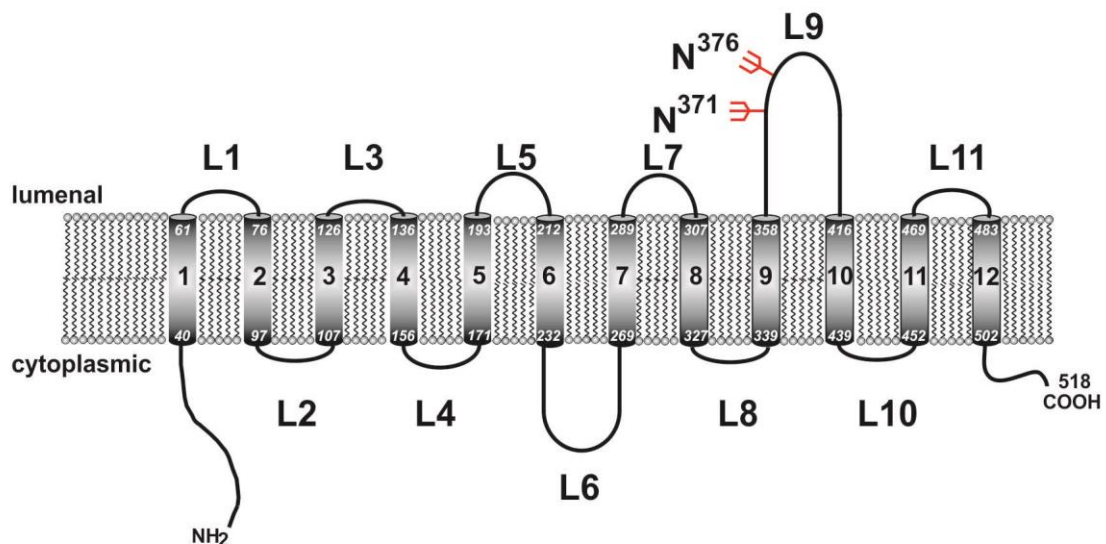


Figure 1.1: Schematic representation of the membrane topology of the CLN7 protein. The transmembrane domains are indicated and numbered 1-12. Loop structures are numbered L1-L11 and the positions of used *N*-glycosylation sites in loop L9 are shown.

1.11.1 Lysosomal targeting of CLN7

An N-terminal dileucine-based lysosomal targeting signal was identified in CLN7 by two independent groups (Sharifi et al., 2010; Steenhuis et al., 2010). Steenhuis and co-workers showed that the transport of CLN7 follows the indirect route via the plasma membrane. CLN7 is delivered to lysosomes along the predominantly used indirect pathway via the plasma membrane and clathrin-mediated endocytosis mediated by an N-terminal dileucine-based motif (Steenhuis et al., 2010).

1.11.2 Function of CLN7

The function of CLN7 is unknown. Sequence homologies of CLN7 with the major facilitator superfamily (MFS) of transporters suggest that it represents a lysosomal transporter. MFS transporters typically consist of 400-600 amino acids and represent single-polypeptide secondary transporters that transport small solutes across membranes, such as carbohydrates and derivatives, drugs, metabolites, amino acids, nucleosides, and vitamins but not macromolecules along an ion gradient (Pao et al., 1998; Sharifi et al., 2010). However, the specific substrate (s) and mode of transport (sym-, uni- or antiport) of CLN7 are unknown (Siintola et al., 2007). It is believed that the accumulation of a monomeric compound (s) which cannot be exported from the lysosomal lumen into the cytosol by mutant CLN7 leads to a LSD.

2. Aim of the study

CLN7 disease is a childhood-onset neurodegenerative lysosomal storage disease caused by the deficiency of the multispanning lysosomal membrane glycoprotein CLN7. Based on its localization, its sequence homologies with the major facilitator superfamily of transporters and the lysosomal disease phenotype in CLN7 patients, CLN7 is predicted to function as a lysosomal transporter. The mode (uni-, sym-, antiport) and directionality (im-/export) of transport and the substrate specificity of CLN7 are unknown and to date only a recently generated mouse model for CLN7 disease exists. The aim of the thesis was to generate a cell-based model for CLN7 disease and to analyze biochemical and cell biological alterations caused by the loss of CLN7 using cells depleted of CLN7. Special emphasis of the project was to analyze biogenesis and functions of lysosomes and the impact of CLN7 depletion on endocytic pathways and macroautophagy.

3. Materials and Methods

3.1 Materials

3.1.1 Equipment and consumables

Table 3.1 Equipment

Equipment	Model	Company
Autoclave	5050ELC and 3850 EL	Systec, Wetttenberg
Balance	AC100	Mettler Toledo, Gießen
	BP2100S OLX-3000	Sartorius, Göttingen Omnilab-Laboratory Center
Block heater	Rotilabo H250	Roth, Karlsruhe
	MHR-23	HLC, Bovenden
Centrifuge	Centrifuges 5415R, 5417R and 5424R and 5804R	Eppendorf, Hamburg
Centrifuge	Minifuge RF	Heraeus Holding GmbH, Hanau
Centrifuge	MC6 Centrifuge	Sarstedt, Nümbrecht
Centrifuge	Ultracentrifuge Discovery M120	Kendro laboratory products, Hanau
Confocal microscope	Leica DM IRE2	Leica, Wetzlar
Cryogenic freezing unit	Cryo 1°C Freezing Container	Thermo Fisher Scientific, Waltham, USA
Electrophoresis chamber	Agagel Midi Wide	Biometra, Göttingen
	SE600	Hofer, Holliston, USA
Imager	Chemi Doc XRS	Bio-Rad, Munich
Incubator (CO ₂)	Incu Safe Mco-17AIC	Ewald Innovationstechnik
Incubator	Innova CO-170P-230	New Brunswick Scientific
Incubator	Heraeus B5060EC-C02	Heraeus Holding
Inverted microscope	Axiovert 25	Carl Zeiss, Oberkochen
Liquid Nitrogen container	Airpege 55	Air Liquide Germany GmbH, Düsseldorf
Magnetic stirrer	MSH-basic	IKA-Werke, Staufen
Microwave	Whirlpool Promicro 825	Bauknecht, Stuttgart
pH meter	MP220	Mettler Toledo, Gießen
Photometer	Biophotometer	Eppendorf, Hamburg
Pipettes	Research and Reference	Eppendorf, Hamburg
Pipette controller	Pipetus	Hirschmann, Eberstadt
Real-time Cycler	Real-Time MX300P	Stratagene Europe, Amsterdam

Shaker	Rocky	Fröbel Labortechnik, Lindau
Shaking incubator	Innova 4230 and 4080	New Brunswick Scientific
Steril bench	Herasafe	Thermo Fisher Scientific, Waltham, USA
Steril bench	Gelaire	Flow Laboratories, Meckenheim
Thermocycler	T Personal Mastercycler Gradient	Biometra, Göttingen Eppendorf, Hamburg
TIRF microscope	Olympus IX81	Olympus, Hamburg
Transfer chamber	TE62 & TE22	Hofer, Holliston, USA
UV transilluminator	Darkroom Evo III	Raytest, Straubenhardt
Vacuum pump	PC 2004 VARIO	Vacuubrand, Wertheim
Vortex	Genie [®] 2	Scientific Industries, New York
Water bath	C 10	Schuett-Biotec, Göttingen

Table 3.2 Consumables

Consumable	Company
Aluminium foil	Roth, Karlsruhe
Centrifuge tubes 15 ml, 50 ml	Greiner Bio-One, Frickenhausen
Cling film	Ecopla, Le Touvet
Coverslips	Glaswarenfabrik Karl Hecht
Cryovials	Nunc, Langensfeldbold
Cuvetes	Sarstedt, Nümbrecht
Disposable gloves (latex, nitril)	Paul Hartmann, Heidenheim
Disposable material for cell culture	Becton Dickinson, Heidelberg Sarstedt, Nümbrecht Nunc, Langensfeldbold
Disposable scraper	Sarstedt, Nümbrecht
Gel electrophoresis combs	Hofer, Holliston, USA
Gel glass plates	GE Healthcare Europe, Freiburg
Lens paper MN 10 B	Carl Zeiss, Oberkochen
Microslides (glass slides)	Glaswarenfabrik Karl Hecht, Sondheim
Needles	Becton Dickinson, Heidelberg
Nitrocellulose membrane	Whatman, Dassel
Parafilm	Pechiney Plastic Packaging, Chicago
Pipette tips	Sarstedt, Nümbrecht

	Eppendorf, Hamburg
Pipette tips with filter	Sarstedt, Nümbrecht
PVDF membranes	B. Braun, Melsungen
Sterile syringe filter (0.22 µm and 0.45 µm)	VWR, Darmstadt
Stripes/lids for Real-time PCR	Life Technologies, Carlsbad, CA
Syringes	B. Braun, Melsungen BD, Heidelberg
UV-cuvettes	Eppendorf, Hamburg
Whatman paper	GE Healthcare Europe, Freiburg

3.1.2 Chemicals and Kits

Table 3.3 Chemicals

Chemical	Company
Acetone	Merck KGaA, Darmstadt
Acrylamide/Bisacrylamide	Roth, Karlsruhe
Agar	Roth, Karlsruhe
Agarose	Biozym Scientific, Hessisch Oldendorf
Albumin Standards	Thermo Scientific, Waltham, USA
Ammonium peroxide sulphate (APS)	Roth, Karlsruhe
Ampicillin	Serva, Heidelberg
Bovine serum albumin (BSA)	Serva, Heidelberg
Carbenicilin	Roth, Karlsruhe
4',6-Diamino-2-phenylindol (DAPI)	Roth, Karlsruhe
Diethylpyrocarbonate (DEPC)	Roth, Karlsruhe
Dimethylsulfoxide (DMSO)	Roth, Karlsruhe
dNTPs (dATP, dCTP, dTTP, dGTP)	Fermentas, St. Leon-Rot
Ethidium bromide	Sigma, Deisenhofen
Ethylenediamin tetraacetic acid (EDTA)	Roth, Karlsruhe
Ethanol, absolute (≥ 99,9 %)	Mallinckrodt Baker, Griesheim
Ethanol 99%, denatured with 1% methyl ethyl ketone	Walter-CMP, Kiel
Fetal Calf Serum (FCS)	PAA Laboratories, Pasching
GlutaMAX -I (100x)	Invitrogen, Darmstadt

Glycerin	Merck KGaA, Darmstadt
Glycin	Roth, Karlsruhe
HEPES	Roth, Karlsruhe
Hydrogen peroxide (H ₂ O ₂), 30%	Merck KGaA, Darmstadt
Immersion oil 518 C	Zeiss, Oberkochen
Isopropanol	Roth, Karlsruhe
Kanamycin sulphate	Roth, Karlsruhe
Methanol	Mallinckrodt Baker, Griesheim
Milk powder (blotting grade)	Roth, Karlsruhe
Mowiol 4-88	Merck KGaA, Darmstadt
NNN'N'-Tetramethylethan-1,2-diamin (TEMED)	Sigma, Deisenhofen
Paraformaldehyde (PFA)	Sigma, Deisenhofen
Protease inhibitor cocktail	Sigma, Deisenhofen
Protein Standard (2mg/ml BSA)	Fisher Scientific, Schwerte
RNase A	Roche Diagnostics, Mannheim
Roti [®] -Quant protein assay	Roth, Karlsruhe
RNase away solution	Roche Diagnostics, Mannheim
Sodium deoxycholate	Merck KGaA, Darmstadt
Sodium dodecyl sulfate (SDS)	Sigma, Deisenhofen
Sodium hydroxide (NaOH)	Roth, Karlsruhe
Tricine	Roth, Karlsruhe
TRI [®] reagent	Sigma, Deisenhofen
Trisma Base	Sigma, Deisenhofen
Trypsin/EDTA 0.05%	Invitrogen, Darmstadt
Tryptone/Peptone	Roth, Karlsruhe
Tris-(hydroxymethyl)-aminomethane	Sigma, Deisenhofen
Triton X-100	Sigma, Deisenhofen
Tween 20	Sigma, Deisenhofen
Yeast extract	Roth, Karlsruhe

Table 3.4: Other reagents

Reagent	Company
Dulbecco's Modified Eagle Medium (DMEM)	Invitrogen, Darmstadt
jetPEI DNA Transfection reagent	Polyplus-Transfection, Illkirch Cedex
Lipofectamine 2000 reagent	Invitrogen, Darmstadt
OptiMEM [®] I Reduced Serum Medium with L-Glutamine, HEPES, without Phenolred	Invitrogen, Darmstadt
EBSS medium	Invitrogen, Darmstadt

Table 3.5: Kits

Kit	Company
GeneJET [™] Gel Extraction Kit	Fermentas, St. Leon-Rot
GeneJET [™] PCR Purification Kit	Fermentas, St. Leon-Rot
GeneJET [™] Plasmid Mini Kit	Fermentas, St. Leon-Rot
GeneJET [™] RNA Purification Kit	Fermentas, St. Leon-Rot
Plasmid Midi Kit	Qiagen, Hilden

3.1.3 Buffers and Solutions

Anode buffer:

0.2 M Tris/HCl (pH 8.9)

Blocking solution:

5 % Milk powder in TBST

Cathode buffer:

0.3 M Tris-base

0.3 M Tricine

0.3 % SDS

CaCl₂ filtered solution:

60 mM CaCl₂ x 2H₂O

15 % Glycerol

10 mM PIPES

2 M NaOH (for pH 7.0)

ECL solution 1:

4.5 ml dd H₂O

500 µl 1 M Tris/HCl (pH 8.5)

100 µl 250 mM Luminol/DMSO

44 µl 90 mM p-cumaric acid/DMSO

ECL solution 2:

4.5 ml	dd H ₂ O
500 µl	1 M Tris/HCl (pH 8.5)
10 µl	30 % H ₂ O ₂

Lysis buffer:

0.5 %	TritonX-100
1X	inhibitor cocktail in PBS

10X PBS:

1.37 M	NaCl
27 mM	KCl
100 mM	Na ₂ HPO ₄ xH ₂ O
17.6 mM	KH ₂ PO ₄ (pH 7.4)

10X TBS:

1.37 M	NaCl
27 mM	KCl
250 mM	Tris/HCl (pH 7.4)

TBST:

0.05 %	Tween 20 in TBS
--------	-----------------

Transfer buffer:

25 mM	Tris/HCl (pH 7.4)
192 mM	Glycine
20 %	Methanol

50X TAE buffer:

2 M	Tris/HCl (pH 8.3)
1 M	Acetic acid
100 mM	EDTA

3.1.4 Enzymes**Table 3.6: Enzymes**

Enzyme	Units	Company
FastAP™ alkaline phosphatase	1 U/µl	Fermentas, St. Leon-Rot -
FastDigest® <i>Hind</i> III	1 FDU/µl	Fermentas, St. Leon-Rot
FastDigest® <i>Bgl</i> II	1 FDU/µl	Fermentas, St. Leon-Rot
FastDigest® <i>Eco</i> RI	1 FDU/µl	Fermentas, St. Leon-Rot
FastDigest® <i>Dpn</i> I	1 FDU/µl	Fermentas, St. Leon-Rot

<i>Maxima</i> TM qPCR master mix		Fermentas, St. Leon-Rot
Multiscribe reverse transcriptase	50U/ μ l	Life Technologies, Carlsbad, CA
<i>Phusion</i> [®] polymerase	2 U/ μ l	New England Biolabs, Ipswich, MA
RNase A		Roche Diagnostics, Mannheim
T4 DNA ligase	400 U/ μ l	New England Biolabs, Ipswich, MA
<i>Taq</i> DNA polymerase		Invitrogen, Darmstadt
T4 polynucleotide kinase		New England Biolabs, Ipswich, MA

3.1.5 Protein and DNA standards

Table 3.7: Molecular weight standards

Molecular weight standard	Company
DNA standard, 1 kb ladder	Invitrogen, Darmstadt
DNA standard, 100 bp ladder	Invitrogen, Darmstadt
DNA standard, <i>FastRuler</i> TM <i>Middle Range</i>	Fermentas, St. Leon-Rot
<i>Full-Range Rainbow</i> TM Protein-Standard	GE Healthcare Europe, Freiburg
<i>Page Ruler</i> TM Protein-Standard	Fermentas, St. Leon-Rot

3.1.6 Mammalian cell lines

Table 3.8 Cell lines

Cell line	Company
HeLa (Human cervical carcinoma cells)	ATCC, Rockville (USA)
HEK293 (human embryonic kidney cells)	ATCC, Rockville (USA)

ATCC - American Type Culture Collection

3.1.7 Media and solutions for cell culture

Dulbecco's modified Eagle's medium (DMEM), Opti-MEM[®], Trypsin/EDTA, Penicillin/Streptomycin (100 IU/ml Pen and 50 mg/ml Strep), LipofectamineTM 2000,

GlutaMAX™ (100 x) and phosphate-buffered saline (PBS) for cell culture (calcium and magnesium free) were obtained from Invitrogen. Fetal calf serum (FCS) was from PAA. HeLa and HEK293 cells were cultured in DMEM containing 10% FCS, 1x Glutamax, and antibiotics (penicillin /streptomycin).

3.1.7.1 Bacterial strains and bacteria medium

Table 3.9 Bacteria

Strain	Company
<i>Escherichia coli</i> TOP10	Invitrogen, Darmstadt

Table 3.10 Bacterial growth medium

Medium	Composition
LB-medium	10 g Tryptone 5 g Yeast extract 5 g NaCl in 1 liter dd H ₂ O

LB-agar plates (Ø 10 cm) were prepared by adding 20 g of agar (final concentration: 2 % w/v) to 1 l of LB medium. After autoclaving, LB-agar suspensions were cooled to 55 °C and antibiotics were added under sterile conditions (ampicillin/carbenicillin: 100 µg/ml; kanamycin: 50 µg/ml). LB plates were allowed to harden at room temperature and stored at 4°C in the dark.

3.1.8 Antibodies

Primary antibodies used for immunofluorescence (IF) and western blotting (WB) are summarized in table 3.11. The dilutions of the antibodies are indicated.

Table 3.11: Primary Antibodies

Primary antibody	Host species	Dilution	Producer
anti-LAMP-1, clone H4A3	Mouse	WB: 1:500 IF: 1:150	Developmental Studies Hybridoma Bank, Iowa City, Iowa
anti-LAMP-2, clone H4B4	Mouse	WB: 1:500 IF: 1:150	Developmental Studies Hybridoma Bank, Iowa City, Iowa
anti-EEA-1	Mouse	IF: 1:100	BD Biosciences, Heidelberg

anti-LC3-II	Rabbit	IF:1:50	Dr. Stephan Storch, UKE Hamburg
Myc, clone 9B11	Mouse	WB: 1:1,000 IF: 1:100	Cell Signalling , Danvers, MA
anti-Beclin 1, sc11427	Rabbit	WB: 1:500	Santa Cruz (Heidelberg)
anti-Cathepsin D, #2284	Rabbit	WB: 1:1,000	Prof. Hasilik, Marburg
anti-Cathepsin Z, AF934	Goat	WB: 1:1,000	R&D Systems, Wiesbaden- Nordenstadt
anti-GFP	Mouse	WB: 1:1,000	Roche Diagnostics, Mannheim
anti-LC3, clone 2G6	Mouse	WB:1:1,000	Nanotools Klon, Teningen
anti-Myc, clone 9B11	Mouse	WB:1:1,000	Cell Signalling Danvers, MA
anti- β -Tubulin, clone E7	Mouse	WB: 1:500	Developmental Studies Hybridoma Bank, Iowa City, Iowa

Table 3.12 Secondary antibodies and fluorophore-coupled transferrin used for immunofluorescence

Secondary antibody	Dilution	Producer
Goat anti-mouse Alexa Fluor [®] 546	1:1.000	Invitrogen, Darmstadt
Goat anti-mouse Alexa Fluor [®] 488	1:1.000	Invitrogen, Darmstadt
Goat anti-rabbit Alexa Fluor [®] 546	1:1.000	Invitrogen, Darmstadt
Goat anti-rabbit Alexa Fluor [®] 488	1:1.000	Invitrogen, Darmstadt
Transferrin Alexa Fluor [®] 546	100 μ g/ml	Invitrogen, Darmstadt

Table 3.13 Secondary antibodies used for Western blots

Secondary antibody	Dilution	Producer
Goat anti-mouse IgG HRP	1:2.000	Dianova, Hamburg
Goat anti-rabbit IgG HRP	1:5.000	Dianova, Hamburg

3.1.9 siRNA

Lyophilized duplex siRNAs (stealth RNAi, invitrogen; Table 3.14) were dissolved in 1000 μ l RNase free ddH₂O to yield a final concentration of 20 μ M. Resuspension to 20 μ M will reconstitute the buffer to 10 mM Tris-Cl, pH 8.0, 20 mM NaCl, 1 mM EDTA. Aliquots were stored at -20°C. A universal siRNA with low amount of GC was used as

a negative control. Three different 25-mer siRNAs annealing to different coding sequences of the *CLN7* mRNA were purchased and tested for their capability to downregulate endogenous *CLN7* mRNA. In preliminary tests stealth siRNA HSS137999 (Table 3.14), which anneals to base pairs 256-280 of the human *CLN7* mRNA (NM_152778), was found to downregulate *CLN7* in HeLa cell lines most effectively .

Table 3.14: Sequences of siRNA

siRNA	Sequenz 5'→3'
<i>CLN7</i> siRNA HSS137999, sense	GGCCAAAUGGUAGCUUCACCUAUAU
<i>CLN7</i> siRNA HSS137999, antisense	AUAUAGGUGAAGCUACCAUUUGGCC

3.1.10 Vectors and primers

All primers used for sequencing, cloning and site-directed mutagenesis were purchased from MWG Biotech (Munich).

Table 3.15: Vectors

Plasmid	Selection marker	Company/reference
pSuper.GFP/neo	Ampicillin	OligoEngine, Seattle, Washington
pcDNA3.1D/V5-His-TOPO-GFP-LC3	Ampicillin	Dr. Stephan Storch, UKE, Hamburg
pcDNA3.1D/V5-His-TOPO-Myc-CLN7	Ampicillin	Steenhuis et al., 2010
mRFP-C1-GFP-LC3	Kanamycin	(Kimura et al., 2007)

Primers for the generation of pSuper constructs were obtained from MWG Biotech. The indicated oligonucleotides were used for the cloning of pSuper.GFP.sh21, pSuper.GFP.sh19, pSuper.GFP.Scr and pSuper GFP-LC3 (Table 3.16 and 3.17).

Table 3.16: Oligonucleotide primers for cloning pSuper.GFP/neo shRNAs

Inserts	5'→3' sequence
CLN7-Scr21-sense	GATCCCCGTTCCATAGGACGCATTCACACTCGAGTGTGAATG CGTCCTATGGAACCTTTTTA

CLN7-Scr21-antisense	AGCTTAAAAAAGCCAAATGGTAGCTTCACCTACTCGAGTAG G TGAAGCTACCATTTGGCGGG
CLN7-sh21-sense	GATCCCCGCCAAATGGTAGCTTCACCTACTCGAGTAGGTG AA GCTACCATTTGGCTTTTTTA
CLN7-sh21-antisense	AGCTTAAAAAAGCCAAATGGTAGCTTCACCTACTCGAGTAG GTG AAGCTACCATTTGGCGGG
CLN7-sh19-sense	GATCCCCCAAATGGTAGCTTCACCTATTCAAGAGATAGGTG AAG CTACCATTTGTTTTTA
CLN7-sh19-antisense	AGCTTAAAAAACAAATGGTAGCTTCACCTATCTCTTGAATAG GT GAAGCTACCATTTGGGG

Table 3.17: Oligonucleotide primers for the generation of the construct pSuper RFP and pSuper GFP-LC3

pSuper-construct	5' → 3' sequence
pSuper-RFP	<i>s</i> : TTA CCG GTC GCC ACC ATGGTGAGCAAGGGCGAGGAGG <i>a</i> : GTG TCAGAA GAA TCA TTA CTT GTA CAG CTC GTC CAT GCC
pSuper-GFP-LC3	<i>s</i> : GGA CTC AGA TCA GCT CCC TCA GAC CGG CCT TTC AAG C <i>a</i> : GTG TCAGAA GAA TCA TCA GAA GCC GAA GGT TTC CTG GG

(s = sense, a=antisense)

Taqman assays for quantitative real-time PCR experiments were obtained from Invitrogen.

Table 3.18: RT PCR assays

Gene	Assay (Sonde + Primer)
<i>CLN 3</i>	Hs00164002_m1
<i>CLN 6</i>	Hs00608557_m1
<i>CLN 7</i>	Hs00380724_m1
<i>CLN 10 (Cathepsin D)</i>	Hs00157205_m1
<i>LAMP-1</i>	Hs00174766_m1
<i>LAMP-2</i>	Hs00174474_m1
<i>LAP (ACP2)</i>	Hs00155636_m1
<i>TRAP (ACP5)</i>	Hs00356261_m1
<i>β-Actin</i>	Hs99999903_m1

3.1.11 Sequencing of DNA samples

Sequencing of DNA samples, which included the PCR reaction in the presence of fluorophore labeled ddNTP, separation of the PCR products and analysis of the chromatograms was performed by Seqlab (Göttingen). The following mixture was prepared for the sequencing reaction:

700	ng	double-stranded plasmid-DNA
20	pmol	primer
x	µl	dd H ₂ O
7	µl	final volume

3.2 Methods

3.2.1 Cell Biology Methods

3.2.1.1 General note

The cultivation of HeLa and HEK293 cells was carried out on a sterile bench. The pipettes and further materials were packed in a sterile way. The bench and further materials used were cleaned with 70% ethanol.

3.2.1.2 Cell culture cultivation and trypsinization

The cell lines were cultivated in 75 cm² cell culture flasks with a CO₂ partial pressure of 5% at 37 °C. Cells were always cultured in pre-warmed complete DMEM medium supplemented with 10 % FCS, Pen/Strep and 1 x GlutaMAXTM-100.

Splitting was carried out twice a week as soon as the cells achieved 70% confluence. The cell culture medium was aspirated and the cells were washed with 5 ml of PBS. Then 1 ml of Trypsin/ EDTA 0.05% was added to the cells for 5 min at 37 °C. The protease activity of trypsin was inhibited by adding 2 ml of fresh cell culture medium and the cell suspension was mixed by pipetting up and down. Cells were seeded in a new flask by using 1 ml of this suspension with 9 ml of fresh complete medium.

3.2.1.3 Cryoconservation and revitalisation of cells

To ensure a permanent stock of different cell lines, cells were frozen in liquid nitrogen. The storage was performed when the cells were actively dividing.

The cells were washed with PBS and trypsinized. Then 5 ml of pre-warmed medium was added. The cell suspension was poured into a 15 ml falcon tube and centrifuged at 1,000 x g for 5 min. The cell pellet was resuspended in 5 ml of freezing medium (DMEM 50% with 40 % FCS and 10 % DMSO). The cells were transferred to 5 cryovials. The cryovials were stored in a Cryo 1 °C Freezing Container filled with isopropanol overnight (ON) at -80 °C and transferred to a liquid nitrogen container the next day.

To revitalize the cells were removed from the liquid nitrogen tank and the cryovials were placed in a 37 °C water bath. Next, the cells were transferred into a 15 ml-falcon tube and 9 ml of culture medium was poured slowly onto them. The cell suspension was centrifuged at 1,000 x g for 5 min and the supernatant was aspirated. The cell pellet was solved in 10 ml of culture medium and the cells were seeded in a new cell culture flask.

3.2.1.4 Transfection of siRNA

HeLa cells grown on 3.5 or 6 cm plates were transfected with silencing RNAs (siRNA) diluted in OptiMEM and Lipofectamine 2000 (LF2000) as described in table 3.19.

Table 3.19: Protocol for the transfection of siRNA

Plate/well	siRNA (pmol)	Opti-MEM [®] (µl)	LF2000 (µl)	Opti-MEM [®] (µl)	Total (µl)	Medium (ml)
6 cm	250	500	10	490	1000	3
3.5 cm	125	200	5	195	400	1.6

3.2.1.5 Transfection of expression- and shRNA vectors

HEK293 and HeLa cells were transfected with expression and shRNA vectors using LF2000 as described in table 3.20.

Table 3.20: Protocol for the transfection of siRNA

Plate/well	cDNA/ shRNA (μg)	Opti-MEM [®] (μl)	LF2000 (μl)	Opti-MEM [®] (μl)	Total (μl)	Medium (ml)
6 cm	5	500	10	490	1000	3.0
3.5 cm	3	200	5	195	400	1.6
24 well	1	50	1	49	100	0.4

Transfection

Before plating HEK293 cells cell culture dishes were incubated with 0.1mg/ ml poly-D-lysine for 30 min at room temperature (RT). Poly-D-lysine was aspirated and the culture dishes were washed twice with PBS (Coating). For immunofluorescence experiments with HeLa cells glass cover slips were coated with gelatin (see chapter 3.2.1.6).

The cells were cultivated on wells until a confluence of 70-80% was achieved. The medium used for the transfection was free of antibiotics to avoid any toxic effect. Mixtures were prepared. Each mixture (see table 3.20) of tube 1 (DNA diluted in Opti-MEM[®]) and tube 2 (LF2000 diluted in Opti-MEM[®]) was incubated for 5 min at room temperature (RT). Next, the contents of tubes 1 and 2 were mixed and incubated for 20 min at RT to ensure the formation of complexes. Simultaneously, the medium was aspirated and exchanged by pre-warmed culture medium lacking antibiotics. Next, the LF2000/cDNA solution was slowly added drop by drop to each well and these were placed back into the 37 °C incubator. 24 hours after the transfection the medium was exchanged by antibiotic-containing culture medium (see 3.1.7). After another 24 hours the second transfection took place and again the medium was exchanged 24 hours afterwards. Cells were analyzed 96 hours after the start of the first transfection.

For co-localization studies using double immunofluorescence cells were co-transfected with 800 ng Myc-CLN7 and 200 ng GFP-LC3 in 24-well plates.

3.2.1.6 Double immunofluorescence microscopy

Coating buffer:	4	%	Gelatine in PBS
Fixation buffer:	4	%	PFA in PBS
Permeabilization buffer:	0.1	% (w/v)	Saponin in PBS (PBS-S)
Blocking buffer:	3	%	BSA in PBS-S
DAPI solution:	0.4	%	DAPI in PBS

Double immunofluorescence microscopy was performed with antibodies against marker proteins of different intracellular compartments to analyze the subcellular localization of CLN7 (Table 3.11). Autoclaved coverslips (diameter: 12 mm) were placed into 24-well plates and incubated with 96% ethanol for 15 min in order to remove traces of fat and dirt. Cover slips were washed twice with PBS and were incubated with coating buffer for 30 min at 37 °C. After two washes with PBS, 50.000 cells were plated onto each cover slip. Transfection of cells was performed at 70% confluency. 72 hours after the start of transfection the cells were washed twice with PBS. Cells were fixed with 2ml 4% PFA in PBS for 15 min at RT, fixation solution was removed and cells were washed twice with PBS. Cover slips were transferred on a strip of parafilm and permeabilized in permeabilization buffer for 10 minutes at RT. Cells were incubated with blocking buffer for 30 min at RT followed by incubation with primary antibodies diluted in blocking buffer for 1 hour. Cells were washed twice with permeabilization buffer followed by incubation with fluorophore-coupled secondary antibodies diluted in blocking buffer at RT in the absence of light for 1 hour. After removal of secondary antibodies cells were washed twice with permeabilization buffer followed by incubation with 4',6-Diamidino-2-phenylindole (DAPI)/PBS for five minutes to stain nuclei. Cells were washed twice with PBS and each cover slip was mounted on a microscope slide using 5 µl Aqua Poly-Mount Medium. After drying overnight, coverslips were sealed with nail polish and stored in the dark.

instructions. To isolate up to 100 µg plasmid DNA a single colony was grown in 5 ml LB containing antibiotics (100 µg/ml carbenicillin or 50 µg/ml kanamycin) for 8 hours. 50 ml LB medium containing antibiotics was inoculated with an aliquot of the preculture (dilution: 1:1,000) and grown overnight at 37 °C with shaking (250 rpm). The cell suspension was centrifuged for 10 min at 3,000 x g at 4 °C, the supernatant was removed and the bacterial pellet processed using the Plasmid Midi Kit (Qiagen) according to the manufacturer's recommendations. Nuclease-free water was used to dissolve the purified DNA.

3.2.3.3 Preparation of glycerol stocks

For long term storage, glycerol stocks were prepared. 800 µl of bacterial culture and 200 µl of sterile-filtered 80 % glycerol were mixed and filled into cryovials. Stocks were stored at -80°C.

3.2.3.4 Photometric measurement of DNA and RNA concentrations

The concentration of nucleic acids was determined photometrically at 260 nm in a UV cuvette. An optical density at 260 nm (OD_{260}) of 1 correlates to a concentration of 50 µg/ml double-stranded DNA and 40 µg/ml single-stranded RNA. The absorbance ratio at 260 and 280 nm ($OD_{260/280}$) is used to estimate the purity of DNA and RNA. Pure solutions of DNA or RNA have OD_{260}/OD_{280} ratios of 1.8 and 2.0, respectively. When low concentrations (100 ng/µl- 1000 ng/µl) were to be expected, 5 µl of DNA/ RNA were diluted in 45 µl dd-water. When high concentrations (over 1000 ng/µl) were to be expected 2 µl of nucleic acid were diluted in 48 µl of water.

3.2.3.5 Cloning of shRNA

To downregulate *MFSD8/CLN7* gene expression, the pSuper.GFP/neo vector was used in combination with a pair of oligonucleotides that contain unique 19- or 21 nucleotide sequences derived from the *MFSD8/CLN7* mRNA transcript targeted for suppression. The vector allows monitoring and studying of cells expressing shRNAs by simultaneous detection of GFP fluorescence. The N19/N21 target sequences correspond to the sense strand of the pSUPER-generated shRNA, which in turn corresponds to a 19-/21-nucleotide sequence within the mRNA. In the mechanism of RNAi (RNA inhibition),

3.2.4 Enzymatic phosphorylation of DNA

Phosphorylation of oligonucleotides was performed as ligases require a 5' phosphate group and a 3' hydroxyl group.

16	μl	double-stranded oligonucleotides (50 ng/μl)
2	μl	10x reaction buffer A
1	μl	ATP (20 pmol)
1	μl	<u>T4 Polynucleotide kinase</u>
20	μl	final volume

Phosphorylation was performed for 30 min at 37 °C. Annealed oligonucleotides were purified using the PCR purification kit according to the manufacturer's instructions.

3.2.5 Linearization of pSuper.GFP/neo

Restriction endonucleases recognize double-stranded DNA at short palindromic nucleotide sequences and hydrolyze phosphodiester bonds. Depending on the used enzyme either blunt ends or 3' and 5' overhanging ends (sticky ends) are generated. The vector pSuper.GFP/neo was sequentially cut with restriction enzymes *Hind* III and *Bgl* II yielding a linearized DNA with overhanging ends.

45	μl	pSuper.GFP/neo (4 μg)
6	μl	FastDigest [®] buffer (10×)
4	μl	<u>FastDigest[®] <i>Hind</i> III</u>

After 1 hour digestion at 37°C:

4	μl	FastDigest [®] <i>Bgl</i> II
1	μl	<u>alkaline phosphatase</u>
60	μl	final volume

The enzymes were added successively to the reaction mixture. First, pSuper.gfp/neo was cleaved by *Hind* III for 1 hour at 37 °C followed by an additional 2 hour incubation with *Bgl* II at 37 °C. Alkaline phosphatase was added to the mixture to dephosphorylate incompletely cut ends to prevent recirculation during the course of ligation. The linearized pSuper.GFP/neo vector was isolated by preparative agarose gel electrophoresis.

3.2.6 Ligation of DNA

For the ligation, phosphorylated oligonucleotides were annealed and ligated with dephosphorylated linearized pSUPER-neo +GFP vector. After generation of 3'- and 5'-overhanging ends (sticky ends) PCR products were ligated with linearized vectors using T4 DNA ligase. DNA ligases catalyze the covalent linkage of DNA fragments by generating phosphodiester bonds between 5' phosphate and 3' hydroxyl groups of free DNA ends. For the ligation, the PCR product was used in a 3-fold molar excess compared to the linearized vector DNA and ligation was performed according to manufacturer's instructions.

x	μl	vector (200 ng)
y	μl	insert (400 ng)
1.4	μl	T4 DNA ligase buffer (10×)
z	μl	dd H ₂ O
1	μl	T4 DNA ligase (1 Unit/μl)
14	μl	final volume

The ligation was performed at room temperature overnight. To reduce background growth the reaction mixture was incubated with *Bgl* II for 30 min afterwards. The complete reaction mixture was used to transform competent *E. coli* cells (see paragraph 3.2.3.1). Transformed cells were plated onto LB-ampicillin agar plates and incubated at 37 °C overnight.

3.2.7 Identification of recombinant clones

For analysis of recombinant clones containing pSuper.GFP.vectors with annealed oligonucleotides, ten clones were picked and incubated in 5 ml LB-amp medium overnight. Plasmid DNA was isolated (see paragraph 3.2.3.1) and 1.5 μg of DNA were digested with the restriction enzyme *Bgl* II as follows:

1.5	μg	Plasmid-DNA in 12μl nuclease-free water
1.5	μl	FastDigest [®] Reaction buffer (10×)
0.75	μl	FastDigest [®] Restriction enzyme <i>Bgl</i> II (20U/ μl)
0.75	μl	dd H ₂ O
15	μl	final volume

Cleavage with restriction enzymes was performed for 1 hour at 37 °C and agarose gel electrophoresis was used to check, if the isolated plasmids contained the desired inserts. Dephosphorylation of vector ends was performed during cleavage by restriction enzymes by adding alkaline phosphatase (0.5 µl) to the reaction mixture.

3.2.8 Cloning of pSuper.RFP.shRNA and pSuper.GFP-LC3.shRNA

For the generation of pSuper.RFP.shRNA and pSuper.GFP-LC3.shRNA cDNA constructs, a two-stage procedure was developed which uses megaprimers that are synthesized in a pre-PCR followed by a Quick Change site-directed mutagenesis protocol using the megaprimers and a template (Wang and Malcolm, 1999). This method is used for insertion and deletion of larger fragments like RFP or LC3 cDNAs. For the amplification of megaprimers containing the insert sequence, short forward and reverse oligonucleotide primers were synthesized, which anneal both to the template sequence (e. g. RFP or LC3, 15 bp) and to the inserted sequence (e.g. EGFP, 21 bp). With these primers the first PCR reaction with 35 cycles resulted in amplification of the insert flanked by short sequences annealing to defined positions in the acceptor DNA sequence.

Table 3.23: Constructs

<i>Construct</i>	<i>Template DNA</i>	<i>Primers</i>
pSuper.RFP.shRNA	mRFP-C1-GFP-LC3	RFP (forward/reverse)
pSuper.GFP-LC3.shRNA	pcDNA3.1-Myc-LC3	GFP-LC3 (forward/ reverse)

PCR reaction mixture for the pre-PCR was prepared as follows:

1	µl	DNA (50 ng/µl)
2.5	µl	Primer 1 (<i>forward</i> , 10pmol/µl)
2.5	µl	Primer 2 (<i>reverse</i> , 10 pmol/µl)
10	µl	HF reaction buffer Phusion (5×)
1	µl	dNTP mix (20 mM)
32.5	µl	PCR water
0.5	µl	<i>Phusion</i> [®] DNA polymerase
50	µl	final volume

Table 3.24: Pre-PCR

Temperature	Period	Number of cycles
98 °C	30 sec	→ 1x
98 °C 72 °C	10 sec 30 sec	→ 35x
72 °C	10 min	→ 1x

PCR products were separated by agarose gels, cut and extracted from the gel using QIAquick Gel Extraction Kit. After photometric determination of DNA concentration, the Quick change mutagenesis PCR was performed using a second template DNA (see paragraph 3.2.9).

3.2.9 Site-directed mutagenesis

The megaprimers (paragraph 3.2.8) were used in a Quick Change site-directed mutagenesis PCR (see table 3.25) using pSuper.GFP shRNA as a template.

Site-directed mutagenesis reaction

1	µl	pSuper.GFP shRNA (50 ng/µl)
300	ng	Megaprimer
10	µl	HF reaction buffer (5×)
1	µl	dNTP mix (20 mM)
32.5	µl	PCR grade water
0.5	µl	<i>Phusion</i> [®] DNA polymerase
50	µl	final volume

Table 3.25: Quick change site-directed mutagenesis PCR

Temperature	Period	Number of cycles
98 °C	30 sec	→ 1x
98 °C 55 °C 72 °C	10 sec 30 sec 10 min	→ 18x

Prior to transformation into *E. coli* TOP 10, 20 µl of the samples were incubated with 2 µl *Dpn* I for 1h at 37°C. The enzyme *Dpn* I recognizes only the parental methylated

plasmid DNA, thus digesting only the template plasmid, but not the mutant PCR product. 10 µl of the samples were used to transform competent *E. coli* top10 cells (paragraph 3.2.3.1). Correct insertion of the RFP- and LC3-sequences, respectively, was verified by sequencing (SEQLAB, Göttingen).

3.2.10 Sequencing of DNA constructs

The generated expression constructs and shRNAs were verified by DNA sequencing at SEQLAB, Göttingen. 700ng of the respective plasmid DNA and 1 µl of the sequencing primer (20 pmol) were added up to a total volume of 7 µl with nuclease-free water in a 200 µl reaction tube and the solutions were mixed. Sequence analyses and comparisons were performed using DNASTAR and Blast N.

3.2.11 Agarose gel electrophoresis

1 x TAE buffer:	DNA sample buffer:
40 mM Tris/HCl (pH 8,5)	0.05 % Bromphenolblue
20 mM acetic acid	0.05 % Xylenecyanol
2 mM EDTA	15 % Ficoll

Agarose gel 1-2 % with ethidium bromide

200 ml	TAE buffer
2-4 g	Agarose
10 µl	Ethidium bromide

DNA fragments were separated according to their molecular weight by electrophoresis for analysis. Depending on the DNA size gel with agarose concentration of 1-2% (w/v) was prepared. Agarose was dissolved in tris acetate-EDTA (TAE) buffer and boiled in a microwave until complete dissolution. Ethidium bromide was added to the chilled agarose solution (55 °C) in a final concentration of 0.5 µg/µl and poured into a gel casting chamber. A comb was inserted immediately and the gel was polymerized at room temperature. After removing the comb the gel was transferred into an electrophoresis chamber filled with 1 x TAE buffer. The DNA samples were mixed with loading dye and loaded on the agarose gel together with a DNA size marker. An electric voltage of 100 V was applied. Intercalation of ethidium bromide into the DNA

was used to make the DNA fragments visible under UV illumination. Images were made by the UV transilluminator. The DNA band was cut out and weighed. DNA was extracted with the GeneJET Gel Extraction Kit (Fermentas) according to the manufacturer`s instructions.

3.2.12 RNA extraction from cultured cells

For RNA extraction the GeneJET™ RNA Isolation kit was used according to the manufacturer`s protocol. Purified RNA was eluted with 50 µl of nuclease-free water. RNA concentrations were measured photometrically at 260 nm. The RNA was stored at -80 °C until further use.

3.2.13 Synthesis of cDNA

Synthesis of complementary DNA (cDNA) from purified mRNA was performed using RNA-dependent DNA polymerase (reverse transcriptase) according to the manufacturer`s instructions. cDNA synthesis is required because only double-stranded DNA can be amplified by quantitative PCR, not single-stranded RNA. The reaction mixture was pipetted into 200 µl PCR reaction tubes, mixed and shortly centrifuged. Synthesis of cDNA was performed in a thermocycler using the following reaction temperatures. cDNA was stored at -20 °C until further use in quantitative real-time PCR.

cDNA reaction mixture	Reaction temperatures
1 µg RNA in 10µl DEPC water	
2 µl 10x RT buffer	25 °C, 10 min
0.8 µl 25x dNTP Mix (100mM)	37 °C, 120 min
2 µl 10x RT Random Primers	85 °C, 5 sec
4.2 µl DEPC water	
<u>1 µl Multiscribe Reverse Transkriptase</u>	
20 µl final volume	

3.2.14 Quantitative real-time PCR

The TaqMan® gene expression assay was used for the quantitative analysis of RNA expression. The assay includes ready-made primers and probes for the respective gene.

The dual-labeled fluorogenic probe is attached to a fluorescent reporter dye on the 5' end and a fluorescent quencher dye at the 3' end. The 3' end is blocked with phosphate to avoid an extension of the probe.

The quencher reduces the fluorescence from the reporter by Fluorescence Resonance Energy Transfer (FRET). During primer extension the Taq polymerase blocks the probe. This leads to an activation of the 5'-3' exonuclease activity of the DNA polymerase and a hydrolysis of the probe follows. This separates the quencher from the reporter and allows the reporter to emit its energy. Hence, the fluorescent signal can be detected. The fluorescence increase is proportional to the increase of the concentration of the amplification product. Initially, the measured fluorescence is not significantly high because the product amounts are too low. During the exponential phase the cycle of threshold (C_T) is reached. The C_T correlates to the number of PCR cycles where fluorescence was significantly higher for the first time. The C_T is used for further calculations.

2 μ l cDNA were pipetted into each 200 μ l reaction tube. 18 μ l of the mixture (see below) was added to the cDNA, samples were mixed by pipetting and the reaction tubes were closed by stripes.

Reaction mixtures for quantitative real-time PCR were prepared as follows:

10 μ l	Maxima Probe/qPCR Master Mix
1 μ l	TaqMan [®] primer mix
2 μ l	cDNA
7 μ l	DEPC water
20 μ l	final volume

Table 3.26: Quantitative real-time PCR

Temperature	Period	Number of cycles
95 °C	10 min	→1x
95 °C 60 °C	30 sec 1 min	→40x

All real-time PCR reactions were performed using a Stratagene thermocycler (model Mx3000P). The information was taken from the real-time PCR manual in the lab (see table 3.26).

3.2.15 Biochemical methods

3.2.15.1 Protein extraction

Lysis buffer:

10	mM	Tris/HCl (pH 7.5)
150	mM	NaCl
5	mM	EDTA
0.1	%	SDS
1	%	Sodium deoxycholate
1	%	Triton X-100

After harvesting the cells (see protocol above) the cell pellet was re-suspended in lysis buffer and incubated on ice for 30 min, every 10 min vortex. Subsequently, the lysate was centrifuged at maximum speed for 10 min at 4 °C in order to remove the supernatant with all the proteins from the cell pellet and to transfer the proteins into a new Eppendorf tube.

3.2.15.2 Protein quantification

Protein quantification was carried out using the Roti[®]-Quant protein assay. A standard curve with different BSA concentrations (0, 2.5, 5, 10 and 15 µg/µl concentration) was used for calibration. 5 µl of protein solved in a solution was mixed with 795 µl of water. 200 µl of Roti[®]-Quant was added to every sample and the samples were vortexed before pouring it into the cuvette to measure the concentration at 595 nm of wavelength in a photometer.

3.2.15.3 SDS-PAGE

Sodium Dodecyl Sulphate PolyAcrylamide Gel Electrophoresis (SDS-PAGE) is used to separate proteins according to their molecular weight. Proteins with lower molecular masses have a higher electrophoretic mobility than those with larger molecular masses. Denatured proteins bear negative charges due to the SDS of the lysis buffer and thus move towards the anodes.

Buffers

Anode buffer	192 mM glycine, 25 mM Tris/HCl (pH 6.8)
Cathode buffer	192 mM glycine, 25 mM Tris/HCl (pH 6.8), 0.1% SDS
4x solubilizer	500 mM Tris/HCl (pH 6.8), 4 % SDS, 40 % Glycerin, Coomassie [®] Blue R, 40 mM DTT

Gel electrophoresis was performed using a vertical slab gel unit (see table 3.27).

Table 3.27: Preparation of the gel for gel electrophoresis

	Stacking gel	Running gel
	4 %	10% or 15%
Acrylamide (30 %), bisacrylamide (0.8 %)	1.3 ml	9.8 ml / 14.6 ml
1.5 M Tris/HCl (pH 8.8)	2.5 ml (pH 6.8)	7.5 ml (pH 8.8)
10 % SDS	100 μ l	300 μ l
H ₂ O	6 ml	7.325 ml (for 15% gel) 12.225 ml (for 10% gel)
10 % APS	100 μ l	250 μ l
TEMED	10 μ l	25 μ l

Preparation of the gel

According to the molecular weight of the protein 10% to 15% acrylamide containing running gel was prepared. The gel substance was poured between two glass plates and air bubbles were removed by adding minimal amounts of water. After 30 min the running gel was done. Water was decanted. The stacking gel was prepared and poured on top of the running gel. Immediately a comb was pushed into the gel. 30 min later the polymerization was finished. The comb was removed. The gel was washed with water.

Preparation of the samples

After measuring the protein concentrations water was added to achieve same total volumes. This was done in order to make the specific protein expression of the samples comparable to each other. The samples (75-150 μ g total protein) were diluted in 100 μ l water and 1% β -mercaptoethanol was added for better solubilisation. Next, the 4x solubilizer was added. After denaturation at 95 °C for 5 min the samples were loaded on a polyacrylamide gel.

Electrophoresis

The electrophoresis chamber was filled with the anode buffer. Samples were loaded on the polyacrylamide gel and placed into the electrophoresis chamber. The cathode buffer was poured onto it. The electrophoresis was performed for 2.5 hours at 50 mA and maximum voltage per gel at RT.

3.2.15.4 Western blot analysis

Buffers

Transfer buffer	25 mM Tris/HCl (pH 7.4), 192 mM glycine, 20 % methanol
Wash buffer	0.1 % Tween 20 in TBS or PBS (TBST or PBST)
Blotto	5 % non-fat dry milk powder in TBST or PBST

Enhanced chemiluminescence (ECL) reaction

Solution 1	5	ml	0.1 M	Tris/HCl (pH 8.5)
	100	μl	250 mM	luminol in DMSO
	50	μl	90 mM	p-cumaric acid in DMSO
Solution 2	5	ml	0.1 M	Tris/HCl (pH 8.5)
	12	μl	30 %	H ₂ O ₂

Electrotransfer of proteins

Proteins are transferred from the gel to a PVDF membrane by applying a current (50 mA/gel) vertically to the membrane. Whatman papers (14 cm x 16 cm) and fiber pads were placed in transfer buffer. The PVDF membrane (13 cm x 15 cm) was soaked in methanol and washed with water for 5 min. After electrophoresis polyacrylamide gel was removed from the chamber and the transfer sandwich (fiber pad, 2 sheets of paper, PVDF membrane, running gel, 2 sheets of paper, fiber pad) was assembled between two grids of a plastic cassette in transfer buffer and placed in a transfer tank. The membrane had to be on the positive pole compared to the gel, as the negatively charged proteins were attracted by the anode. Electrotransfer of proteins was performed at 900 mA for 3 hours.

Immunodetection

After protein transfer, the membrane was cut into appropriate pieces for the different proteins with specific molecular weights. First, the membrane was washed with wash buffer. Then, the membrane was incubated with shaking in the appropriate blocking solution (Blotto) for 1 hour at RT to block free antigen binding sites on the membrane. Next, the membrane was incubated with shaking using the primary antibody diluted in Blotto for 3 hours at RT. The membrane was incubated four times (1.5 min, 5 min, 10 min, 10 min) in wash buffer with constant shaking at RT. Finally the membrane was incubated with the horse-radish-peroxidase (HRP)-coupled secondary antibodies diluted in Blotto for 1 hour at RT in the absence of light. The membrane was washed 4 times with wash buffer and 3 times with PBS or TBS.

Enhanced Chemiluminescence (ECL)-Detection

For detection of secondary antibodies on the membranes a home-made reaction mixture was used. Equal volumes of ECL solutions 1 and 2 were mixed and applied on the membranes for 1 min. The detection of chemiluminescence on the membranes was performed immediately using the ChemiDocXRS imager. Intensities of immunoreactive bands were quantified using Image J.

4. Results

CLN7 is a multispinning lysosomal membrane glycoprotein of unknown function, which is ubiquitously expressed with tissue- and cell-type differences in expression levels (Siintola et al., 2007). Since no model organisms existed at the start of the present study, a cell-based model generated via shRNA-mediated depletion of *MFSD8/CLN7* mRNA was generated for biochemical and cell biological studies. Aim of the study was to analyze lysosomal biogenesis, lysosomal function and endocytic, autophagic and biosynthetic pathways to lysosomes in *MFSD8/CLN7*-depleted cultured cells.

4.1 *MFSD8/CLN7* mRNA expression in cultured human cell lines

To identify cells suitable for silencing RNA (siRNA)- and short hairpin RNA (shRNA)-mediated down-regulation, endogenous *MFSD8/CLN7* mRNA expression was quantified in two human cell lines, the HeLa tumor and the HEK293 embryonic fibroblast cell lines derived from cervix and kidney, respectively. High *MFSD8/CLN7* mRNA levels would suggest an important functional role for CLN7 in the analyzed cell line. HeLa and HEK293 cells were grown to confluency, total mRNA was harvested and *MFSD8/CLN7* mRNA levels were determined by quantitative real-time PCR. Real-time PCR analyses of *MFSD8/CLN7* mRNA expression were performed in triplicate with three independent cell culture plates. In HEK293 cells statistically significant 8-fold higher amounts of *MFSD8/CLN7* mRNA compared to HeLa cells were detected (Figure 4.1). Due to the higher *MFSD8/CLN7* mRNA levels in HEK293 cells, these were chosen for siRNA-/shRNA-mediated *MFSD8/CLN7*-downregulation and analysis of the cellular phenotypes.

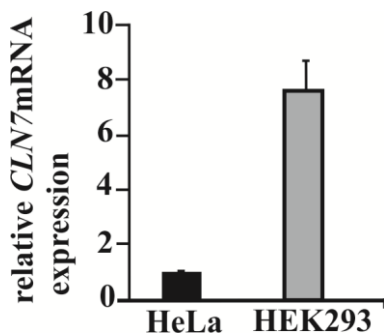


Figure 4.1 *MFSD8/CLN7* mRNA expression levels in cultured HeLa and HEK293 cells. *MFSD8/CLN7* mRNA expression normalized to β -actin expression was quantified in cultured HeLa and HEK293 cells. The data are the mean \pm standard deviation (SD) of three independent RNA preparations. Relative expression of *MFSD8/CLN7* mRNA in HeLa cells was arbitrarily set as 1. Black bar: HeLa; grey bar: HEK293.

4.2 siRNA-mediated down-regulation of *MFSD8/CLN7* mRNA

To deplete endogenous *MFSD8/CLN7* mRNA in HeLa and HEK293 cells, siRNA-mediated down-regulation was performed. To identify mRNA sequences which specifically bind to *MFSD8/CLN7* mRNA a commercially available algorithm was used. By these algorithms off-target effects caused by unspecific silencing of unrelated mRNAs can be minimized. Three independent siRNAs targeted against *MFSD8/CLN7* coding sequences were synthesized and tested for their efficacy to down-regulate endogenous *MFSD8/CLN7* mRNA in both HEK293 and HeLa cells. Transfection of single siRNAs twice in 48h-intervalls resulted in a reduction of *MFSD8/CLN7* mRNA by 50% as determined by quantitative real-time PCR (data not shown).

4.3 shRNA-mediated down-regulation of *MFSD8/CLN7* mRNA

4.3.1 Generation of vector pSuper.GFP.CLN7-shRNA

shRNA is a sequence of RNA that makes a tight hairpin turn that can be used to silence target gene expression via RNA interference (RNAi, Brummelkamp et al., 2002). In contrast to chemically synthesized siRNAs, shRNAs are delivered by plasmids and have a relatively low rate of degradation and turnover. In the used, commercially available pSuper.GFP/neo vector the cloned shRNA of *MFSD8/CLN7* is under control of the H1 promoter, which results in a robust shRNA expression. Since GFP (green fluorescent protein) is transcribed from an internal ribosome entry site (IRES) sequence, expression of shRNAs in single cells can be monitored by detection of GFP-fluorescence. Two 61

bp and 63 bp specific oligonucleotides directed against coding sequences of human *MFSD8/CLN7*-cDNA were cloned into the *Hind* III /*Bgl* II restriction sites of vector pSuper.GFP/neo to generate the pSuper.GFP /neo CLN7-shRNA plasmid (Figure 4.2 A and B). A schematic representation of the pSuper.GFP/neo vector and the sequences of oligonucleotides containing the 19 and 21 bp targeted *MFSD8/ CLN7* sequences are shown (Figure 4.2 A and B).

Transient transfection of pSuper.GFP.CLN7-shRNA plasmid allowed both the downregulation of *MFSD8/CLN7* in cultured cells and the identification of individual CLN7-downregulated cells by GFP fluorescence using confocal laser scan microscopy.

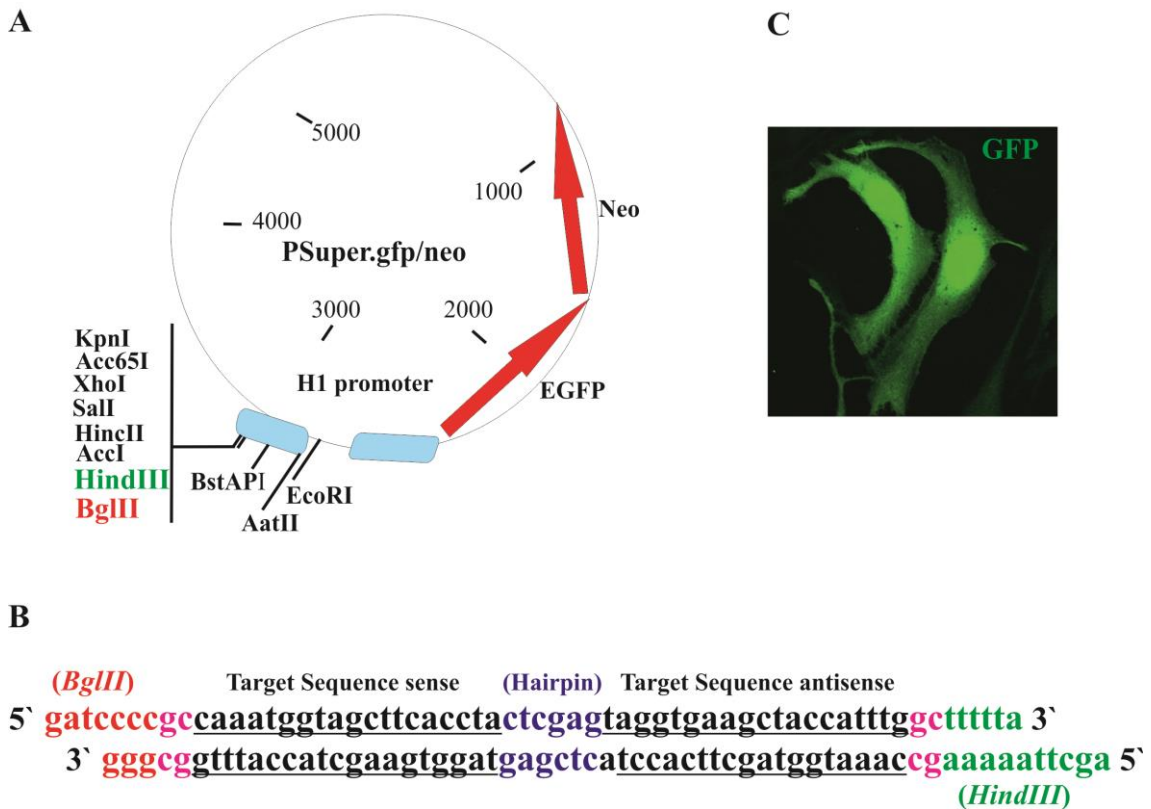


Figure 4.2 Schematic representation of vector pSuper.GFP/neo

(A) Schematic representation of the vector pSuper.GFP/neo. The used *Hind* III/*Bgl* II restriction sites are indicated in green and red letters, respectively. The positions of the H1 promoter, the EGFP and neomycin expression genes are indicated (red arrows). (B) Sequences of oligonucleotides used for specific downregulation of *MFSD8/CLN7* mRNA. Targeted *MFSD8/CLN7* and hairpin sequences are indicated in black and purple, respectively. The 5' overhanging sequences used for cloning into *Bgl* II (red) and *Hind* III (green) restriction sites of vector pSuper.GFP/neo are given. The additional two nucleotides present in sh21 are shown in pink. (C) HeLa cells were transiently transfected with pSuper.GFP.shRNA and fixed 72 hours after the start of transfection. GFP fluorescence (green) was detected by confocal laser scanning microscopy.

4.3.2 shRNA-mediated down-regulation of *MFSD8/CLN7* mRNA in HeLa cells

HeLa cells were transfected with pSuper.GFP.CLN7 carrying a scrambled (scr)-shRNA (negative control), pSuper GFP carrying a 21-mer shRNA (-sh21-shRNA) and pSuper GFP carrying a 19-mer shRNA (-sh19-shRNA) twice at 48-h intervals to deplete endogenous *MFSD8/CLN7* mRNA. 96 hours after the start of transfection cells were harvested and *MFSD8/CLN7* mRNA amounts were determined by quantitative real-time PCR. In sh21-shRNA and sh19-shRNA transfected cells *MFSD8/CLN7* mRNA was downregulated by 73% and 77%, respectively, compared to scrambled shRNA transfected control cells (Figure 4.3).

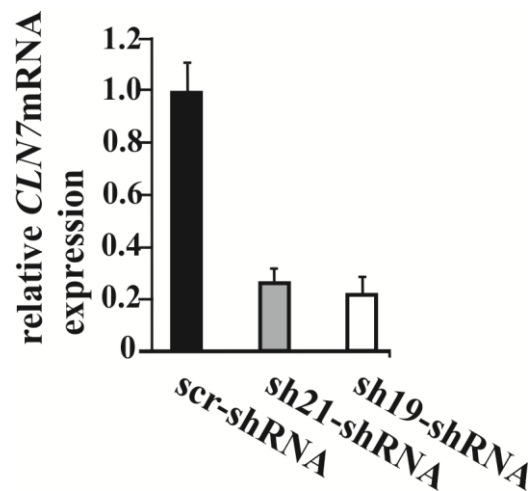


Figure 4.3: Depletion of endogenous *MFSD8/CLN7* mRNA by shRNA.

HeLa cells were transfected twice in 48-h intervals with scr-shRNA, sh21-shRNA or sh19-shRNA and total mRNA was harvested 96 hours after the start of transfection. *MFSD8/CLN7* mRNA levels were measured by quantitative real-time PCR and normalized to β -actin mRNA expression. The data are the mean \pm SD of one transfection each. Expression in scr-shRNA transfected HeLa cells was arbitrarily set as 1. Black bar: scr-shRNA; gray bar: sh21-shRNA; white bar: sh19-shRNA.

Confirmation of CLN7 depletion on the protein level could not be performed due to the lack of an antibody detecting endogenous CLN7.

4.3.3 Reduced amounts of *CLN6* and *CLN8* mRNAs in *MFSD8/CLN7*-depleted HeLa cells

To study whether depletion of *MFSD8/CLN7* mRNA leads to changes in the mRNA expression of genes coding for NCL-related membrane proteins, quantitative real-time PCR analyses were performed on downregulated cells. HEK293 and HeLa cells were transfected twice in 48h-intervals with pSuper-GFP-scr (controls), -sh19 and -sh21 cDNAs and cells harvested 96 hours after the first transfection. After isolation of total mRNA and synthesis of cDNA quantitative real-time PCR analyses were performed to quantify the degree of down-regulation of *MFSD8/CLN7* mRNA and the amounts of *CLN3*, *CLN6* and *CLN8* mRNA in *MFSD8/CLN7*-depleted HEK293 cells and *CLN3*, *CLN6*, *CLN8* and *CLN10* mRNA in *MFSD8/CLN7*-depleted HeLa cells (Figure 4.4).

Quantitative real-time PCR revealed that in HEK293 cells expression of sh21- and sh19-shRNAs down-regulated endogenous *MFSD8/CLN7* mRNA by 77% and 80%, respectively, compared to scr-shRNA transfected cells (Figure 4.4.A). In HeLa cells expression of sh21- and sh19-shRNAs down-regulated endogenous *MFSD8/CLN7* mRNA by 75% and 70%, respectively, compared to scr-shRNA transfected cells (Figure 4.4.B).

In sh21-RNA transfected HEK293 cells a reduction of *CLN3* mRNA by 40%, of *CLN6* mRNA by 45% and of *CLN8* mRNA by 35% compared to scr-shRNA transfected control cells was detected (Figure 4.4 A). In sh19-RNA transfected HEK293 cells a decrease of *CLN3* mRNA by 15%, of *CLN6* mRNA by 35% and of *CLN8* mRNA by 13% was observed. In sh21-RNA transfected HeLa cells a reduction of *CLN3* mRNA by 11%, of *CLN6* mRNA by 24% and of *CLN8* mRNA by 47% compared to scr-shRNA transfected control cells was detected (Figure 4.4 B). A minor increase of *CLN10* mRNA by 12% was detected. In sh19-RNA transfected HeLa cells a decrease of *CLN3* mRNA by 26%, of *CLN6* mRNA by 27%, of *CLN8* mRNA by 50% and of *CLN10* mRNA by 10% was observed. Although the degree of decrease varied between *MFSD8/CLN7* downregulated HEK293 and HeLa cells, there was trend towards decreased *CLN3*-, *CLN6*- and *CLN8*-mRNA levels in *MFSD8/CLN7* depleted cells.

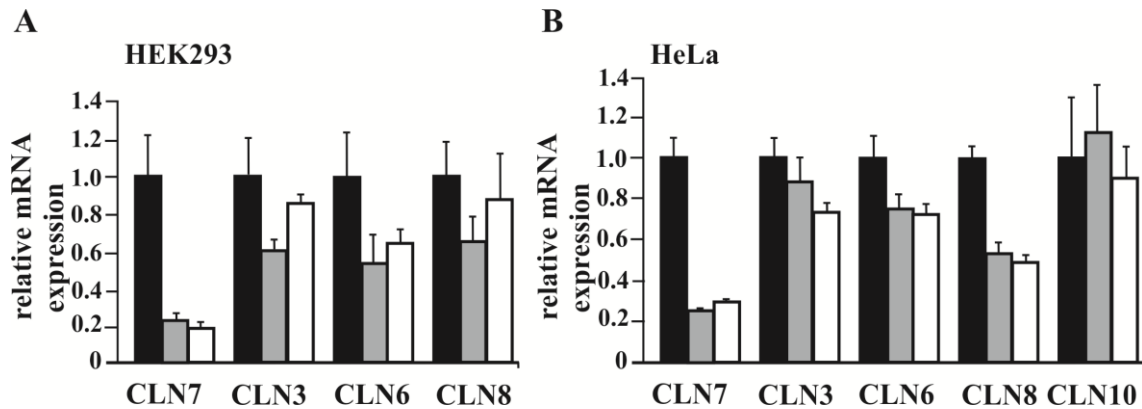


Figure 4.4 Expression of NCL-related genes in *MFSD8/CLN7*-depleted cells. (A) HEK293 and (B) HeLa cells were transfected twice in 48-h intervals with scr-, sh21- and sh19-shRNAs and total mRNA was harvested after 96 hours. The amounts of *MFSD8/CLN7*, *CLN3*, *CLN6*, *CLN8* and *CLN10* mRNAs were measured by quantitative real-time PCR and relative mRNA expression was normalized to β -actin mRNA expression. The relative mRNA amount in scr-shRNA transfected cells was arbitrarily set as 1. Bars are the mean expression \pm SD. Black bar: scr-shRNA, gray bar: sh21-shRNA, white bar: sh19-shRNA.

4.3.4 *MFSD8/CLN7*-depletion does not alter mRNA expression levels of lysosomal proteins

It has been shown that transcription of most lysosomal genes and autophagy-related genes is regulated by the transcription factor TFEB (Sardiello et al., 2009). In addition, starvation or depletion of nutrients in cells is sensed by the LYNUS system which activates TFEB via a TORC1-dependent pathway (Settembre et al., 2013). To analyze whether depletion of *MFSD8/CLN7* affects the transcription of lysosomal genes, quantitative real-time PCR analyses were performed in *MFSD8/CLN7*-downregulated HEK293 cells and HeLa cells. After shRNA-mediated *MFSD8/CLN7* depletion the *MFSD8/CLN7* mRNA amounts were reduced by 66% (sh21-shRNA) in HEK293 cells compared to scr-shRNA transfected control cells and by 71% (sh21-shRNA) and 74% (sh19-shRNA) in HeLa cells compared to negative control cells (scr-shRNA; Figure 4.5 A and B).

Results showed a reduction of *LAMP-1* mRNA by 13%, of *tartrate-resistant acid phosphatase* (TRAP) mRNA by 12%, of *cathepsin D* mRNA by 13% and equal lysosomal acid phosphatase (*LAP*) levels in sh21-shRNA transfected HEK293 cells compared to scr-shRNA-transfected control cells (Figure 4.5 A). Student's t-test revealed no statistical significant differences.

Consistent with the data no significant decrease of *LAMP-1* and *LAP* mRNA levels were detected in *MFSD8/CLN7* down-regulated HeLa cells (Figure 4.5 B). A significant 4-fold increase of *TRAP* mRNA was observed in cells transfected with sh21-shRNA compared to scr-shRNA expressing control cells. Interestingly, no significant changes in *TRAP* mRNA levels were detected in cells transfected with sh19-shRNA (Figure 4.5 B).

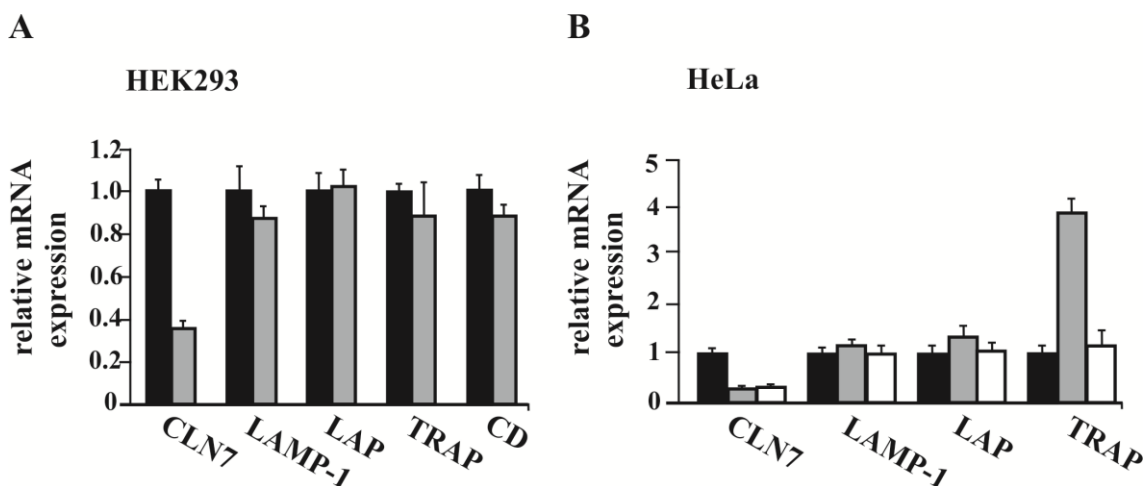


Figure 4.5 mRNA expressions of genes encoding lysosomal proteins in *MFSD8/CLN7*-depleted cells. (A) HEK293 and (B) HeLa cells were transfected twice in 48-h intervals with scr-, sh21- and sh19-shRNAs and total mRNA was harvested after 96 hours. Relative mRNA expression levels of *LAMP-1*, *LAP*, *TRAP* and *cathepsin D* (CD) were measured by quantitative real-time PCR in *MFSD8/CLN7*-depleted cells. mRNA levels were normalized to the expression of β -actin. Relative amounts of mRNAs in scr shRNA transfected cells were arbitrarily set as 1 and presented in a bar diagram (mean \pm SD). Black bars: scr-shRNA, grey bars: sh21-shRNA, white bars: sh19-shRNA.

4.3.5 Clathrin-mediated endocytosis of the transferrin receptor is not altered in *MFSD8/CLN7*-depleted HeLa cells

Transferrin (Tf) is a monomeric serum glycoprotein that binds Fe^{3+} in the blood. The transferrin- Fe^{3+} complexes are bound by the homodimeric transferrin receptor (Tfr) at the cell surface. After internalization by receptor-mediated, clathrin-dependent endocytosis, Tfr-Tf- Fe^{3+} complexes are transported to endosomal compartments, where Fe^{3+} is released due to the low pH. The Tfr-apo Tf complexes are recycled back to the plasma membrane enabling apo Tf to scavenge more Fe^{3+} after release from the Tfr (Luck and Mason, 2012).

Clathrin-mediated endocytosis in *MFSD8/CLN7*-depleted HeLa and control cells was studied by the uptake of the marker protein Tf coupled to Alexa Fluor[®] 546 (Tf-AF546). Cells were transiently transfected with pSuper-GFP.*CLN7* shRNA twice in 48-h intervals. Scrambled shRNA transfected cells served as controls. Seventy two hours after the start of transfection, cells were starved for 30 min in DMEM lacking amino acids and fetal calf serum and subsequently incubated in medium containing Tf-AF546 for 30 minutes on ice. After removal of the medium, cells were chased in full medium at 37 °C for 1 hour, fixed and analyzed by confocal laser scan microscopy.

Both in scr-shRNA and *CLN7*-shRNA transfected cells transferrin was detected in intracellular vesicles indicating clathrin-mediated uptake of Tf by the Tfr at the plasma membrane, internalization and subsequent transport to intracellular organelles (Figure 4.6). Quantification of intracellular Tf-AF546 fluorescence in GFP-positive scr-shRNA and sh21-shRNA transfected cells revealed an increase by 15% in *MFSD8/CLN7*-down-regulated cells compared to control cells (Figure 4.6 B). However changes in the distribution of endocytosed Tf in *MFSD8/CLN7*-depleted cells compared to negative control (scr-shRNA) and non-transfected neighbouring cells were observed. In *CLN7*-down-regulated cells Tf was detected in peripheral vesicles, whereas in scr-transfected and GFP-negative non-transfected cells endocytosed Tf was observed perinuclear (Figure 4.6A). However these findings could not be detected in all *MFSD8/CLN7*-depleted cells. The results suggest that clathrin-mediated endocytosis of the Tfr and transport to intracellular vesicles is not impaired by the depletion of *CLN7*.

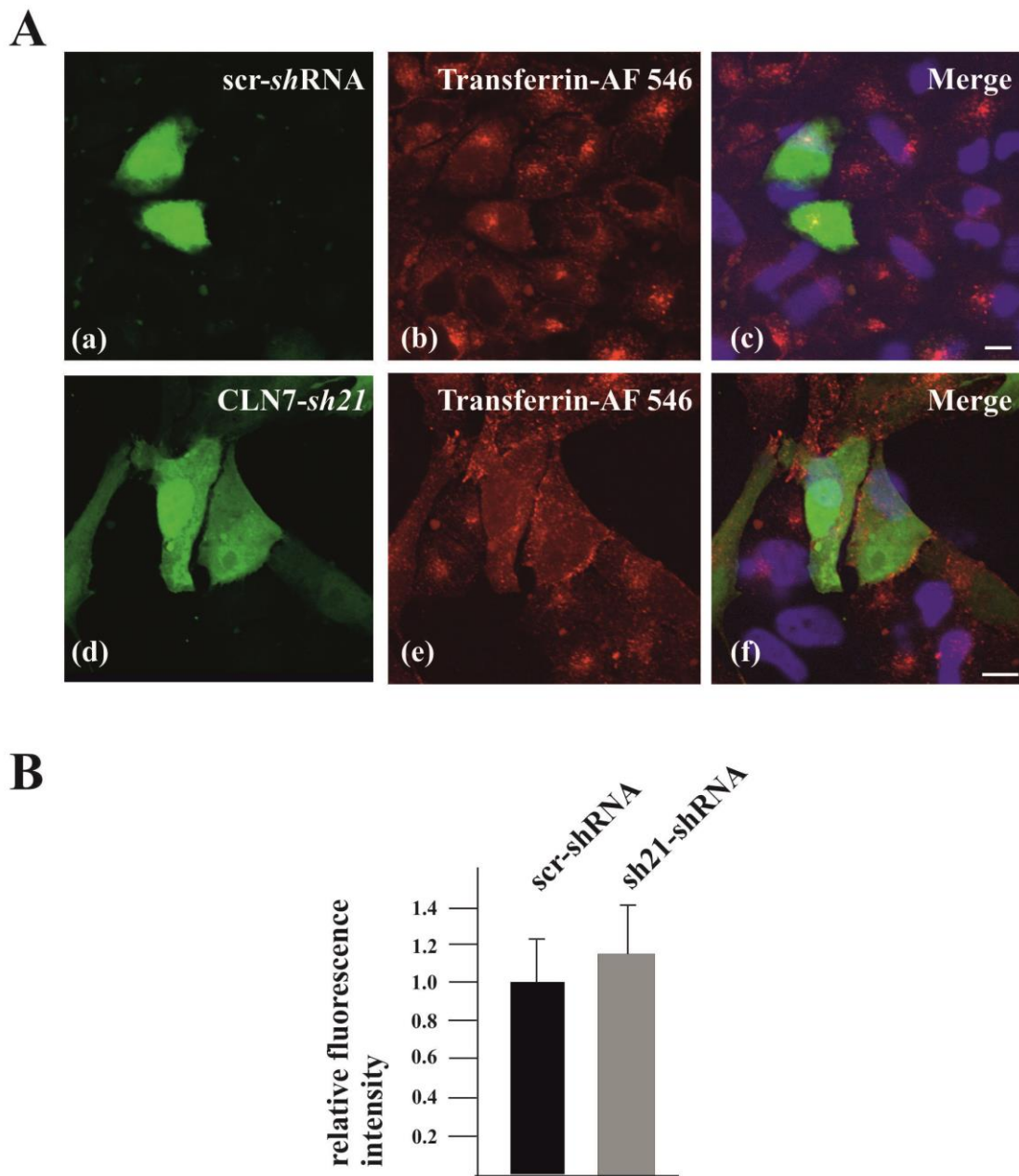


Figure 4.6 Clathrin-mediated endocytosis of Tfr is not altered in *MFSD8/CLN7*-depleted HeLa cells. (A) HeLa cells were transfected twice with pSuper-GFP-*scr* shRNA (*scr-shRNA*, a-c) and *-CLN7* shRNA (*sh21-shRNA*, d-f) plasmids in 48-h intervals. Seventy two hours after the first transfection, cells were incubated with Tf-AF546 on ice for 30 minutes and chased for 1 hour at 37°C. Cells were fixed and analyzed for GFP-fluorescence (green) and intracellular Tf-AF 546 (red) by confocal microscopy. Nuclei were stained with DAPI (blue). Merged images indicate the amount of endocytosed Tf-AF546 in *scr-shRNA* (c) and *sh21-shRNA* (f) expressing cells. Scale bars: 15 μ m. (B) Quantification of intracellular Tf-AF546 fluorescence. Intensity of Tf-AF546 fluorescence was measured in 16 independent GFP-positive cells. Bars are the mean fluorescence intensity \pm standard deviation of endocytosed Tf-AF546 in *scr-shRNA* (negative control, black bar) and *CLN7-shRNA* transfected cells (gray bar). Fluorescence intensity in *scr-shRNA* transfected control cells was arbitrarily set as 1.

4.3.6 Number, size and distribution of LAMP-1 and LAMP-2 positive compartments were not affected in *MFSD8/CLN7*-depleted cells

To analyze whether depletion of *MFSD8/CLN7* affects the number, size, distribution and morphology of lysosomes, immunofluorescence analyses on scr-shRNA and sh21-shRNA expressing HeLa cells were performed. HeLa cells were transfected twice with shRNAs, fixed 72 hours after the start of transfection and stained with antibodies against the lysosomal marker proteins LAMP-1 and LAMP-2. Cells expressing shRNAs were identified by detection of GFP-fluorescence (Figure 4.7). In GFP-positive, *MFSD8/CLN7*-depleted cells a grossly normal morphology of LAMP-1 positive compartments was observed. No obvious changes in the size, number, intracellular distribution and morphology of LAMP-1 positive compartments were detected (Figure 4.7). Both in control and *MFSD8/CLN7*-depleted cells lysosomes were evenly distributed within cells (Figure 4.7).

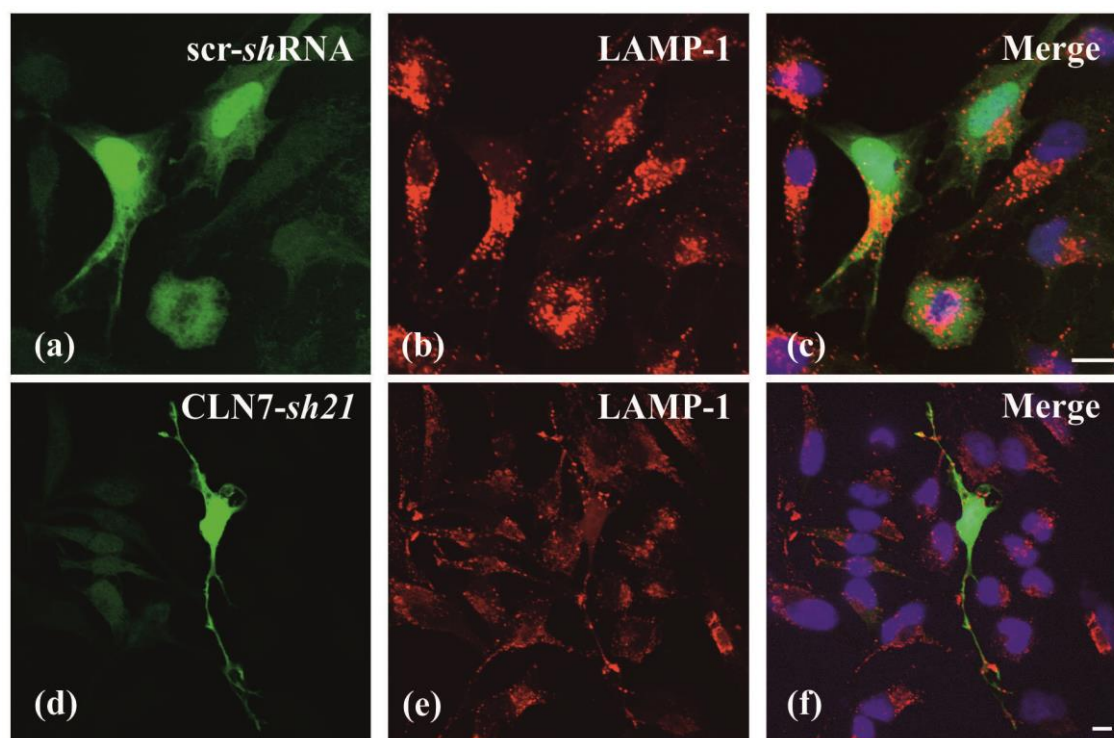


Figure 4.7 No changes in the size, number, distribution and morphology of LAMP-1 positive compartments in *MFSD8/CLN7*-depleted HeLa cells. HeLa cells were transfected twice with pSuper-GFP-scr-shRNA (a-c) and -sh21-shRNA plasmids (d-f) and fixed 72 hours after the start of transfection. Cells were incubated with antibodies against the lysosomal marker protein LAMP-1 (red, b and e) followed by staining with secondary antibodies conjugated to AF546. GFP-fluorescence was detected simultaneously (green, a and d) and nuclei were stained with DAPI (blue). Merged images show LAMP-1 positive compartments (red) in scr-shRNA (c) and sh21-shRNA-transfected cells (f). Scale bars: 15 μ m.

Consistent with these results no obvious alterations were found in number, size, distribution and morphology of LAMP-2-positive compartments (Figure 4.8).

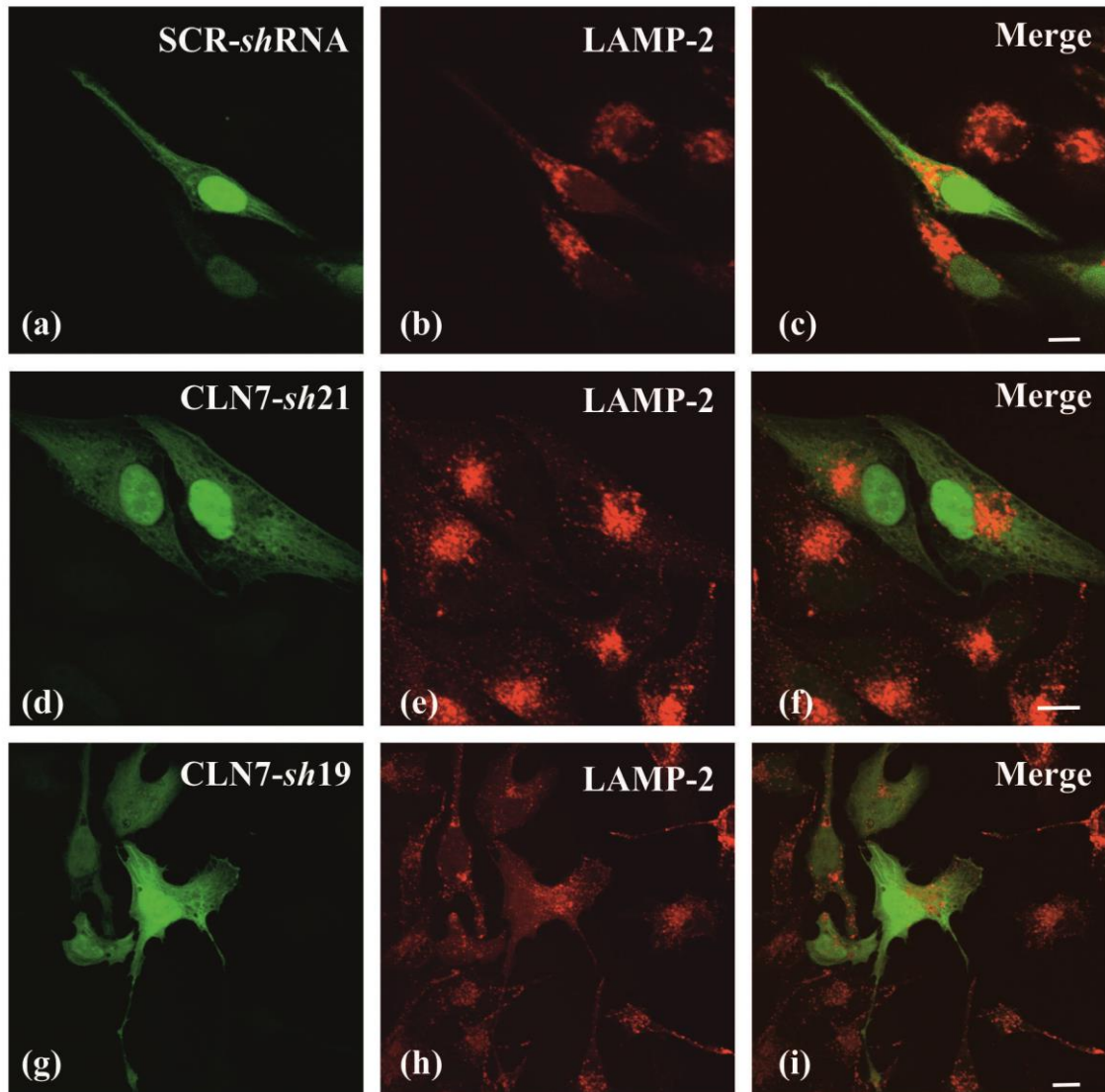


Figure 4.8 No changes in the size, number, distribution and morphology of LAMP-2 positive compartments in *MFSD8/CLN7*-depleted HeLa cells. HeLa cells grown on glass cover slips were transfected twice with pSuper.GFP-scr-shRNA (a-c), -CLN7-sh21 (d-f) and -CLN7-sh19 RNA (g-i) plasmids and were fixed 72 hours after the first transfection. Cells were stained with antibodies against the lysosomal marker protein LAMP-2 (red) followed by incubation with secondary antibodies conjugated to AF546. GFP-fluorescence was detected simultaneously (green). Merged images show LAMP-2 positive compartments (red) in scr-sh RNA- (c), sh21-shRNA (f) and sh19-shRNA (i) -transfected cells. Scale bars: 15 μ m.

4.3.7 Expression of LAMP-1 and LAMP-2 in *MFSD8/CLN7*-depleted cells

Increased amounts of lysosomal membrane proteins have been reported in *CLN3*-depleted HeLa cells, in cultured skin fibroblasts of *CLN3* patients and in mouse models of other LSDs, like mucopolipidosis II (Kollmann et al., 2012; Pohl et al., 2007). To analyze whether depletion of *CLN7* affects the levels of major lysosomal membrane proteins, the amounts of the highly abundant LAMP-1 and -2 proteins were quantified in *MFSD8/CLN7*-depleted HEK293 cells and compared to scr-sh RNA transfected control cells. HEK293 cells were transfected twice with pSuper.GFP.scr - and sh21-shRNA at intervals of 48 hours. 90 hours after the start of transfection, cells were either grown in full medium or starved in EBSS medium for additional 6 hours and subsequently harvested. Total protein homogenates were separated by SDS-PAGE and analyzed by LAMP-1, LAMP-2, and β -tubulin immunoblotting (Figure 4.9.A). In *MFSD8/CLN7*-depleted HEK293 cells the amounts of LAMP-1 were reduced by 65% compared to scr-shRNA transfected control cells. Starvation in EBSS medium lacking amino acids and growth factors for 6 hours resulted in a reduction of LAMP-1 protein levels by 40% (Figure 4.9, B). In *MFSD8/CLN7*-down-regulated HEK293 cells no significant changes in the amounts of LAMP-2 proteins were detected both in non-starved and in starved cells (Figure 4.9 C).

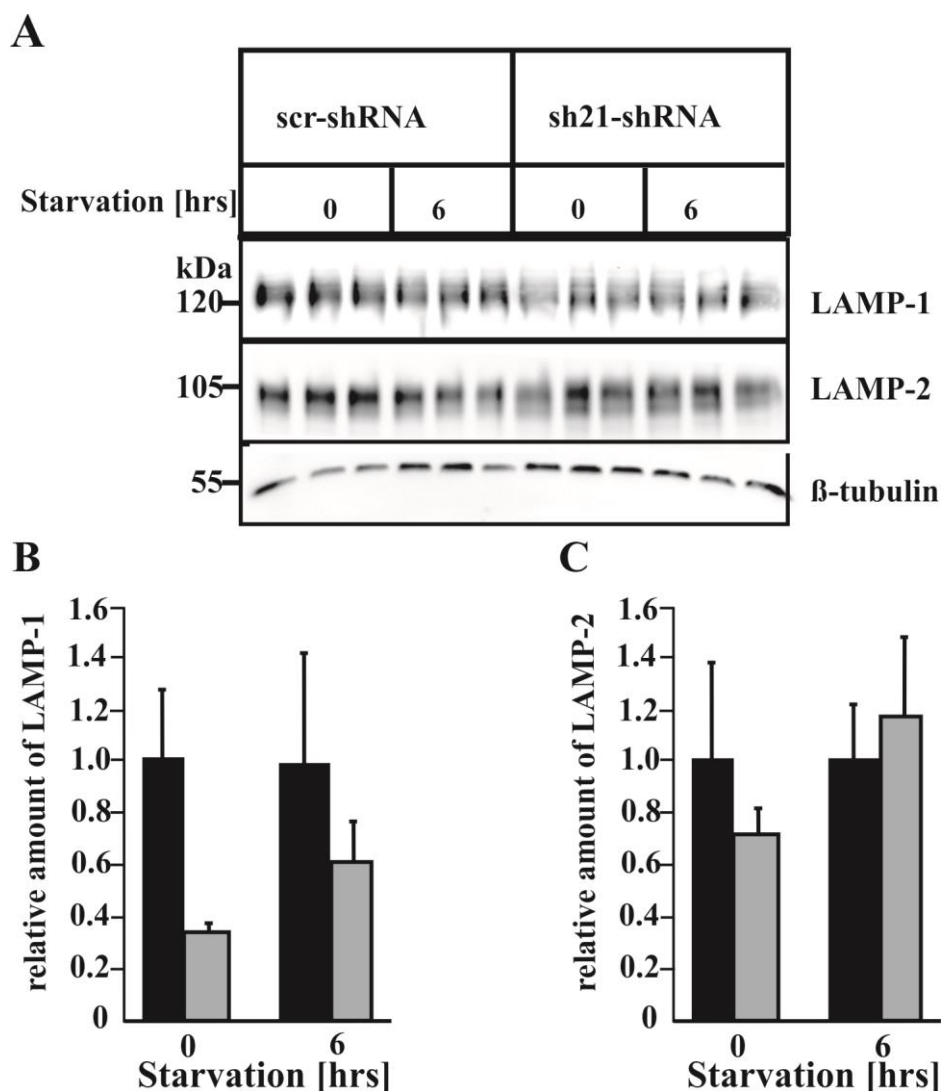


Figure 4.9 Expression of LAMP-1 and LAMP-2 in non-starved and starved *MFSD8/CLN7*-depleted HEK293 cells. (A) HEK293 cells were transfected twice with scr-shRNA and sh21-shRNA. 90 hours after the start of transfection cells were either grown in full medium or starved in EBSS medium for additional 6 hours. Total protein homogenates (100 μ g protein) were separated by SDS-PAGE and analyzed by LAMP-1 and LAMP-2 immunoblotting. β -tubulin western blotting was performed to control the loading. The positions of molecular mass proteins are indicated. (B) Quantification of LAMP-1. The densities of immunoreactive bands were quantified and normalized to the amounts of β -tubulin. The mean values \pm SD are shown (black bars: scr-shRNA-transfected cells; gray bars: sh21-shRNA-transfected cells). The time period or starvation prior to harvesting the cells is indicated. (C) Protein quantification of LAMP-2. Black bar: scr-shRNA, gray bar: sh21-shRNA.

To confirm results obtained in HEK293 cells, *MFSD8/CLN7*-downregulation was performed in HeLa cells. Quantification of immunoreactive band intensities showed no significant changes in the amounts of LAMP-1 and LAMP-2 in *MFSD8/CLN7* down-regulated HeLa cells compared to scrambled shRNA transfected control cells (Figure 4.10).

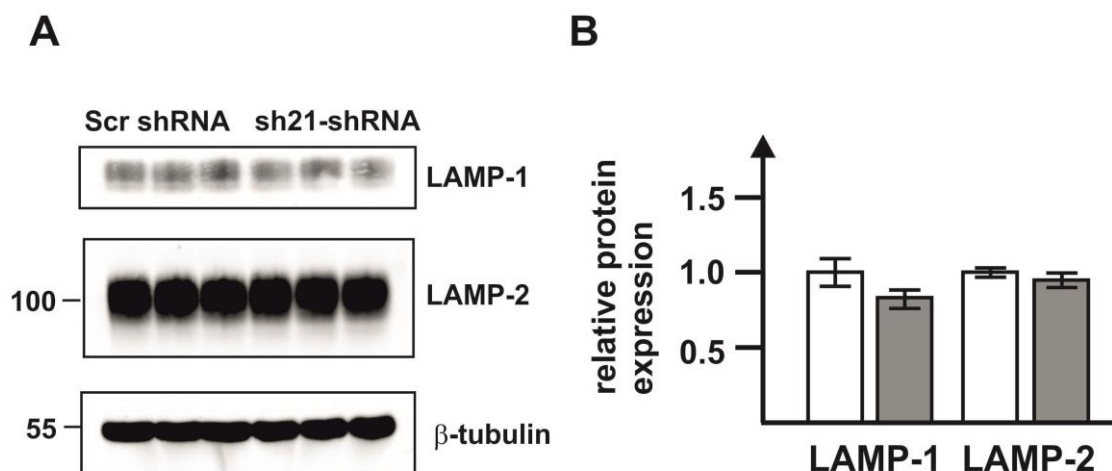


Figure 4.10 No significant changes in the amounts of LAMP-1 and LAMP-2 in *MFSD8/CLN7*-depleted HeLa cells. (A) HeLa cells were transfected with scr- and sh21-shRNAs and harvested 96 h after the first transfection. Total homogenates (150 μ g protein) were separated by SDS-PAGE and analyzed by LAMP-1, LAMP-2, and β -tubulin western blotting. Positions of molecular weight markers are indicated. (B) Densitometric quantification of immunoreactive band intensities. The densities were quantified and normalized to the amounts of β -tubulin. The mean values \pm SD are shown (white bars: scr-shRNA-transfected cells; gray bars: sh21-shRNA-transfected cells).

4.3.8 Proteolytic processing of cathepsin D and Z is not altered in *MFSD8/CLN7*-depleted HeLa cells

To analyze whether expression, lysosomal transport and processing of soluble lysosomal proteins are affected by CLN7 depletion, aspartic protease cathepsin D and the cysteine protease cathepsin Z were analyzed by western blotting in *MFSD8/CLN7*-down-regulated cells. HeLa cells were transfected twice with pSuper.GFP.scr - and sh21-shRNA in 48-h intervals and cells were harvested 96 hours after the start of transfection. Total homogenates were separated by SDS-PAGE and analyzed by cathepsin D and -Z immunoblotting (Figure 4.11). Both in scr-shRNA and sh21-shRNA HeLa cells mature 28 kDa and 15 kDa cathepsin D forms were detected indicating that lysosomal transport and proteolytic processing were not impaired in CLN7 depleted cells (Figure 4.11 A). Precursor and intermediate cathepsin D forms were not detected by the used polyclonal antibody. In CLN7-depleted cells both the 38 kDa precursor and the 36 kDa mature cathepsin Z forms were detected (Figure 4.11 A). Densitometric quantification of immunoreactive band intensities revealed decreased amounts of cathepsin D and Z by 12% and 24%, respectively (Figure 4.11 B).

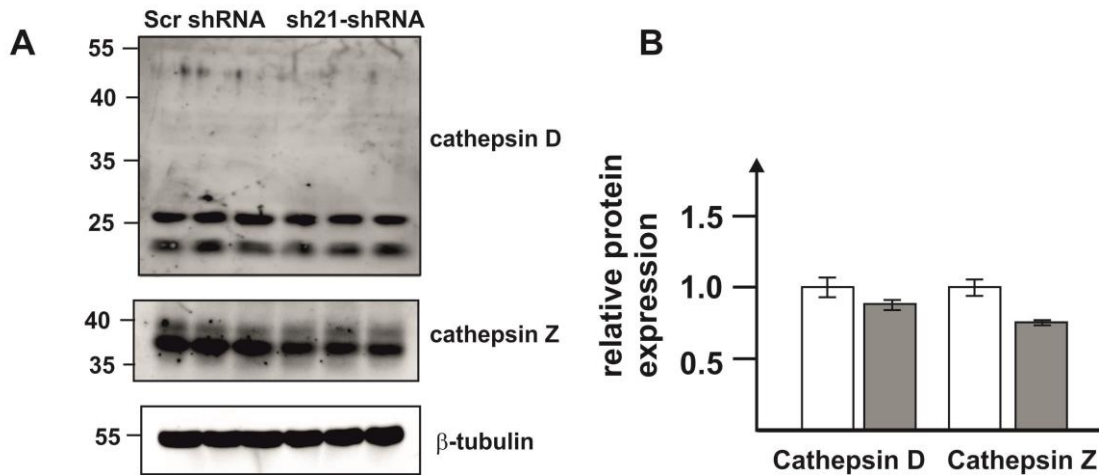


Figure 4.11 Reduced amounts of cathepsin Z in *MFSD8/CLN7* depleted HeLa cells. (A) HeLa cells were transfected with scr- and sh21-shRNAs and harvested 96 h after the first transfection. Total homogenates (150 μ g protein) were separated by SDS-PAGE and analyzed by cathepsin D, cathepsin Z and β -tubulin western blotting. Positions of molecular weight markers (in kDa) are indicated. (B) Densitometric quantification of immunoreactive band intensities. The densities were quantified and normalized to the expression of β -tubulin. The mean values \pm SD are shown (white bars: scr-shRNA-transfected cells; gray bars: sh21-shRNA-transfected cells).

4.3.9 Number, size and distribution of early endosomes are not changed in *MFSD8/CLN7*-depleted HeLa cells

The early endosomal antigen-1 (EEA-1) was used as a marker protein to analyze the number, size and distribution of early endosomes in *MFSD8/CLN7*-depleted cells. HeLa cells grown on glass cover slips were transfected twice with pSuper.GFP.shRNA. Seventy two hours after the start of transfection cells were fixed and analyzed by confocal laser scan microscopy.

Both in scr and sh21-transfected GFP-positive HeLa cells endosomes were evenly distributed intracellularly. No obvious differences in the size and number of early endosomes were observed between sh21-transfected cells, *CLN7*-depleted cells and scr-shRNA or non-transfected cells (Figure 4.12).

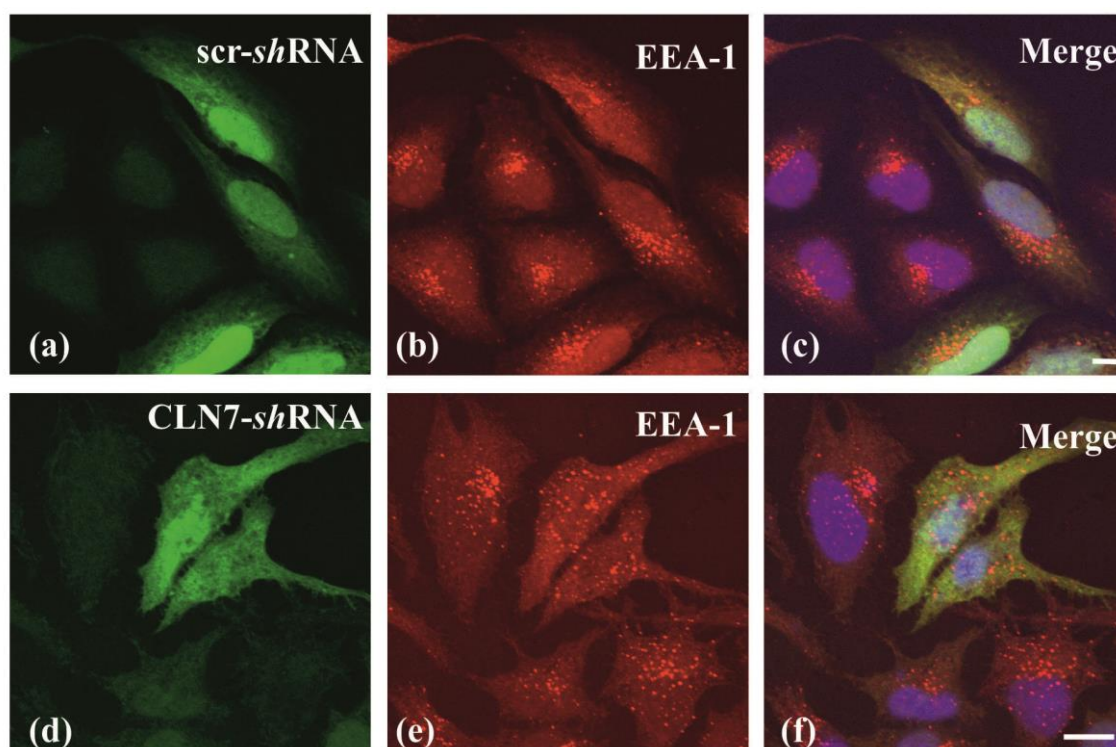


Figure 4.12 Analysis of early endosomal compartments in *MFSD8/CLN7* depleted HeLa cells. HeLa cells were transfected twice with pSuper.GFP-*scr-shRNA* (a-c) and *sh21-shRNA* (d-f) plasmids in 48-h intervals and fixed 96 hours after the start of transfection. Cells were stained with antibodies against the early endosomal marker protein EEA-1 (b and e, red) followed by incubation with secondary antibodies coupled to AF546. *Scr* and *shRNA* expressing cells were visualized by GFP-fluorescence (a and d, green) and nuclei were stained with DAPI (blue). Merged images indicate the size and distribution of early endosomes in *scr-sh-* (c) and *sh21-shRNA* transfected (f) cells. Scale bars: 15 μ m.

4.4 Effects of *MFSD8/CLN7* depletion on macroautophagy

The microtubule associated protein LC3 exists in two forms: LC3-I represents the unlipidated cytosolic form and LC3-II is the membrane-bound, lipidated form which is associated with autophagosomal membranes and is regarded as a marker for macroautophagy (Kabeya et al., 2000). LC3-II can be distinguished from LC3-I by a higher electrophoretic mobility on SDS-PAGE (Tanida et al., 2008) and thus detection of LC3-II by immunoblotting is a routine method for monitoring macroautophagy.

LC3-II levels were quantified in cultured *MFSD8/CLN7*-depleted cells in full medium under steady-state conditions. HEK293 cells were either transfected with GFP-LC3 or transfected with the vector pSuper.GFP-LC3.shRNA twice in 48-hour intervals and cells were harvested 96 hours after the start of transfection. Total homogenates were separated by SDS-PAGE and analyzed by LC3 and β -tubulin immunoblotting,

respectively (Figure 4.13A). Both in non-transfected, scr- and sh21-transfected HEK293 cells the 18 kDa LC3-I and the 16 kDa LC3-II forms were detected, indicating the formation of autophagosomes and unchanged autophagic flux in *MFSD8/CLN7*-depleted cells. Densitometric quantification and normalization to the amounts of β -tubulin revealed a 2.8-fold increase in the amounts of LC3-II in sh21-transfected cells compared to scr-shRNA transfected control cells (Figure 4.13B).

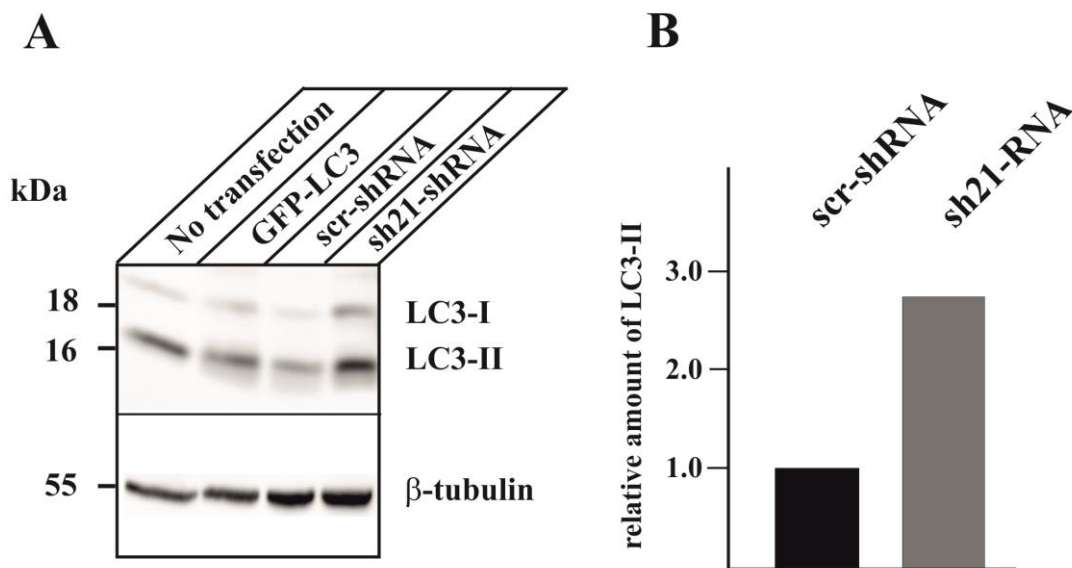


Figure 4.13 Increased amounts of LC3-II in *MFSD8/CLN7*-depleted HEK293 cells. (A) HEK293 cells were either non-transfected, transfected with GFP-LC3 or transfected twice with scr-shRNA and sh21-shRNA in 48-h intervals. Ninety six hours after the start of transfection cells were harvested and total homogenates (150 μ g protein) were separated by SDS-PAGE and analyzed by LC3- and β -tubulin immunoblotting. The positions of LC3-I, LC3-2 and molecular weight markers (in kDa) are indicated. (B) Densitometric quantification of LC3-II amounts. LC3-II levels were normalized to the amounts of β -tubulin. LC3-II amounts in homogenates of scr-shRNA transfected control cells were arbitrarily set as 1. Black bar: scr-shRNA, gray bar: sh21-shRNA

To confirm increased amounts of LC3-II in *MFSD8/CLN7*-depleted HEK293 cells, experiments were repeated in shRNA-downregulated HeLa cells. For statistical evaluation three independent tissue plates were transfected and analyzed. Total homogenates were prepared, separated by SDS-PAGE and analyzed by LC3, p62 and β -tubulin immunoblotting (Figure 4.14). The intensities of immunoreactive bands were normalized to β -tubulin expression and relative protein expression of p62 and LC3-II were quantified. In *MFSD8/CLN7*-downregulated HeLa cells a 1.5-fold increase in the

amounts of LC3-II was detected compared to scr-shRNA transfected control cells (Figure 4.14 B). Interestingly the levels of p62 in *MFSD8/CLN7*-depleted HeLa cells were not significantly changed.

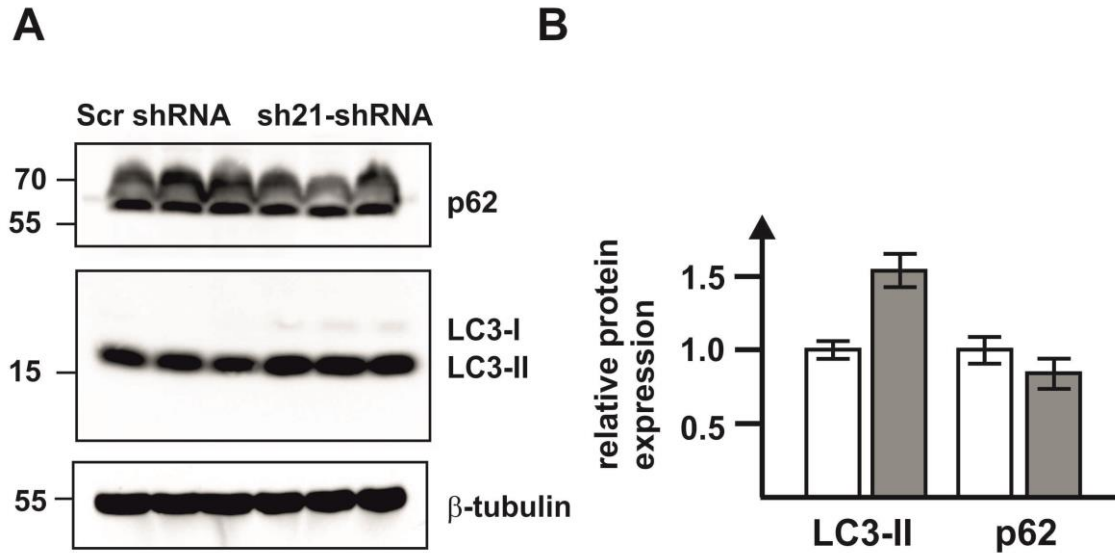


Figure 4.14 Increased LC3-II levels in *MFSD8/CLN7*-depleted HeLa cells. (A) HeLa cells were transfected with scr- or sh21-shRNAs and harvested 96 hours after the first transfection. Total homogenates (150 μ g protein) were separated by SDS-PAGE and analyzed by p62, LC3-, and β -tubulin western blotting. Positions of molecular weight markers (in kDa) are indicated. (B) Densitometric quantification of immunoreactive band intensities. The densities were quantified and normalized to the expression of β -tubulin. The mean values \pm SD are shown (white bars: scr-shRNA-transfected cells; gray bars: sh21-shRNA-transfected cells).

To examine whether the increase in the amount of LC3-II-positive autophagosomes is due to signalling events initiating autophagy (Mizushima et al., 2008), the expression of beclin 1 was determined in down-regulated HEK293 cells. The 60 kDa beclin 1 represents a multifunctional protein known to have regulatory functions in autophagy (Wirawan et al., 2012). Cells were transfected with scr- and sh21-shRNAs, harvested 96 hours after the start of transfection and analyzed by beclin 1 and β -tubulin immunoblotting (Figure 4.15A). In *MFSD8/CLN7*-downregulated HEK293 cells a 1.3-fold increase in the amounts of beclin 1 was detected compared to scr-shRNA transfected control cells (Figure 4.15 B).

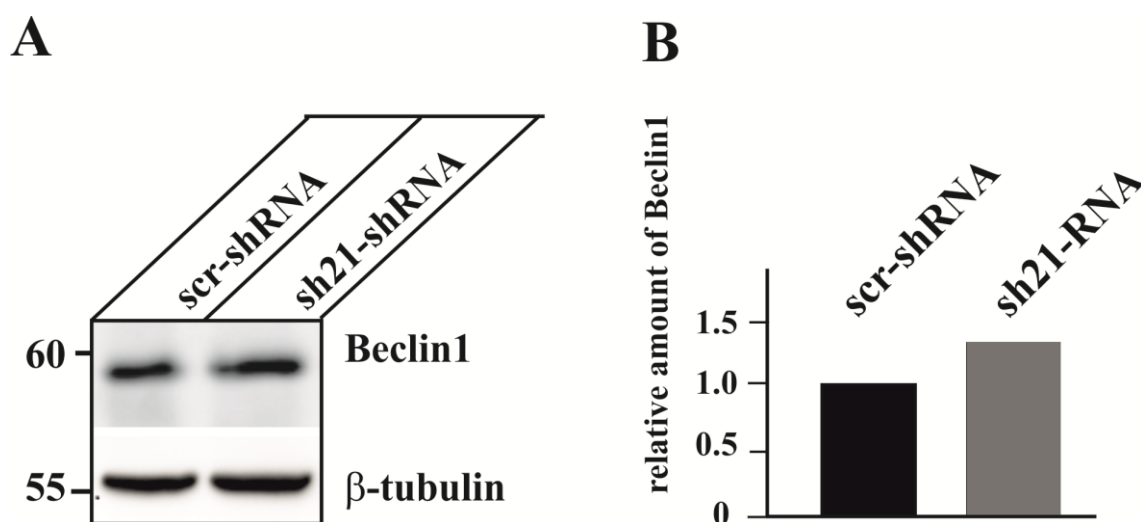


Figure 4.15 Increased amounts of beclin 1 in *MFSD8/CLN7*-depleted HEK293 cells. (A) HEK293 cells were transfected with scr-shRNA (negative control) and sh21-shRNA and were harvested 96 hours after the first transfection. Total protein homogenates (150 μ g protein) were solubilized, separated by SDS-PAGE and analyzed by beclin 1 and β -tubulin immunoblotting. Positions of molecular weight markers (in kDa) are indicated. (B) Densitometric evaluation of intensities of immunoreactive bands. Bars represent the mean of beclin amounts in scr-shRNA (black bar) and sh21-shRNA (gray bar) transfected cells normalized to the levels of β -tubulin. The amounts of beclin 1 in scr-shRNA transfected control cells were arbitrarily set as 1.

4.4.1 Detection of autophagosomes by imaging the autophagosomal marker GFP-LC3-II in *MFSD8/CLN7*-down-regulated cells

To study the formation of autophagosomes in *MFSD8/CLN7* down-regulated cells by imaging, the cDNA coding for LC3 was fused in frame with an N-terminal GFP sequence (GFP-LC3) in vector pSuper.GFP.sh21RNA. HeLa cells were transfected with the generated pSuper.GFP-LC3.sh21RNA cDNA construct and analyzed 72 hours after the start of transfection using confocal laser scan microscopy. In cells transfected with pSuper.GFP-LC3.sh21RNA cDNA both cytosolic GFP-LC3-I and membrane-bound GFP-LC3-II were detected (Figure 4.16). These results indicate that formation of autophagosomes in HeLa cells can be monitored by the formation of GFP-LC3-II in *MFSD8/CLN7*-depleted cells.

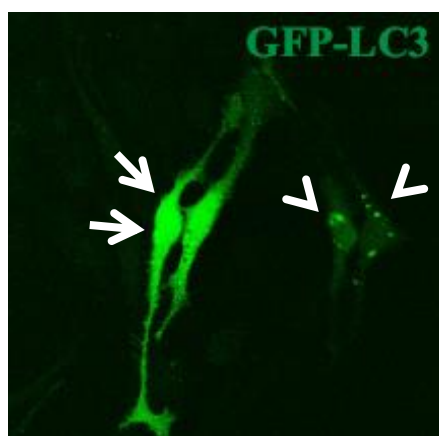


Figure 4.16 Localization of GFP-LC3 in pSuper.GFP-LC3 sh21RNA transfected HeLa cells. HeLa cells were transfected with pSuper.GFP-LC3 sh21RNA cDNA construct and analyzed 72 hours after the start of transfection by confocal laser scan microscopy (63x magnification). Cells expressing either cytosolic GFP-LC3-I (arrows) or membrane bound, lipidated GFP-LC3-II (arrowhead) are indicated.

4.4.2 Increased number of autophagosomes in *MFSD8/CLN7*-depleted HeLa cells

To confirm increased numbers of autophagosomes in *MFSD8/CLN7* depleted HeLa cells observed by LC3-II immunoblotting, cells grown on glass cover slips were transfected once with pSuper.GFP-LC3-scr shRNA and -*CLN7* shRNA GFP-LC3. Cells were fixed 72 hours after the start of transfection followed by detection of GFP-LC3 by immunofluorescence. In transfected cells, both, scrambled shRNA and *CLN7* shRNAs, are co-expressed with the autophagosomal marker protein GFP-LC3. The GFP-LC3-I form is cytosolic and the GFP-LC3-II form is associated with autophagosomal membranes (Klionsky et al., 2012). In scr shRNA expressing control cells, GFP fluorescence was mainly detected in the cytosol indicating the presence of mainly LC3-I (Figure 4.17 c). In *CLN7* shRNA transfected cells, GFP fluorescence was associated with vacuolar structures of different diameters indicating localization of LC3-II on autophagosomal membranes (Figure 4.17 a).

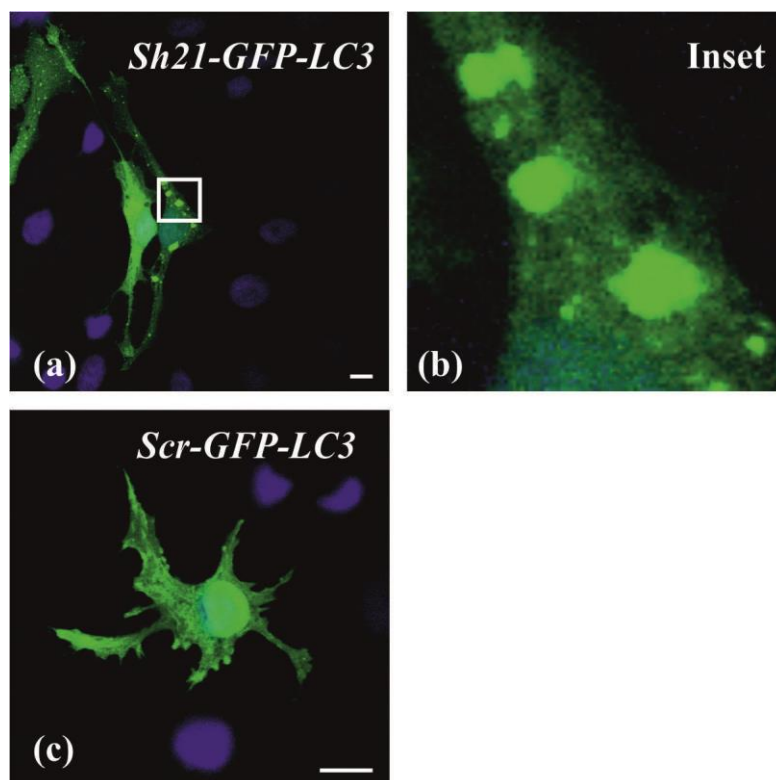


Figure 4.17 Increased number of GFP-LC3-II positive autophagosomes in *MFSD8/CLN7*-depleted HeLa cells. HeLa cells were transfected once with pSuper.GFP-LC3-scr shRNA (c) and -CLN7 shRNA plasmids (a). Cells were fixed 72 hours after the start of transfection and analyzed for GFP-fluorescence (green) by confocal microscopy. The inset (b) shows a 9.5-fold magnification of the region marked by the white rectangle. Nuclei were stained with DAPI (blue). Merged images are shown. Scale bars: 15 μ m.

In a next experiment cells were transfected once with pSuper.GFP-LC3-SCR shRNA and -CLN7 shRNA GFP-LC3 and cells were starved 72 hours after the start of transfection in EBSS medium lacking amino acids and growth medium for 2 or 4 hours to induce autophagy. Both in scr and CLN7 shRNA transfected cells increased numbers of GFP-LC3-II positive vacuolar structures were observed indicating higher numbers of autophagosomes and an activation of macroautophagy, both in control and *MFSD8/CLN7* depleted cells (Figure 4.18).

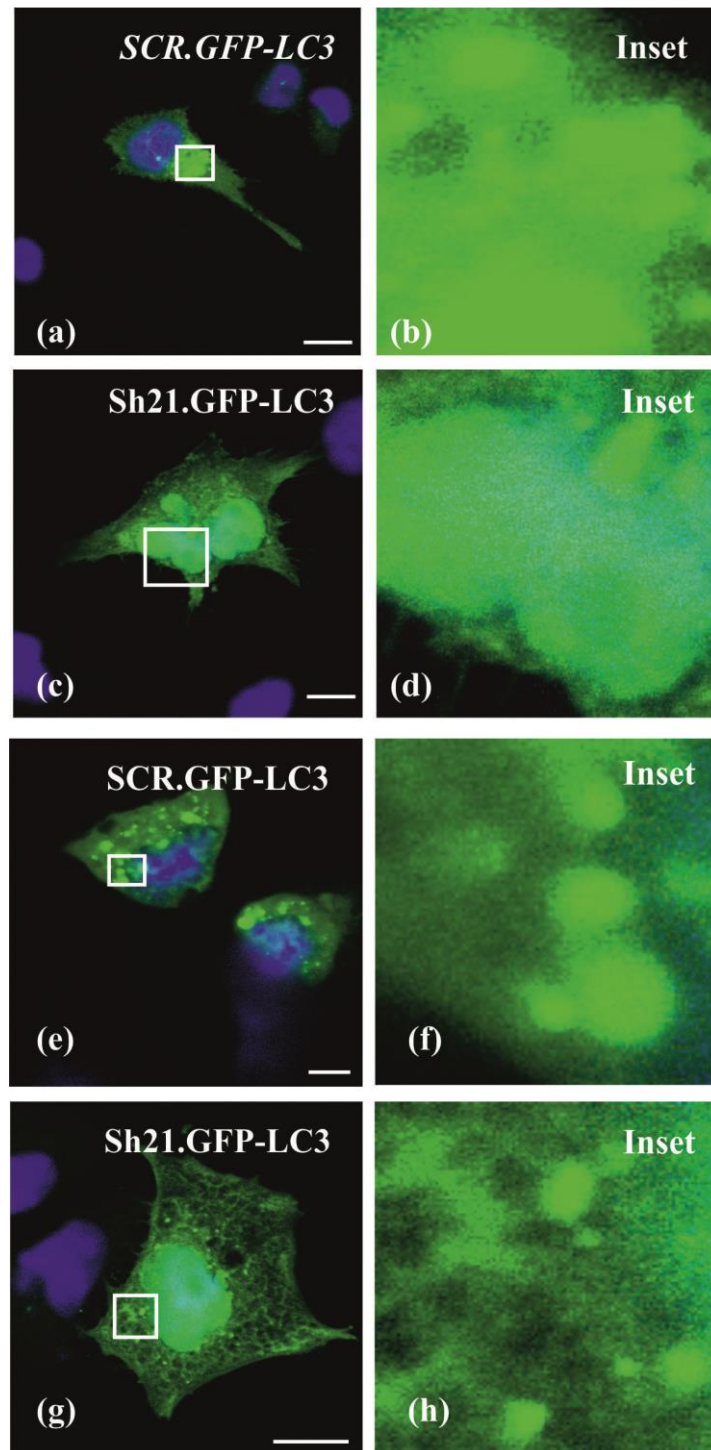


Figure 4.18 Increased number of autophagosomes in starved *MFSD8/CLN7* depleted HeLa cells and control cells (A) *MFSD8/CLN7*-depleted cells and LC3-II are detected via GFP-tag. Inserts show GFP-LC3 accumulation. HeLa cells were transfected once with pSuper.GFP-LC3-scr shRNA and $-CLN7$ shRNA plasmids. Cells were starved for 2 hours/ 4 hours after the transfection and were fixed. Cells were analyzed for GFP-fluorescence (green) by confocal microscopy. Nuclei were stained with DAPI (blue). Merged images are shown. The insets are 10-fold (b), 5.5-fold (d), 10-fold (f) and 8-fold (h) magnifications of the regions marked by the white rectangles. a) SCR, 2 hours starvation, c) shRNA 21, 2 hours starvation, e) SCR, 4 hours starvation, g) shRNA 21, 4 hours starvation. Scale bars: 15 μ m.

4.4.3 Increased number of autophagosomes in CLN7 overexpressing HeLa cells

Depletion of *MFSD8/CLN7* in HeLa cells resulted in increased number of autophagosomes as shown by higher levels of LC3-2 by immunoblotting and increased numbers of GFP-LC3-II positive autophagosomes. To analyze whether increased CLN7 levels result in enhanced formation of autophagosomes, HeLa cells grown on glass cover slips were co-transfected with Myc-CLN7 and GFP-LC3 in a ratio of 0.8:0.2. Cells co-transfected with empty vector and GFP-LC3 were used as negative controls. Cells were fixed 72 hours after the start of transfection, stained with antibodies against the Myc epitope followed by incubation with Alexa Fluor 546 conjugated secondary antibodies (Figure 4.19). Cells were imaged by confocal laser scan microscopy and LC-3 was detected by monitoring GFP fluorescence (Figure 4.19). In both control and CLN7 overexpressing cells, cytosolic GFP-LC3-I and small GFP-LC3-II positive vesicles of variable size were observed indicating conversion of GFP-LC3-I to GFP-LC3-II and the association with autophagosomal membranes. In CLN7 overexpressing cells the size and number of autophagosomes were increased compared to mock transfected control cells (Figure 4.19). Small numbers of GFP-LC3-II positive autophagosomes colocalized with Myc-CLN7 suggesting a fusion of autophagosomes with lysosomes.

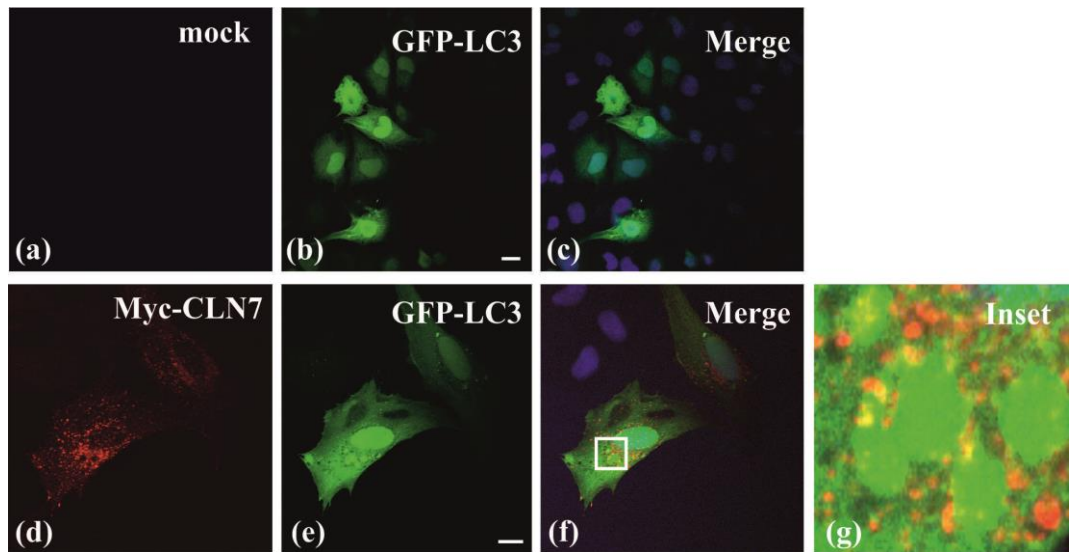


Figure 4.19 Increased numbers of autophagosomes in HeLa cells overexpressing Myc-CLN7. HeLa cells were transiently transfected with GFP-LC3 (a-c) or co-transfected with GFP-LC3 and Myc-CLN7 (d-f). 72 hours after the start of transfection cells were fixed and stained with antibodies against Myc (red, a and d) followed by incubation with secondary antibodies coupled to Alexa-Fluor 546. GFP-LC3-I and -II were detected by GFP-fluorescence (b and e) and nuclei were visualized with DAPI (blue). The merged image indicates partial co-localization of Myc-CLN7 and LC3-II (f). The inset (g) shows a 9-fold magnification of the region marked by the white rectangle. Scale bars 15 μ m.

5. Discussion

CLN7 is a lysosomal membrane glycoprotein of unknown function which is deficient in CLN7 disease, a neurodegenerative lysosomal storage disorder of childhood (Steenhuis et al., 2010). CLN7 is located in lysosomes in neuronal and non-neuronal cells (Sharifi et al., 2010; Siintola et al., 2007). *MFSD8/CLN7* mRNA is lowly abundant and is mainly expressed in neuronal cells of the hippocampus and the cortex of mouse and rat brain with minor expression in the cerebellum (Damme et al., 2014; Sharifi et al., 2010). Based on its sequence homologies with transporters of the major facilitator superfamily (MFS), CLN7 is believed to be a lysosomal transporter with unknown substrate specificity (Siintola et al., 2007). It is unclear, how mutations in CLN7 lead to lysosomal storage and to the specific damage and loss of photoreceptors and neurons in different brain regions (Elleder, 2011; Sharifi et al., 2010). Due to the rarity of the disease and the limited availability of skin fibroblasts from CLN7 patients, the aim of the study was to generate a cell-based model of the disease by siRNA and shRNA-mediated down-regulation of the endogenous *MFSD8/CLN7* mRNA.

5.1 Expression analyses of *MFSD8/CLN7* in cultured human cell lines

Low abundant expression of *MFSD8/CLN7* mRNA has been shown in different human tissues and in rat brain by Northern blot analyses and quantitative real-time PCR analyses, respectively (Sharifi et al., 2010; Siintola et al., 2007). Analyses of cultured neuronal rat cells showed 6- and 12-fold higher *Mfsd8/Cln7* expression levels in neurons compared to astrocytes and microglia cells, respectively (Sharifi et al., 2010). To choose a cell line with high *MFSD8/CLN7* abundance, expression levels of *MFSD8/CLN7* mRNA were quantified in cultured HEK293 and HeLa cells by real-time PCR. Expression in HEK293 fibroblast cell line derived from kidney was 8-fold higher compared to the HeLa tumor cell line derived from cervix. Delta CT values revealed low abundant *MFSD8/CLN7* mRNA amounts in both cell lines confirming low expression in tissues revealed by Northern blot analyses of human brain (Siintola et al., 2007) and real-time PCR analyses of rat brain (Sharifi et al., 2010). In agreement with abundant expression of *MFSD8/CLN7* mRNA in HEK293 cells, high CLN7 expression in kidney was observed in wild type mice by immunoblotting and in *Mfsd8-lacZ*

reporter gene mice by *lacZ* expression, suggesting an important functional role for CLN7 in the kidney (Damme et al., 2014). Tissue-dependent *MFSD8/CLN7* mRNA expression could not be verified by immunoblotting as no antibody detecting the endogenous human CLN7 protein existed. Based on abundant CLN7 expression, HEK293 cells were chosen for siRNA- and shRNA-mediated downregulation of *CLN7/MFSD8*.

5.2 Generation of a cell-based model for CLN7 disease

To down-regulate endogenous *MFSD8/CLN7* mRNA two experimental strategies were performed on cultured HEK293 and HeLa cells. First, *MFSD8/CLN7* was down-regulated by chemically synthesized siRNAs directed against a sequence of the coding human *MFSD8/CLN7* mRNA. Since the exact half-life time of the CLN7 protein in these cells is unknown, siRNA-mediated knockdown was performed for 96 hours to deplete newly synthesized CLN7 protein. The rather long duration of siRNA knockdown should guarantee that endogenous CLN7 protein is turned over during the time period. To test transfection efficiency, efficacy of depletion and toxicity of siRNA-mediated knockdown both HEK293 and HeLa cells were down-regulated for 96 hours and *MFSD8/CLN7* mRNA was quantified by real-time PCR. In both cell lines a reduction of *MFSD8/CLN7* mRNA levels by 50% was detected. Reasons for the incomplete down-regulation of *MFSD8/CLN7* mRNA could be that strong down-regulation of CLN7 leads to an immediate apoptosis of cells, which would favour the survival of cells with lower degree of CLN7 depletion. However, data from a mouse model of CLN7 disease argue against the possibility that CLN7 is required for cell survival and maintenance because *Cln7*-deficient mice are viable and fertile (Damme et al., 2014). Furthermore primary *Cln7*-deficient fibroblasts can be cultivated without obvious cell loss and with unaltered proliferation compared to control cells (L. Brandenstein, personal communication).

In a second approach the pSuper RNAi system, a vector based system for efficient and specific down-regulation of gene expression by short hairpin RNA (shRNA) was used for transient transfection of HEK293 and HeLa cells (Brummelkamp et al., 2002). 19 bp and 21 bp custom oligonucleotides derived from the *MFSD8/CLN7* mRNA sequence were cloned into the multiple cloning site of vector pSuper.GFP.shRNA, which allowed

simultaneous expression of shRNA and GFP. Transient transfection of pSuper.GFP.sh19RNA and -sh21RNA resulted in a down-regulation by 77% and 73% in HeLa cells, respectively, and by 74% and 72% in HEK293 cells, respectively. The data indicate that the shRNA-mediated downregulation of *MFSD8/CLN7* mRNA was more efficient than siRNA-mediated depletion in both HeLa and HEK293 cells and that the sh19RNA was more efficient than the sh21RNA. However, a complete knockout of the *MFSD8/CLN7* mRNA was not achieved by shRNA-mediated down-regulation.

5.3 Analyses of *MFSD8/CLN7*-depleted cells

5.3.1 Expression of NCL-related and lysosomal genes in *MFSD8/CLN7*-depleted cells

Quantitative real-time PCR analyses were performed in *MFSD8/CLN7* down-regulated HEK293 and HeLa cells to quantify changes in the expression of selected NCL-related genes and lysosomal genes. Due to the related biochemical and clinical phenotype of NCL diseases it was suggested that NCL-related proteins interact and may share common biochemical pathways (Getty and Pearce, 2011; Siintola et al., 2006a; Vesa et al., 2002). It is conceivable that short-term depletion of CLN7 leads to a compensatory up-regulation in the expression of NCL-related genes having overlapping or redundant functions with CLN7 or alternatively resulting in alterations in biochemical pathways shared with other NCL-related proteins. Furthermore, the loss of CLN7 could result in a depletion of the exported metabolite in the cytosol, e.g. amino acids, dipeptides, monosaccharides, leading to cellular starvation and lysosomal stress. This would lead to decreased phosphorylation of TFEB and its nuclear translocation which would result in a global increase in the expression of all lysosomal and autophagy genes (Settembre et al., 2013). The lysosomal NCL-related genes *CLN1*, *CLN2*, *CLN3*, *CLN5*, *MFSD8/CLN7*, *CLN10* and *CLN13* have been identified as potential TFEB targets (Kollmann et al., 2013).

For gene expression analyses the NCL-related genes *CLN3*, *CLN6* and *CLN8* were chosen. The *CLN3* gene encodes an integral lysosomal membrane protein of unknown function and the *CLN6* and *CLN8* genes encode for integral membrane proteins located in the ER (Kollmann et al., 2013). The amounts of *CLN3*, *CLN6* and *CLN8* mRNAs

were decreased in *MFSD8/CLN7*-depleted cells. Reasons for lower amounts of *CLN3*, *CLN6* and *CLN8* mRNAs are unclear and remain to be investigated. It has to be noted that both *CLN6* and *CLN8* encode integral membrane proteins located in the ER and hence their gene expression is not regulated by TFEB. The primary functions of *CLN6* and *CLN8* are unknown.

To analyze whether short term down-regulation of *MFSD8/CLN7* mRNA leads to compensatory changes in the mRNA expression of lysosomal genes, quantitative real-time PCR analyses were performed. Expression of genes coding for lysosomal membrane proteins (*LAMP-1*, *LAP*) and soluble lysosomal enzymes (*TRAP*, *cathepsin D*) were chosen for analyses. In down-regulated HEK293 cells no transcriptional upregulation of *LAMP-1*, *LAP*, *TRAP* and *cathepsin D* mRNAs was observed. The absence of significant up-regulation of mRNAs coding for lysosomal proteins suggests that TFEB is not activated and translocated to the nucleus in *MFSD8/CLN7* short-term depleted cells. The absence of TFEB activation further suggests that short-term depletion of *MFSD8/CLN7* does not lead to lysosomal stress or cellular starvation.

5.3.2 Unaltered transferrin-receptor mediated endocytosis in *MFSD8/CLN7*-depleted cells

Transferrin (Tf) is a monomeric serum glycoprotein that binds Fe^{3+} in the blood. This complex binds to a specific homodimeric transmembrane protein called transferrin receptor (Tfr) at the cell surface (Schneider et al., 1982). The receptor-ligand complexes are internalized by clathrin-mediated endocytosis. In the endosomal acidic environment Fe^{3+} is released from the Tfr/Tf- complex. Iron-free Tf bound to Tfr is recycled to the plasma membrane to scavenge more iron after release from the Tfr (Luck and Mason, 2012), whereas Fe^{3+} is reduced to Fe^{2+} and transported via the dimetal transporter 1 (DMT1) to the cytosol for reutilization (Rouault, 2013). To study clathrin-mediated endocytosis Tf coupled to Alexa Fluor[®] 546 (Tf-AF546) was used as a marker protein. Cells were transfected twice with scr shRNA or *CLN7* sh21-shRNA, incubated in the presence of Tf-AF546 at 4°C for 30 min and chased for 60 min at 37°C. With these analyses both the receptor-mediated uptake of transferrin and the vesicular intracellular

transport of the Tfr/Tf-complexes from the plasma membrane to endosomal compartments can be analyzed. GFP-positive single cells expressing scr- or CLN7-shRNAs were analyzed and the intracellular Tf-AF546 fluorescence was quantified. Immunofluorescence analyses showed uptake of Tf both in scr- and CLN7-sh21 transfected cells indicating that cell surface localization and clathrin-mediated endocytosis of Tfr was not affected by the deficiency of CLN7. Quantification of intracellular Tf-AF546 fluorescence showed no alterations in the amount of intracellular transferrin in *MFSD8/CLN7*-depleted cells compared to scr shRNA transfected control cells. Endocytosed Tf-AF546 co-localized with the early endosomal marker protein EEA1 in *MFSD8/CLN7*-depleted cells indicating correct intracellular transport to endosomal compartments after internalization. However, in *MFSD8/CLN7*-downregulated cells endocytosed Tf was distributed more peripherally, whereas in scr transfected cells Tf-positive compartments were located in the perinuclear region. These results suggest that the amount of Tfrs at the plasma membrane, the binding of Tf to its receptors, the rate of endocytosis and the recycling from endosomes to the plasma membrane is not affected by the deficiency of CLN7. It remains to be investigated why a peripheral distribution of endocytosed Tf is observed in *MFSD8/CLN7*-depleted cells. Unaltered Tfr-mediated endocytosis has also been observed in CLN3- and CLN6-deficient cells. In CLN6-deficient human, mouse and sheep fibroblasts comparable amounts of [¹²⁵I] transferrin were internalized compared to control cells (Heine et al., 2004). In fibroblasts of patients with CLN3 disease no changes in transferrin endocytosis were observed compared to control cells (Luiro et al., 2004). Uptake of low density lipoprotein was unaltered, but transport in the endocytic pathway from early endosomes to lysosomes was delayed in CLN3-deficient cells (Luiro et al., 2004). It has been reported that fluid-phase endocytosis of the marker substrate dextran was up-regulated in CLN3- and reduced in CLN6-deficient cerebellar cell lines (Cao et al., 2011; Fossale et al., 2004). These cerebellar cell lines derived from the *Cln3* delta *ex7/ex8* knockin mouse and the natural *Cln6*-deficient *nclf* mutant mouse (Bronson et al., 1998; Cotman et al., 2002). The deletions and mutations in the *Cln3* and *Cln6* genes, respectively, have been reported to result in a complete loss of *Cln3* and *Cln6* function. Although transferrin-mediated endocytosis was not affected in CLN6-deficient cells, the MPR-300 mediated endocytosis of the lysosomal enzyme arylsulfatase A was increased

(Heine et al., 2004). As M6P-receptor and transferrin receptor-mediated endocytosis are both clathrin-mediated, these differences imply that not all the endocytic pathways are affected in the same way. In the future, it will be interesting to examine mannose 6-phosphate receptor (MPR) dependent endocytosis, by examining internalization of M6P-ligands in the absence or presence of M6P, and fluid-phase endocytosis, by measuring the uptake of BSA coupled to fluorophore using FACS analyses, in *MFSD8/CLN7*-depleted and deficient cells.

5.3.3 Decreased LAMP-1 protein amounts in *MFSD8/CLN7*-depleted cells

In several lysosomal storage disorders elevated levels of lysosomal membrane proteins have been observed. Increased size and number of lysosomes from >1% to as much as 50% of total cellular volume have been reported (Meikle et al., 1997). LAMP-1 has been used as a diagnostic marker in LSD-affected human skin fibroblasts and soluble LAMP-1 forms in the plasma of patients (Meikle et al., 1997). We could demonstrate by immunoblotting that LAMP-1 amounts were significantly decreased in *MFSD8/CLN7*-depleted HEK293 cells compared to control cells. LAMP-2 protein amounts were not changed in *MFSD8/CLN7*-depleted cells. *LAMP-1* mRNA amounts were slightly decreased in *MFSD8/CLN7*-depleted cells. The reason for reduced LAMP-1 protein amounts in *MFSD8/CLN7*-depleted cells remains to be investigated. The concomitant decrease of both mRNA and protein levels suggest that LAMP-1 is transcriptionally down-regulated. Alternatively, depletion of *MFSD8/CLN7* could lead to impaired lysosomal sorting of LAMP-1 or could result in increased degradation of LAMP-1 in lysosomes. To study accelerated turnover of LAMP-1 in lysosomes in more detail, pulse-chase analyses of metabolically labeled cells in the absence and presence of inhibitors of lysosomal proteases or vacuolar ATPases to determine the half-life times of LAMP-1 have to be performed. In tissues of Lamp-1 deficient mice a compensatory upregulation of Lamp-2 was reported (Andrejewski et al., 1999). Altered expression of LAMP-1 and LAMP-2 were shown in *CLN3* knock-down cells. (Pohl et al., 2007). In *CLN3* knock-down HeLa cells decreased expression of LAMP-1 on both mRNA and protein level was accompanied by highly increased LAMP-2 levels.

In contrast to decreased LAMP-1 levels in *MFSD8/CLN7*-depleted cultured cells used in this study, increased levels of Lamp-1 and Lamp-2 were shown in the brain of 10 month old *Mfsd8* knockout mice (L. Brandenstein, personal communication). Discrepancies of LAMP-1 levels between the cell-based model and the CLN7 mouse model may be explained by i) changes in LAMP-1 being cell-type specific, e.g. occurring mainly in postmitotic cells with high MFSD8/CLN7 expression, like neurons (Sharifi et al., 2010), ii) progressive accumulation of lysosomal storage material requiring a longer time period which is not reached during the short-term induced depletion of endogenous *MFSD8/CLN7* mRNA in cultured cells and iii) the metabolism of cultured HeLa and HEK293 cells being different from the affected tissues *in vivo*. Cultured cells have an excess of nutrients and growth factors and therefore the lack of monomeric compounds in the cytosol caused by CLN7 deficiency is probably not as severe as in tissues. A further explanation could be the residual putative transporter function of active, wild type CLN7 protein in down-regulated HeLa and HEK293 cells. In contrast to the *Mfsd8* knockout mouse, shRNA-mediated depletion of *CLN7/MFSD8* mRNA only results in a reduction by 75%, leaving 25% of *CLN7/MFSD8* mRNA left. Residual amounts of CLN7 may lead to the reduced accumulation of the unknown transported metabolite in lysosomes resulting in the absence or slower progression of lysosomal storage and consequently to a lack of increase in the size and number of lysosomes. In agreement with this hypothesis, Lamp-1 levels were not significantly altered in the brain of a *lacZ Mfsd8*-gene trap mouse model, which has been described as hypomorphic *Cln7* mouse model (Damme et al., 2014). In summary, the data suggest that number and size of lysosomes are not altered and that lysosomal storage is absent in short term *MFSD8/CLN7*-depleted cells.

We have not analyzed whether *MFSD8/CLN7*-depleted cells show lysosomal storage which can be quantified by autofluorescence and by the accumulation of subunit c of mitochondrial ATP synthase in lysosomes. Accumulation of autofluorescent ceroid lipopigments and lysosomal storage of subunit c are hallmarks of CLN7 disease and have been observed in the brains of 6 and 10 month old *Mfsd8* knockout mice and of CLN7 patients post mortem (L. Brandenstein, personal communication, Elleder, 2011; Sharifi et al., 2010).

5.3.4 Analysis of expression, biosynthetic sorting and proteolytic processing of soluble lysosomal enzymes in *MFSD8/CLN7*-depleted cells

For a number of lysosomal storage diseases increased amounts of soluble lysosomal proteins have been reported. Analyses of soluble lysosomal enzymes in *MFSD8/CLN7*-depleted cells by immunoblotting showed unaltered levels of cathepsin D and a minor reduction in cathepsin Z amounts compared to control cells. In contrast, the levels of cathepsin Z and cathepsin D were upregulated in the brain of 10 months old *Mfsd8* knockout mice (L. Brandenstein, personal communication). The discrepancy in expression levels of selected lysosomal enzymes between the down-regulated cultured cells and the brain of *Cln7*-deficient mice could be due to i) short-term shRNA-mediated down-regulation of *MFSD8/CLN7*, ii) residual *MFSD8/CLN7* mRNA amounts in shRNA downregulated cells iii) cell type-specific consequences of *CLN7* depletion, e. g. neuronal versus non-neuronal cells or iv) decreased degradation due to lysosomal dysfunction. Increased cathepsin Z and D levels in the brains of *Cln7*-deficient mouse models could be due to a proliferation of microglial cells which mainly express cathepsin Z and D in the brain.

Amounts and the appearance of mature cathepsin D forms in *MFSD8/CLN7* down-regulated cells were unaltered indicating that expression, biosynthetic sorting to lysosomes and proteolytic processing were not impaired by the loss of *CLN7*. This indicates that lysosomal acidification is not impaired in *MFSD8/CLN7*-depleted cells. In agreement with this study, processing of cathepsin D was not altered in the brain of *Mfsd8 lacZ* gene trap and *Cln7* knockout mice (Damme et al., 2014, L. Brandenstein, personal communication). Furthermore, *Cln7*-deficient primary embryonic fibroblasts showed normal lysosomal transport and processing of cathepsin D to the mature forms (L. Brandenstein; personal communication). In *CLN3*-deficient human fibroblasts and in *CLN6/Cln6*-deficient human, mouse and sheep fibroblasts intracellular transport and processing of cathepsin D were not impaired (Heine et al., 2004; Pohl et al., 2007).

5.3.5 Increased number of autophagosomes in *MFSD8/CLN7*-depleted cells

Macroautophagy is a constitutive process, which can be induced by the starvation of cells and an increase in the unfolded protein response. It involves the engulfment of cytosolic proteins or whole organelles (e.g. ribosomes, mitochondria) by a double membrane (Klionsky and Codogno, 2013). These double-membraned vesicles, called autophagosomes, fuse with endosomes and finally with lysosomes to form autolysosomes where the autophagic cargo is released and subsequently degraded (Eskelinen and Saftig, 2009). Macroautophagy is the major cellular pathway for recycling damaged and aged mitochondria (Raben et al., 2009b) and is important for cell renewal, especially in non-dividing cells as neurons, where altered proteins and damaged organelles cannot be cleared by redistribution to daughter cells by cell division (Wong and Cuervo, 2010). Thus impairment of autophagy is implicated in the pathogenesis of neurodegenerative disorders (Komatsu et al., 2006; Nedelsky et al., 2008; Ventruti and Cuervo, 2007) and lysosomal storage disorders (Lieberman et al., 2012).

To analyze the role of *CLN7* for macroautophagy, *MFSD8/CLN7* mRNA was depleted by shRNA and the endogenous levels of the autophagic marker protein microtubule-associated protein1 light chain 3-II (LC3-II) were quantified by western blotting. In *MFSD8/CLN7* shRNA transfected HEK293 cells a statistically significant 2.76-fold increase in LC3-II levels was detected compared to scr shRNA transfected control cells. To confirm our results, we performed LC3-II immunoblotting with total homogenates from *MFSD8/CLN7*-depleted HeLa cells. In agreement with the results in HEK293 cells, increased amounts of LC3-II were observed in *MFSD8/CLN7*-depleted HeLa cells. The data indicate that increased numbers of autophagosomes are present in *MFSD8/CLN7*-depleted cultured cells. In agreement, increased numbers of GFP-LC3-II positive autophagosomes were detected in *MFSD8/CLN7* down-regulated HeLa cells compared to scrambled shRNA transfected control cells in immunofluorescence experiments. Interestingly, increased numbers of GFP-LC3-II positive autophagosomes were also observed in *MFSD8/CLN7* overexpressed HeLa cells.

Autophagy is induced under starvation conditions to provide metabolites for cellular survival (Cao et al., 2006). During a 2-hour and a 4-hour starvation period elevated numbers of GFP-LC3-II positive autophagosomes were detected in both *MFSD8/CLN7*-

depleted cells and in control cells. The data indicate that during nutrient withdrawal the formation of new autophagosomes occurs both in control and in *MFSD8/CLN7*-depleted cells. These results suggest that in the presence of amino acids, nutrients and growth factors only *MFSD8/CLN7*-depleted cells are unable to compensate for the loss of *MFSD8/CLN7* leading to increased numbers of autophagosomes, whereas cells containing *MFSD8/CLN7* show unchanged autophagosomes. Under starvation conditions even the control cells expressing *CLN7* become unable to compensate the nutrient withdrawal and hence an increase is shown here, too. It was reported that lack of amino acids and growth factors induces autophagy generally (Ishibashi et al., 2009).

Increased levels of LC3-II could be caused by an impaired degradation in autolysosomes, decreased fusion of autophagosomes with lysosomes or an induction of macroautophagy (Klionsky et al., 2012). To discriminate between these possibilities expression levels of beclin were further analyzed. Beclin1 is a multifunctional protein and is known to have regulatory functions in autophagy (Wirawan et al., 2012). It is required for the formation of the PtdIns3K-beclin-1-complex and is essential for the induction of autophagy (Funderburk et al., 2010). Western blot analyses revealed that beclin1 levels were not significantly altered in *MFSD8/CLN7*-downregulated HEK293 cells. The data suggest that increased numbers of autophagosomes in *MFSD8/CLN7*-depleted cells are not due to an activation of autophagy, but rather a reduced removal/degradation of autophagosomes either by a block of fusion with lysosomes, altered mobility of autophagosomes or decreased degradation after fusion with lysosomes in autolysosomes. Increased LC3-II levels accompanied by unaltered beclin amounts were also observed in the brains of mouse models for mucopolipidosis II (ML-II) (Kollmann et al., 2012), *CLN2* disease (Micsenyi et al., 2013), *CLN6* disease (Thelen et al., 2012) and *CLN7* disease (L. Brandenstein, personal communication).

A gradual age-dependent increase in LC3-II and higher numbers of autophagosomes have also been reported in the brain of mouse models for *CLN2* disease (Micsenyi et al., 2013), *CLN3* disease (Cao et al., 2006), *CLN6* disease (Thelen et al., 2012) and *CLN10* disease (Koike et al., 2005; Shacka and Roth, 2007). However the changes in the number of autophagosomes, except for *CLN10* disease, were mild and were mostly observed in older mice indicating a progressive accumulation of autophagosomes

during the course of the disease (Raben et al., 2009b). In addition, increased LC3-II levels have been observed for a number of lysosomal storage diseases like ML-II (Kollmann et al., 2012) and -IV (Vergarajauregui et al., 2008), Niemann Pick type C (Pacheco et al., 2007), Pompe disease (Raben et al., 2009a), multiple sulfatase deficiency, and mucopolysaccharidosis type IIIA (Settembre et al., 2008).

From this study it cannot be concluded whether the accumulation of autophagosomes in *MFSD8/CLN7*-depleted cells is due to decreased mobilization of autophagosomes, decreased fusion of autophagosomes with lysosomes or impaired lysosomal degradation (Wong and Cuervo, 2010). However, reduced lysosomal acidification, accumulation of storage material and decreased content or activity of lysosomal hydrolases have been reported to result in incomplete degradation of the content of autophagosomes. Based on the data of this study impaired acidification and lysosomal accumulation of storage material are unlikely to contribute to increased numbers of autophagosomes. However, alterations in lysosomal Ca^{2+} levels have been shown to inhibit fusion of lysosomes with other organelles, mainly in the endocytic pathway (Luzio et al., 2007). Defects in the lysosomal Ca^{2+} channel mucolipin 1 result in increased number of autophagosomes in neurons of mucolipin-1-deficient mouse brain (Curcio-Morelli et al., 2010) and in skin fibroblasts of MLIV patients (Vergarajauregui et al., 2008). It is possible that *CLN7* may be involved in the export of divalent cations from the lysosomal lumen into the cytosol with Ca^{2+} , Zn^{2+} , Mn^{2+} and Fe^{2+} being potential substrates. The levels of *MFSD8/CLN7* mRNA in the brain were reported to be altered by acute dietary iron loading and chronic iron accumulation in a mouse model in *Hfe*^{-/-} mice, a mouse model for hemochromatosis (Johnstone et al., 2012; Johnstone and Milward, 2010). It is possible that *CLN7* contributes to the transport of Fe^{2+} across lysosomal membranes.

However, transport studies on isolated lysosomes from wild type and *Cln7* knockout mice with Fe^{2+} as substrate have to be performed to show direct transport by *CLN7*.

In summary, the data obtained in *MFSD8/CLN7*-down-regulated HEK293 and HeLa cells and the *CLN7* mouse model suggest that *CLN7* disease has a macroautophagy inefficiency which is not due to a lysosomal acidification defect or the accumulation of storage material in lysosomes.

5.4 Comparison of *MFSD8/CLN7*-downregulated cells with *Cln7*-deficient fibroblasts from *Mfsd8/Cln7*-knockout mice

During the course of the studies an *Mfsd8-lacZ* gene trap and a *Mfsd8* knockout mouse model were generated by targeted disruption of the homologous *Mfsd8/Cln7* gene by deletion of the critical exon 2 (S. Storch, personal communication, Damme et al., 2014). The comparison of the data from this study and new data from the *Mfsd8/Cln7*-knockout mouse model indicate that the alterations of the protein composition of lysosomes was more pronounced in *Cln7*-deficient cells compared to *MFSD8/CLN7*-depleted cells. The data suggest that residual function of *MFSD8/CLN7* caused by the incomplete depletion may weaken the phenotype in shRNA-mediated downregulated cells. In contrast to other *CLN* diseases (e. g. *CLN1* disease, *CLN2* disease), where different mutations in the same gene lead to a variety of phenotypes, defects in the *MFSD8/CLN7* gene primarily result in the severe late-infantile NCL form suggesting that the majority of mutations lead to a complete loss of function. However, the cell culture model has some disadvantages compared to the mouse model. Increased numbers of autophagosomes in specific cell types (e. g. neurons in the brain) could be due to a long-term starvation period due to defective supply of monomeric compounds caused by lysosomal dysfunction with decreased degradation of macromolecules or export of catabolic monomers. It is unlikely, that a similar starvation occurs in cells cultured in full medium. Furthermore the rather late manifestation of *CLN7* disease in patients suggest that either a critical threshold has to be exceeded or that other lysosomal membrane proteins with redundant functions can partially compensate for the loss of *MFSD8/CLN7*. In cerebellar precursor cells of cultured mouse *Cln3 Δ ex7/8* storage of subunit c could only be detected upon aging of cells at confluency (Fossale et al., 2004). The rather late manifestation of *CLN7* disease in patients suggests that either a critical threshold has to be exceeded or that other lysosomal membrane proteins with redundant functions can partially compensate for the loss of *CLN7*.

5.5 Outlook

To date, only one hypomorphic mouse model for CLN7 disease exists which recapitulates partially the phenotype of human CLN7 patients (Damme et al., 2014). It will be of interest whether the complete knockout of the *Cln7/Mfsd8* gene in mice leads to neurodegeneration in the brain and in the retina, accumulation of autofluorescent ceroid lipopigments, neuroinflammation and the activation of the lysosomal/autophagy machinery and on the biochemical level to lysosomal storage, missorting and altered processing of lysosomal enzymes, changed expression of lysosomal proteins and proteins involved in macroautophagy. The generated cell-based model of CLN7 disease is only partially valuable as a tool to study the cellular phenotype of CLN7 disease because a reduction of *MFSD8/CLN7* by 75 % was achieved by shRNA-mediated transfection, leaving 25% of residual *MFSD8/CLN7* mRNA. Phenotypic differences between the mild phenotype observed in hypomorphic *Mfsd8/lacZ* gene trap mice (Damme et al., 2014) and the more severe phenotype observed in *Mfsd8* knockout mice (L. Brandenstein, personal communication) and the presence of late-infantile (majority of mutations) and juvenile forms (e. g. p.Ala157Pro) of CLN7 disease (Kousi et al., 2012) suggest that minor residual activity of wild type and mutant *Cln7* might alter the onset and course of the disease and the cellular phenotype of CLN7-depleted cells. It is possible that the lack of cellular phenotypes in *MFSD8/CLN7*-depleted cells was due to residual amounts of wild type CLN7. Furthermore it is likely that both the cell type and the duration of CLN7 deficiency contribute to the pathological phenotypes observed in CLN7 disease.

In contrast to the neuropathological analyses of human CLN7 disease and the phenotype of the *Mfsd8/lacZ* mouse model, only consequences of short term depletion in mitotically active non-neuronal cells up to 96 hours were analyzed in this study. The data obtained in *MFSD8/CLN7* down-regulated cells suggest that macroautophagy is impaired even in the presence of residual CLN7 levels, whereas the expression, biosynthetic sorting, and processing of cathepsin Z and D were not altered.

In the future interruption of the *CLN7/MFSD8* gene by new techniques like the CRISPR/Cas9 genome editing system, has to be performed in HEK293 and HeLa cells to generate *CLN7* knockout cells lines (Ran et al., 2013). With this technique a complete

knockout of *MFSD8/CLN7* can be achieved in any cell line circumventing the problem of low residual *CLN7* amounts. The analyses of these cells will clarify whether accumulation of autofluorescent ceroid lipopigments, increased levels of soluble lysosomal proteins, storage of subunit c of mitochondrial ATP-synthase in lysosomes and increased levels of autophagosomes can be observed in confluent *CLN7*-deficient cells upon aging. These knockout cell lines would contribute to study *CLN7* disease-specific mechanisms.

6. Summary

1. Quantitative real-time PCR analyses showed low abundance of *MFSD8/CLN7* mRNA in cultured HEK293 and HeLa cells. *MFSD8/CLN7* mRNA expression was 8-fold higher in the human kidney derived cell line HEK293 compared to the HeLa cell line.

2. Comparison of siRNA- and shRNA-mediated down-regulation of *MFSD8/CLN7* mRNA in HeLa and HEK293 revealed a higher reduction by shRNAs resulting in a decrease of *MFSD8/CLN7* mRNA by 75% after 96 hours of expression compared to scrambled shRNA transfected cells.

3. Quantitative real-time PCR analyses of NCL-related and lysosomal genes in *MFSD8/CLN7*-depleted HeLa and HEK293 cells showed a reduction of *CLN3*, *CLN6* and *CLN8* mRNA levels. No significant changes in mRNAs coding for lysosomal proteins LAMP-1, lysosomal acid phosphatase, and cathepsin D in *MFSD8/CLN7* down-regulated cells were detected suggesting no global transcriptional activation of lysosomal genes by TFEB in cells with short-term depletion of CLN7.

4. Endocytosis of the transferrin receptor at the cell surface and transport of transferrin-transferrin receptor complexes to endosomal compartments were unaltered in *MFSD8/CLN7*-downregulated HeLa cells.

5. In *MFSD8/CLN7*-depleted HEK293 cells decreased LAMP-1 and unaltered LAMP-2 protein levels were observed. In down-regulated HeLa cells amounts of LAMP-1 and LAMP-2 were unchanged and no gross changes in the number, size and distribution of LAMP-1 and LAMP-2 positive compartments were observed.

6. Biosynthetic sorting and processing of cathepsin D and cathepsin Z were unchanged in *MFSD8/CLN7*-depleted HeLa cells indicating that intracellular transport to lysosomes and lysosomal acidification were not impaired due to loss of CLN7.

7. Increased LC3-II amounts and an elevated number of autophagosomes in *MFSD8/CLN7*-depleted HEK293 and HeLa cells indicate an impairment of

macroautophagy. Unaltered beclin amounts showed that macroautophagy was not induced due to loss of CLN7.

8. In summary, the cell-based model for CLN7 disease generated by shRNA-mediated depletion did not replicate all changes observed in *Cln7*-deficient fibroblasts of a knockout mouse model for CLN7 disease. However, an increased number of autophagosomes was detected in CLN7-depleted cells making the cell-based model for CLN7 disease suitable to study macroautophagy. The data suggest that both the cell type and the duration of CLN7 deficiency contribute to the pathological phenotypes observed in CLN7 disease. In addition, residual amounts of wild type CLN7 protein may lead to the absence or later onset of cellular phenotypes.

7. References

- Aiello, C., Terracciano, A., Simonati, A., Discepoli, G., Cannelli, N., Claps, D., Crow, Y.J., Bianchi, M., Kitzmüller, C., Longo, D., *et al.* (2009). Mutations in *MFSD8/CLN7* are a frequent cause of variant-late infantile neuronal ceroid lipofuscinosis. *Human mutation* 30, E530-540.
- Aldahmesh, M.A., Al-Hassnan, Z.N., Aldosari, M., and Alkuraya, F.S. (2009). Neuronal ceroid lipofuscinosis caused by *MFSD8* mutations: a common theme emerging. *Neurogenetics* 10, 307-311.
- Anderson, G.W., Goebel, H.H., and Simonati, A. (2013). Human pathology in NCL. *Biochim Biophys Acta* 1832, 1807-1826.
- Andrejewski, N., Punnonen, E.L., Guhde, G., Tanaka, Y., Lüllmann-Rauch, R., Hartmann, D., von Figura, K., and Saftig, P. (1999). Normal lysosomal morphology and function in LAMP-1-deficient mice. *J Biol Chem* 274, 12692-12701.
- Bagshaw, R.D., Mahuran, D.J., and Callahan, J.W. (2005). A proteomic analysis of lysosomal integral membrane proteins reveals the diverse composition of the organelle. *Molecular & cellular proteomics : MCP* 4, 133-143.
- Ballabio, A., and Gieselmann, V. (2009). Lysosomal disorders: from storage to cellular damage. *Biochim Biophys Acta* 1793, 684-696.
- Beck, M. (2010). Therapy for lysosomal storage disorders. *IUBMB Life* 62, 33-40.
- Bjorkoy, G., Lamark, T., Brech, A., Outzen, H., Perander, M., Overvatn, A., Stenmark, H., and Johansen, T. (2005). p62/SQSTM1 forms protein aggregates degraded by autophagy and has a protective effect on huntingtin-induced cell death. *J Cell Biol* 171, 603-614.
- Bonifacino, J.S., and Traub, L.M. (2003). Signals for sorting of transmembrane proteins to endosomes and lysosomes. *Annual review of biochemistry* 72, 395-447.
- Bras, J., Verloes, A., Schneider, S.A., Mole, S.E., and Guerreiro, R.J. (2012). Mutation of the parkinsonism gene *ATP13A2* causes neuronal ceroid-lipofuscinosis. *Human molecular genetics* 21, 2646-2650.
- Braulke, T., and Bonifacino, J.S. (2009). Sorting of lysosomal proteins. *Biochim Biophys Acta* 1793, 605-614.
- Bronson, R.T., Donahue, L.R., Johnson, K.R., Tanner, A., Lane, P.W., and Faust, J.R. (1998). Neuronal ceroid lipofuscinosis (*nclf*), a new disorder of the mouse linked to chromosome 9. *Am J Med Genet* 77, 289-297.
- Brummelkamp, T.R., Bernards, R., and Agami, R. (2002). A system for stable expression of short interfering RNAs in mammalian cells. *Science* 296, 550-553.
- Cao, Y., Espinola, J.A., Fossale, E., Massey, A.C., Cuervo, A.M., MacDonald, M.E., and Cotman, S.L. (2006). Autophagy is disrupted in a knock-in mouse model of juvenile neuronal ceroid lipofuscinosis. *J Biol Chem* 281, 20483-20493.
- Cao, Y., Staropoli, J.F., Biswas, S., Espinola, J.A., Macdonald, M.E., Lee, J.M., and Cotman, S.L. (2011). Distinct early molecular responses to mutations causing *vLINCL* and *JNCL* presage ATP synthase subunit C accumulation in cerebellar cells. *PLoS One* 6, e17118.
- Ciechanover, A. (2005). Proteolysis: from the lysosome to ubiquitin and the proteasome. *Nature reviews Molecular cell biology* 6, 79-87.

- Cotman, S.L., Vrbanac, V., Lebel, L.A., Lee, R.L., Johnson, K.A., Donahue, L.R., Teed, A.M., Antonellis, K., Bronson, R.T., Lerner, T.J., *et al.* (2002). Cln3(Deltaex7/8) knock-in mice with the common JNCL mutation exhibit progressive neurologic disease that begins before birth. *Hum Mol Genet* *11*, 2709-2721.
- Curcio-Morelli, C., Charles, F.A., Micsenyi, M.C., Cao, Y., Venugopal, B., Browning, M.F., Dobrenis, K., Cotman, S.L., Walkley, S.U., and Slaugenhaupt, S.A. (2010). Macroautophagy is defective in mucopolipin-1-deficient mouse neurons. *Neurobiol Dis* *40*, 370-377.
- Damme, M., Brandenstein, L., Fehr, S., Jankowiak, W., Bartsch, U., Schweizer, M., Hermans-Borgmeyer, I., and Storch, S. (2014). Gene disruption of *Mfsd8* in mice provides the first animal model for CLN7 disease. *Neurobiol Dis* *65*, 12-24.
- Dell'Angelica, E.C., Mullins, C., Caplan, S., and Bonifacino, J.S. (2000). Lysosome-related organelles. *FASEB J* *14*, 1265-1278.
- Elleder, M., Kousi, M., Lehesjoki, A. E., Mole, S. E., Siintola, E., Topcu, M., ed. (2011). The neuronal ceroid lipofuscinoses (Batten disease), 2 nd edn (Oxford University Press).
- Eskelinen, E.L., and Saftig, P. (2009). Autophagy: a lysosomal degradation pathway with a central role in health and disease. *Biochim Biophys Acta* *1793*, 664-673.
- Eskelinen, E.L., Tanaka, Y., and Saftig, P. (2003). At the acidic edge: emerging functions for lysosomal membrane proteins. *Trends Cell Biol* *13*, 137-145.
- Fossale, E., Wolf, P., Espinola, J.A., Lubicz-Nawrocka, T., Teed, A.M., Gao, H., Rigamonti, D., Cattaneo, E., MacDonald, M.E., and Cotman, S.L. (2004). Membrane trafficking and mitochondrial abnormalities precede subunit c deposition in a cerebellar cell model of juvenile neuronal ceroid lipofuscinosis. *BMC Neurosci* *5*, 57.
- Funderburk, S.F., Wang, Q.J., and Yue, Z. (2010). The Beclin 1-VPS34 complex--at the crossroads of autophagy and beyond. *Trends Cell Biol* *20*, 355-362.
- Futerman, A.H., and van Meer, G. (2004). The cell biology of lysosomal storage disorders. *Nature reviews Molecular cell biology* *5*, 554-565.
- Gao, H., Boustany, R.M., Espinola, J.A., Cotman, S.L., Srinidhi, L., Antonellis, K.A., Gillis, T., Qin, X., Liu, S., Donahue, L.R., *et al.* (2002). Mutations in a novel CLN6-encoded transmembrane protein cause variant neuronal ceroid lipofuscinosis in man and mouse. *American journal of human genetics* *70*, 324-335.
- Getty, A.L., and Pearce, D.A. (2011). Interactions of the proteins of neuronal ceroid lipofuscinosis: clues to function. *Cell Mol Life Sci* *68*, 453-474.
- Ghosh, P., Dahms, N.M., and Kornfeld, S. (2003). Mannose 6-phosphate receptors: new twists in the tale. *Nature reviews Molecular cell biology* *4*, 202-212.
- Haltia, M. (2003). The neuronal ceroid-lipofuscinoses. *Journal of neuropathology and experimental neurology* *62*, 1-13.
- Heine, C., Koch, B., Storch, S., Kohlschütter, A., Palmer, D.N., and Bräulke, T. (2004). Defective endoplasmic reticulum-resident membrane protein CLN6 affects lysosomal degradation of endocytosed arylsulfatase A. *J Biol Chem* *279*, 22347-22352.
- Hobert, J.A., and Dawson, G. (2006). Neuronal ceroid lipofuscinoses therapeutic strategies: past, present and future. *Biochim Biophys Acta* *1762*, 945-953.
- Hunziker, W., and Geuze, H.J. (1996). Intracellular trafficking of lysosomal membrane proteins. *Bioessays* *18*, 379-389.

- Ishibashi, S., Yamazaki, T., and Okamoto, K. (2009). Association of autophagy with cholesterol-accumulated compartments in Niemann-Pick disease type C cells. *J Clin Neurosci* *16*, 954-959.
- Jabs, S., Quitsch, A., Kakela, R., Koch, B., Tyynela, J., Brade, H., Glatzel, M., Walkley, S., Saftig, P., Vanier, M.T., *et al.* (2008). Accumulation of bis(monoacylglycero)phosphate and gangliosides in mouse models of neuronal ceroid lipofuscinosis. *J Neurochem* *106*, 1415-1425.
- Jalanko, A., and Braulke, T. (2009). Neuronal ceroid lipofuscinoses. *Biochim Biophys Acta* *1793*, 697-709.
- Jentsch, T.J. (2008). CLC chloride channels and transporters: from genes to protein structure, pathology and physiology. *Crit Rev Biochem Mol Biol* *43*, 3-36.
- Jezeqou, A., Llinares, E., Anne, C., Kieffer-Jaquinod, S., O'Regan, S., Aupetit, J., Chabli, A., Sagne, C., Debacker, C., Chadeaux-Vekemans, B., *et al.* (2012). Heptahelical protein PQLC2 is a lysosomal cationic amino acid exporter underlying the action of cysteamine in cystinosis therapy. *Proc Natl Acad Sci U S A* *109*, E3434-3443.
- Johnstone, D., Graham, R.M., Trinder, D., Delima, R.D., Riveros, C., Olynyk, J.K., Scott, R.J., Moscato, P., and Milward, E.A. (2012). Brain transcriptome perturbations in the *Hfe*(*-/-*) mouse model of genetic iron loading. *Brain Res* *1448*, 144-152.
- Johnstone, D., and Milward, E.A. (2010). Genome-wide microarray analysis of brain gene expression in mice on a short-term high iron diet. *Neurochem Int* *56*, 856-863.
- Kabeya, Y., Mizushima, N., Ueno, T., Yamamoto, A., Kirisako, T., Noda, T., Kominami, E., Ohsumi, Y., and Yoshimori, T. (2000). LC3, a mammalian homologue of yeast Apg8p, is localized in autophagosome membranes after processing. *Embo J* *19*, 5720-5728.
- Kang, R., Zeh, H.J., Lotze, M.T., and Tang, D. (2011). The Beclin 1 network regulates autophagy and apoptosis. *Cell Death Differ* *18*, 571-580.
- Kimura, S., Noda, T., and Yoshimori, T. (2007). Dissection of the autophagosome maturation process by a novel reporter protein, tandem fluorescent-tagged LC3. *Autophagy* *3*, 452-460.
- Klionsky, D.J., Abdalla, F.C., Abeliovich, H., Abraham, R.T., Acevedo-Arozena, A., Adeli, K., Agholme, L., Agnello, M., Agostinis, P., Aguirre-Ghiso, J.A., *et al.* (2012). Guidelines for the use and interpretation of assays for monitoring autophagy. *Autophagy* *8*, 445-544.
- Klionsky, D.J., and Codogno, P. (2013). The mechanism and physiological function of macroautophagy. *J Innate Immun* *5*, 427-433.
- Klionsky, D.J., and Emr, S.D. (2000). Autophagy as a regulated pathway of cellular degradation. *Science* *290*, 1717-1721.
- Kohan, R., Cismondi, I.A., Oller-Ramirez, A.M., Guelbert, N., Anzolini, T.V., Alonso, G., Mole, S.E., de Kremer, D.R., and de Halac, N.I. (2011). Therapeutic approaches to the challenge of neuronal ceroid lipofuscinoses. *Curr Pharm Biotechnol* *12*, 867-883.
- Kohlschütter, A., Goebel, H. H., Schulz, A., Lukacs, Z. (2005). Die neuronalen Ceroid-Lipofuszinosen. *Deutsches Ärzteblatt* *102*, 284-288.
- Kohlschütter, A., and Schulz, A. (2009). Towards understanding the neuronal ceroid lipofuscinoses. *Brain Dev* *31*, 499-502.

- Koike, M., Shibata, M., Waguri, S., Yoshimura, K., Tanida, I., Kominami, E., Gotow, T., Peters, C., von Figura, K., Mizushima, N., *et al.* (2005). Participation of autophagy in storage of lysosomes in neurons from mouse models of neuronal ceroid-lipofuscinoses (Batten disease). *Am J Pathol* 167, 1713-1728.
- Kollmann, K., Damme, M., Markmann, S., Morelle, W., Schweizer, M., Hermans-Borgmeyer, I., Rochert, A.K., Pohl, S., Lubke, T., Michalski, J.C., *et al.* (2012). Lysosomal dysfunction causes neurodegeneration in mucopolidosis II 'knock-in' mice. *Brain* 135, 2661-2675.
- Kollmann, K., Pohl, S., Marschner, K., Encarnacao, M., Sakwa, I., Tiede, S., Poorthuis, B.J., Lübke, T., Müller-Loennies, S., Storch, S., *et al.* (2010). Mannose phosphorylation in health and disease. *European journal of cell biology* 89, 117-123.
- Kollmann, K., Uusi-Rauva, K., Scifo, E., Tyynelä, J., Jalanko, A., and Braulke, T. (2013). Cell biology and function of neuronal ceroid lipofuscinosis-related proteins. *Biochim Biophys Acta* 1832, 1866-1881.
- Komatsu, M., Waguri, S., Chiba, T., Murata, S., Iwata, J., Tanida, I., Ueno, T., Koike, M., Uchiyama, Y., Kominami, E., *et al.* (2006). Loss of autophagy in the central nervous system causes neurodegeneration in mice. *Nature* 441, 880-884.
- Kornfeld, R., Bao, M., Brewer, K., Noll, C., and Canfield, W.M. (1998). Purification and multimeric structure of bovine N-acetylglucosamine-1-phosphodiester alpha-N-acetylglucosaminidase. *J Biol Chem* 273, 23203-23210.
- Kornfeld, S., and Mellman, I. (1989). The biogenesis of lysosomes. *Annu Rev Cell Biol* 5, 483-525.
- Kousi, M., Lehesjoki, A.E., and Mole, S.E. (2012). Update of the mutation spectrum and clinical correlations of over 360 mutations in eight genes that underlie the neuronal ceroid lipofuscinoses. *Human mutation* 33, 42-63.
- Kousi, M., Siintola, E., Dvorakova, L., Vlaskova, H., Turnbull, J., Topcu, M., Yuksel, D., Gokben, S., Minassian, B.A., Elleder, M., *et al.* (2009). Mutations in *CLN7/MFSD8* are a common cause of variant late-infantile neuronal ceroid lipofuscinosis. *Brain : a journal of neurology* 132, 810-819.
- Kurz, T., Terman, A., Gustafsson, B., and Brunk, U.T. (2008). Lysosomes in iron metabolism, ageing and apoptosis. *Histochem Cell Biol* 129, 389-406.
- Lerner, T.J., Boustany, R.M., Anderson, J.W., D'Arigo, K.L., Schlumpf, K., Buckler, A.J., Gusella, J.F., and Haines, J.L. (1995). Isolation of a novel gene underlying batten disease, *CLN3*. *Cell* 82, 949-957.
- Levine, B., and Kroemer, G. (2008). Autophagy in the pathogenesis of disease. *Cell* 132, 27-42.
- Lieberman, A.P., Puertollano, R., Raben, N., Slaugenhaupt, S., Walkley, S.U., and Ballabio, A. (2012). Autophagy in lysosomal storage disorders. *Autophagy* 8, 719-730.
- Lübke, T., Lobel, P., and Sleat, D.E. (2009). Proteomics of the lysosome. *Biochim Biophys Acta* 1793, 625-635.
- Luck, A.N., and Mason, A.B. (2012). Transferrin-mediated cellular iron delivery. *Curr Top Membr* 69, 3-35.
- Luiro, K., Yliannala, K., Ahtiainen, L., Maunu, H., Jarvela, I., Kyttälä, A., and Jalanko, A. (2004). Interconnections of *CLN3*, *Hook1* and *Rab* proteins link Batten disease to defects in the endocytic pathway. *Human molecular genetics* 13, 3017-3027.

- Luzio, J.P., Bright, N.A., and Pryor, P.R. (2007). The role of calcium and other ions in sorting and delivery in the late endocytic pathway. *Biochem Soc Trans* 35, 1088-1091.
- Meikle, P.J., Brooks, D.A., Ravenscroft, E.M., Yan, M., Williams, R.E., Jaunzems, A.E., Chataway, T.K., Karageorgos, L.E., Davey, R.C., Boulter, C.D., *et al.* (1997). Diagnosis of lysosomal storage disorders: evaluation of lysosome-associated membrane protein LAMP-1 as a diagnostic marker. *Clin Chem* 43, 1325-1335.
- Mellman, I. (1996). Endocytosis and molecular sorting. *Annu Rev Cell Dev Biol* 12, 575-625.
- Micsenyi, M.C., Sikora, J., Stephney, G., Dobrenis, K., and Walkley, S.U. (2013). Lysosomal membrane permeability stimulates protein aggregate formation in neurons of a lysosomal disease. *J Neurosci* 33, 10815-10827.
- Mindell, J.A. (2012). Lysosomal acidification mechanisms. *Annu Rev Physiol* 74, 69-86.
- Mizushima, N., Levine, B., Cuervo, A.M., and Klionsky, D.J. (2008). Autophagy fights disease through cellular self-digestion. *Nature* 451, 1069-1075.
- Mole SE, G.H. (2011). The Neuronal Ceroid Lipofuscinoses (Batten Disease).
- Mole, S.E., Williams, R.E., and Goebel, H.H. (2005). Correlations between genotype, ultrastructural morphology and clinical phenotype in the neuronal ceroid lipofuscinoses. *Neurogenetics* 6, 107-126.
- Muzaffar, N.E., and Pearce, D.A. (2008). Analysis of NCL Proteins from an Evolutionary Standpoint. *Curr Genomics* 9, 115-136.
- Nedelsky, N.B., Todd, P.K., and Taylor, J.P. (2008). Autophagy and the ubiquitin-proteasome system: collaborators in neuroprotection. *Biochim Biophys Acta* 1782, 691-699.
- Noskova, L., Stranecky, V., Hartmannova, H., Pristoupilova, A., Baresova, V., Ivanek, R., Hulkova, H., Jahnova, H., van der Zee, J., Staropoli, J.F., *et al.* (2011). Mutations in *DNAJC5*, encoding cysteine-string protein alpha, cause autosomal-dominant adult-onset neuronal ceroid lipofuscinosis. *American journal of human genetics* 89, 241-252.
- Ohsumi, Y. (2001). Molecular dissection of autophagy: two ubiquitin-like systems. *Nature reviews Molecular cell biology* 2, 211-216.
- Pacheco, C.D., Kunkel, R., and Lieberman, A.P. (2007). Autophagy in Niemann-Pick C disease is dependent upon Beclin-1 and responsive to lipid trafficking defects. *Human molecular genetics* 16, 1495-1503.
- Palmer, D.N., Martinus, R.D., Barns, G., Reeves, R.D., and Jolly, R.D. (1988). Ovine ceroid-lipofuscinosis. I: Lipopigment composition is indicative of a lysosomal proteinosis. *Am J Med Genet Suppl* 5, 141-158.
- Pao, S.S., Paulsen, I.T., and Saier, M.H., Jr. (1998). Major facilitator superfamily. *Microbiol Mol Biol Rev* 62, 1-34.
- Perez-Poyato, M.S., Mila-Recasens, M., Ferrer-Abizanda, I., Cusi-Sanchez, V., Vazquez-Lopez, M., Camino-Leon, R., Coll-Rosell, M.J., Gort, L., and Pineda-Marfa, M. (2012). [Neuronal ceroid lipofuscinosis: diagnostic algorithm and clinical description of the variants late infantile Finnish (CLN5) and Turkish (CLN7)]. *Rev Neurol* 54, 544-550.
- Piper, R.C., and Lehner, P.J. (2011). Endosomal transport via ubiquitination. *Trends Cell Biol* 21, 647-655.

- Platt, F.M., Boland, B., and van der Spoel, A.C. (2012). The cell biology of disease: lysosomal storage disorders: the cellular impact of lysosomal dysfunction. *J Cell Biol* *199*, 723-734.
- Platt, F.M., and Lachmann, R.H. (2009). Treating lysosomal storage disorders: current practice and future prospects. *Biochim Biophys Acta* *1793*, 737-745.
- Pohl, S., Marschner, K., Storch, S., and Braulke, T. (2009). Glycosylation- and phosphorylation-dependent intracellular transport of lysosomal hydrolases. *Biol Chem* *390*, 521-527.
- Pohl, S., Mitchison, H.M., Kohlschütter, A., van Diggelen, O., Braulke, T., and Storch, S. (2007). Increased expression of lysosomal acid phosphatase in CLN3-defective cells and mouse brain tissue. *J Neurochem* *103*, 2177-2188.
- Raben, N., Baum, R., Schreiner, C., Takikita, S., Mizushima, N., Ralston, E., and Plotz, P. (2009a). When more is less: excess and deficiency of autophagy coexist in skeletal muscle in Pompe disease. *Autophagy* *5*, 111-113.
- Raben, N., Shea, L., Hill, V., and Plotz, P. (2009b). Monitoring autophagy in lysosomal storage disorders. *Methods Enzymol* *453*, 417-449.
- Ran, F.A., Hsu, P.D., Wright, J., Agarwala, V., Scott, D.A., and Zhang, F. (2013). Genome engineering using the CRISPR-Cas9 system. *Nat Protoc* *8*, 2281-2308.
- Ranta, S., Zhang, Y., Ross, B., Lonka, L., Takkunen, E., Messer, A., Sharp, J., Wheeler, R., Kusumi, K., Mole, S., *et al.* (1999). The neuronal ceroid lipofuscinoses in human EPMR and *mnd* mutant mice are associated with mutations in *CLN8*. *Nat Genet* *23*, 233-236.
- Rouault, T.A. (2013). Iron metabolism in the CNS: implications for neurodegenerative diseases. *Nat Rev Neurosci* *14*, 551-564.
- Ruivo, R., Anne, C., Sagne, C., and Gasnier, B. (2009). Molecular and cellular basis of lysosomal transmembrane protein dysfunction. *Biochim Biophys Acta* *1793*, 636-649.
- Rutsch, F., Gailus, S., Miousse, I.R., Suormala, T., Sagne, C., Toliat, M.R., Nürnberg, G., Wittkamp, T., Buers, I., Sharifi, A., *et al.* (2009). Identification of a putative lysosomal cobalamin exporter altered in the cblF defect of vitamin B12 metabolism. *Nat Genet* *41*, 234-239.
- Saftig, P., ed. (2005). *Lysosomes* (Landes Bioscience).
- Saftig, P., and Klumperman, J. (2009). Lysosome biogenesis and lysosomal membrane proteins: trafficking meets function. *Nature reviews Molecular cell biology* *10*, 623-635.
- Sagne, C., and Gasnier, B. (2008). Molecular physiology and pathophysiology of lysosomal membrane transporters. *J Inher Metab Dis* *31*, 258-266.
- Santavuori, P., Vanhanen, S.L., and Autti, T. (2001). Clinical and neuroradiological diagnostic aspects of neuronal ceroid lipofuscinoses disorders. *Eur J Paediatr Neurol* *5 Suppl A*, 157-161.
- Sardiello, M., Palmieri, M., di Ronza, A., Medina, D.L., Valenza, M., Gennarino, V.A., Di Malta, C., Donaudy, F., Embrione, V., Polishchuk, R.S., *et al.* (2009). A gene network regulating lysosomal biogenesis and function. *Science* *325*, 473-477.
- Savukoski, M., Klockars, T., Holmberg, V., Santavuori, P., Lander, E.S., and Peltonen, L. (1998). *CLN5*, a novel gene encoding a putative transmembrane protein mutated in Finnish variant late infantile neuronal ceroid lipofuscinosis. *Nat Genet* *19*, 286-288.

- Schneider, C., Sutherland, R., Newman, R., and Greaves, M. (1982). Structural features of the cell surface receptor for transferrin that is recognized by the monoclonal antibody OKT9. *J Biol Chem* 257, 8516-8522.
- Schröder, B., Wrocklage, C., Pan, C., Jager, R., Kösters, B., Schäfer, H., Elsässer, H.P., Mann, M., and Hasilik, A. (2007). Integral and associated lysosomal membrane proteins. *Traffic* 8, 1676-1686.
- Schröder, B.A., Wrocklage, C., Hasilik, A., and Saftig, P. (2010). The proteome of lysosomes. *Proteomics* 10, 4053-4076.
- Schultz, M.L., Tecedor, L., Chang, M., and Davidson, B.L. (2011). Clarifying lysosomal storage diseases. *Trends Neurosci* 34, 401-410.
- Schulz, A., Dhar, S., Rylova, S., Dbaibo, G., Alroy, J., Hagel, C., Artacho, I., Kohlschütter, A., Lin, S., and Boustany, R.M. (2004). Impaired cell adhesion and apoptosis in a novel CLN9 Batten disease variant. *Ann Neurol* 56, 342-350.
- Schulze, H., Kolter, T., and Sandhoff, K. (2009). Principles of lysosomal membrane degradation: Cellular topology and biochemistry of lysosomal lipid degradation. *Biochim Biophys Acta* 1793, 674-683.
- Schulze, H., and Sandhoff, K. (2011). Lysosomal lipid storage diseases. *Cold Spring Harb Perspect Biol* 3, a004804.
- Schwake, M., Schröder, B., and Saftig, P. (2013). Lysosomal membrane proteins and their central role in physiology. *Traffic* 14, 739-748.
- Settembre, C., Di Malta, C., Polito, V.A., Garcia Arencibia, M., Vetrini, F., Erdin, S., Erdin, S.U., Huynh, T., Medina, D., Colella, P., *et al.* (2011). TFEB links autophagy to lysosomal biogenesis. *Science* 332, 1429-1433.
- Settembre, C., Fraldi, A., Jahreiss, L., Spampinato, C., Venturi, C., Medina, D., de Pablo, R., Tacchetti, C., Rubinsztein, D.C., and Ballabio, A. (2008). A block of autophagy in lysosomal storage disorders. *Human molecular genetics* 17, 119-129.
- Settembre, C., Fraldi, A., Medina, D.L., and Ballabio, A. (2013). Signals from the lysosome: a control centre for cellular clearance and energy metabolism. *Nature reviews Molecular cell biology* 14, 283-296.
- Shacka, J.J., and Roth, K.A. (2007). Cathepsin D deficiency and NCL/Batten disease: there's more to death than apoptosis. *Autophagy* 3, 474-476.
- Sharifi, A., Kousi, M., Sagne, C., Bellenchi, G.C., Morel, L., Darmon, M., Hulkova, H., Ruivo, R., Debacker, C., El Mestikawy, S., *et al.* (2010). Expression and lysosomal targeting of CLN7, a major facilitator superfamily transporter associated with variant late-infantile neuronal ceroid lipofuscinosis. *Hum Mol Genet* 19, 4497-4514.
- Siintola, E., Lehesjoki, A.E., and Mole, S.E. (2006a). Molecular genetics of the NCLs-status and perspectives. *Biochim Biophys Acta* 1762, 857-864.
- Siintola, E., Partanen, S., Strömme, P., Haapanen, A., Haltia, M., Maehlen, J., Lehesjoki, A.E., and Tynnelä, J. (2006b). Cathepsin D deficiency underlies congenital human neuronal ceroid-lipofuscinosis. *Brain : a journal of neurology* 129, 1438-1445.
- Siintola, E., Topcu, M., Aula, N., Lohi, H., Minassian, B.A., Paterson, A.D., Liu, X.Q., Wilson, C., Lahtinen, U., Anttonen, A.K., *et al.* (2007). The novel neuronal ceroid lipofuscinosis gene *MFSD8* encodes a putative lysosomal transporter. *American journal of human genetics* 81, 136-146.

- Sleat, D.E., Donnelly, R.J., Lackland, H., Liu, C.G., Sohar, I., Pullarkat, R.K., and Lobel, P. (1997). Association of mutations in a lysosomal protein with classical late-infantile neuronal ceroid lipofuscinosis. *Science* 277, 1802-1805.
- Sleat, D.E., Sohar, I., Pullarkat, P.S., Lobel, P., and Pullarkat, R.K. (1998). Specific alterations in levels of mannose 6-phosphorylated glycoproteins in different neuronal ceroid lipofuscinoses. *The Biochemical journal* 334 (Pt 3), 547-551.
- Smith, K.R., Dahl, H.H., Canafoglia, L., Andermann, E., Damiano, J., Morbin, M., Bruni, A.C., Giaccone, G., Cossette, P., Saftig, P., *et al.* (2013). Cathepsin F mutations cause Type B Kufs disease, an adult-onset neuronal ceroid lipofuscinosis. *Hum Mol Genet* 22, 1417-1423.
- Smith, K.R., Damiano, J., Franceschetti, S., Carpenter, S., Canafoglia, L., Morbin, M., Rossi, G., Pareyson, D., Mole, S.E., Staropoli, J.F., *et al.* (2012). Strikingly different clinicopathological phenotypes determined by progranulin-mutation dosage. *Am J Hum Genet* 90, 1102-1107.
- Staropoli, J.F., Karaa, A., Lim, E.T., Kirby, A., Elbalalesy, N., Romansky, S.G., Leydiker, K.B., Coppel, S.H., Barone, R., Xin, W., *et al.* (2012). A homozygous mutation in *KCTD7* links neuronal ceroid lipofuscinosis to the ubiquitin-proteasome system. *American journal of human genetics* 91, 202-208.
- Steenhuis, P., Froemming, J., Reinheckel, T., and Storch, S. (2012). Proteolytic cleavage of the disease-related lysosomal membrane glycoprotein CLN7. *Biochim Biophys Acta* 1822, 1617-1628.
- Steenhuis, P., Herder, S., Gelis, S., Braulke, T., and Storch, S. (2010). Lysosomal targeting of the CLN7 membrane glycoprotein and transport via the plasma membrane require a dileucine motif. *Traffic* 11, 987-1000.
- Steinfeld, R., Reinhardt, K., Schreiber, K., Hillebrand, M., Kraetzner, R., Bruck, W., Saftig, P., and Gärtner, J. (2006). Cathepsin D deficiency is associated with a human neurodegenerative disorder. *American journal of human genetics* 78, 988-998.
- Stogmann, E., El Tawil, S., Wagenstaller, J., Gaber, A., Edris, S., Abdelhady, A., Assem-Hilger, E., Leutmezer, F., Bonelli, S., Baumgartner, C., *et al.* (2009). A novel mutation in the *MFSD8* gene in late infantile neuronal ceroid lipofuscinosis. *Neurogenetics* 10, 73-77.
- Tanida, I., Ueno, T., and Kominami, E. (2008). LC3 and autophagy. *Methods in molecular biology* 445, 77-88.
- Thelen, M., Damme, M., Schweizer, M., Hagel, C., Wong, A.M., Cooper, J.D., Braulke, T., and Galliciotti, G. (2012). Disruption of the autophagy-lysosome pathway is involved in neuropathology of the *nclf* mouse model of neuronal ceroid lipofuscinosis. *PLoS One* 7, e35493.
- Tiede, S., Storch, S., Lübke, T., Henrissat, B., Bargal, R., Raas-Rothschild, A., and Braulke, T. (2005). Mucopolidosis II is caused by mutations in *GNPTA* encoding the alpha/beta GlcNAc-1-phosphotransferase. *Nat Med* 11, 1109-1112.
- Topcu, M., Tan, H., Yalnizoglu, D., Usubutun, A., Saatci, I., Aynaci, M., Anlar, B., Topaloglu, H., Turanli, G., Kose, G., *et al.* (2004). Evaluation of 36 patients from Turkey with neuronal ceroid lipofuscinosis: clinical, neurophysiological, neuroradiological and histopathologic studies. *Turk J Pediatr* 46, 1-10.

- Tyynelä, J., Palmer, D.N., Baumann, M., and Haltia, M. (1993). Storage of saposins A and D in infantile neuronal ceroid-lipofuscinosis. *FEBS letters* 330, 8-12.
- Ventrucci, A., and Cuervo, A.M. (2007). Autophagy and neurodegeneration. *Curr Neurol Neurosci Rep* 7, 443-451.
- Vergarajauregui, S., Connelly, P.S., Daniels, M.P., and Puertollano, R. (2008). Autophagic dysfunction in mucopolipidosis type IV patients. *Human molecular genetics* 17, 2723-2737.
- Verheijen FW, M.G., ed. (2005). *Lysosomal transporters and associated diseases*. (Landes Bioscience / Eurekah.com, Georgetown, Texas, USA).
- Vesa, J., Chin, M.H., Oelgeschlager, K., Isosomppi, J., DellAngelica, E.C., Jalanko, A., and Peltonen, L. (2002). Neuronal ceroid lipofuscinoses are connected at molecular level: interaction of CLN5 protein with CLN2 and CLN3. *Molecular biology of the cell* 13, 2410-2420.
- Vesa, J., Hellsten, E., Verkruyse, L.A., Camp, L.A., Rapola, J., Santavuori, P., Hofmann, S.L., and Peltonen, L. (1995). Mutations in the palmitoyl protein thioesterase gene causing infantile neuronal ceroid lipofuscinosis. *Nature* 376, 584-587.
- Walkley, S.U., and Vanier, M.T. (2009). Secondary lipid accumulation in lysosomal disease. *Biochim Biophys Acta* 1793, 726-736.
- Wang, W., and Malcolm, B.A. (1999). Two-stage PCR protocol allowing introduction of multiple mutations, deletions and insertions using QuikChange Site-Directed Mutagenesis. *Biotechniques* 26, 680-682.
- Wheeler, R.B., Sharp, J.D., Schultz, R.A., Joslin, J.M., Williams, R.E., and Mole, S.E. (2002). The gene mutated in variant late-infantile neuronal ceroid lipofuscinosis (*CLN6*) and in *nclf* mutant mice encodes a novel predicted transmembrane protein. *American journal of human genetics* 70, 537-542.
- Wirawan, E., Lippens, S., Vanden Berghe, T., Romagnoli, A., Fimia, G.M., Piacentini, M., and Vandenabeele, P. (2012). Beclin1: a role in membrane dynamics and beyond. *Autophagy* 8, 6-17.
- Wong, E., and Cuervo, A.M. (2010). Autophagy gone awry in neurodegenerative diseases. *Nature neuroscience* 13, 805-811.

8. Curriculum Vitae

Persönliche Daten:

Name: Jana Farhana Galal, geb. Helal
Adresse: Agathenstrasse 11, 20357 Hamburg
Geburtstag: 04.10.1987
Geburtsort: Köln
Familienstand: Verheiratet

Schulischer Werdegang:

1994-1997 India International School, Bangladesch
1997-1999 Grundschule Franzosenkoppel, Hamburg
1999-2008 Helene-Lange-Gymnasium, Hamburg (bilingual)

Studium

UKE, Hamburg; Humanmedizin (seit Oktober 2008)
1. Staatsexamen (Sommer 2010), Note: 2,0
experimentelle Doktorarbeit, seit März 2011
Kinder- und Jugendmedizin
Thema: Lysosomale Speichererkrankungen

Famulaturen:

Nephrologie Station 5B, UKE Juli 2012
Hausarztpraxis Melderis August 2012
Neurologie, Asklepios-Klinik Altona April 2013
Anästhesie, Asklepios-Klinik St. Georg Mai 2013

Praktisches Jahr:

Wahltertial Neurologie, Institute of Neurology, London
August-Dezember 2013
Innere Medizin, Regio Klinikum Pinneberg Dezember 2013 -
März 2014
Chirurgie, Regio Klinikum Elmshorn April-Juli 2014

Sprachkenntnisse:

Englisch (sehr gut),
Bengali (sehr gut),
Französisch (Schulkenntnisse)

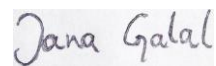
9. Affidavit (Eidesstattliche Erklärung)

Ich versichere ausdrücklich, dass ich die Arbeit selbständig und ohne fremde Hilfe verfasst, andere als die von mir angegebenen Quellen und Hilfsmittel nicht benutzt und die aus den benutzten Werken wörtlich oder inhaltlich entnommenen Stellen einzeln nach Ausgabe (Auflage und Jahr des Erscheinens), Band und Seite des benutzten Werkes kenntlich gemacht habe.

Ferner versichere ich, dass ich die Dissertation bisher nicht einem Fachvertreter an einer anderen Hochschule zur Überprüfung vorgelegt oder mich anderweitig um Zulassung zur Promotion beworben habe.

Ich erkläre mich einverstanden, dass meine Dissertation vom Dekanat der Medizinischen Fakultät mit einer gängigen Software zur Erkennung von Plagiaten überprüft werden kann.

Unterschrift:

The image shows a handwritten signature in cursive script that reads "Jana Galal". The signature is written in black ink on a light-colored background.

10. Acknowledgements

I want to thank Prof Thomas Braulke and PD Dr. Stephan Storch for providing the topic.

I would like to express my special appreciation and thanks to the “team CLN7”: My advisor Dr. Stephan Storch for the dedicated support and critical examination of my thesis.

Furthermore I want to thank my supervisor Dr. Pieter Steenhuis for a friendly and patient training during the experimental works and various inspiring discussions.

Also, I want to thank all of the members of the biochemical/ molecular biological laboratory for their helpfulness and friendly company during work.

My sincerest thanks go to my family for encouraging and supporting me throughout my life. Mama, Papa, Nadia, Elaine, I cannot express how grateful I am for all the sacrifices that you have made on my behalf. Danke, Rami, für die liebevolle Unterstützung!

I would also like to thank my friends for motivating me and everybody who believed in me.